FPGA-Based DOCSIS Upstream Demodulation

A Thesis Submitted

to the College of Graduate Studies and Research

in Partial Fulfillment of the Requirements

for the Degree of Doctor of Philosophy

in the Department of Electrical and Computer Engineering

University of Saskatchewan

by

Brian Berscheid

Saskatoon, Saskatchewan, Canada

Permission to Use

In presenting this thesis in partial fulfillment of the requirements for a Postgraduate degree from the University of Saskatchewan, it is agreed that the Libraries of this University may make it freely available for inspection. Permission for copying of this thesis in any manner, in whole or in part, for scholarly purposes may be granted by the professors who supervised this thesis work or, in their absence, by the Head of the Department of Electrical and Computer Engineering or the Dean of the College of Graduate Studies and Research at the University of Saskatchewan. Any copying, publication, or use of this thesis, or parts thereof, for financial gain without the written permission of the author is strictly prohibited. Proper recognition shall be given to the author and to the University of Saskatchewan in any scholarly use which may be made of any material in this thesis.

Request for permission to copy or to make any other use of material in this thesis in whole or in part should be addressed to:

Head of the Department of Electrical and Computer Engineering

57 Campus Drive

University of Saskatchewan

Saskatoon, Saskatchewan, Canada

S7N 5A9

Acknowledgments

I would like to express my appreciation to my supervisors, Professor J. Eric Salt and Professor Ha H. Nguyen for their guidance and teaching throughout my pursuit of this degree. They have truly taken an interest in my work, and have provided outstanding support over the years. I feel very fortunate to have had the opportunity to work with such wonderful supervisors.

I would also like to thank Professors Robert Johanson, Aryan Saadat-Mehr, and Doug Degenstein for acting as members of my Ph.D. advisory committee. Their questions and comments have helped to direct my research.

I would like to thank fellow students Eric Pelet and Zohreh Andalibi, with whom I have enjoyed many thoughtful discussions and collaborations.

Finally, I would like to express my gratitude to my parents, Bruce and Barbara Berscheid, who have provided tremendous support, encouragement, and inspiration over the years.

Abstract

In recent years, the state-of-the-art in field programmable gate array (FPGA) technology has been advancing rapidly. Consequently, the use of FPGAs is being considered in many applications which have traditionally relied upon application-specific integrated circuits (ASICs). FPGA-based designs have a number of advantages over ASIC-based designs, including lower up-front engineering design costs, shorter time-to-market, and the ability to reconfigure devices in the field. However, ASICs have a major advantage in terms of computational resources. As a result, expensive high performance ASIC algorithms must be redesigned to fit the limited resources available in an FPGA.

Concurrently, coaxial cable television and internet networks have been undergoing significant upgrades that have largely been driven by a sharp increase in the use of interactive applications. This has intensified demand for the so-called upstream channels, which allow customers to transmit data into the network. The format and protocol of the upstream channels are defined by a set of standards, known as DOCSIS 3.0, which govern the flow of data through the network.

Critical to DOCSIS 3.0 compliance is the upstream demodulator, which is responsible for the physical layer reception from all customers. Although upstream demodulators have typically been implemented as ASICs, the design of an FPGA-based upstream demodulator is an intriguing possibility, as FPGA-based demodulators could potentially be upgraded in the field to support future DOCSIS standards. Furthermore, the lower non-recurring engineering costs associated with FPGA-based designs could provide an opportunity for smaller companies to compete in this market.

The upstream demodulator must contain complicated synchronization circuitry to detect, measure, and correct for channel distortions. Unfortunately, many of the synchronization algorithms described in the open literature are not suitable for either upstream cable channels or FPGA implementation. In this thesis, computationally inexpensive and robust synchronization algorithms are explored. In particular, algo-

rithms for frequency recovery and equalization are developed.

The many data-aided feedforward frequency offset estimators analyzed in the literature have not considered intersymbol interference (ISI) caused by micro-reflections in the channel. It is shown in this thesis that many prominent frequency offset estimation algorithms become biased in the presence of ISI. A novel high-performance frequency offset estimator which is suitable for implementation in an FPGA is derived from first principles. Additionally, a rule is developed for predicting whether a frequency offset estimator will become biased in the presence of ISI. This rule is used to establish a channel excitation sequence which ensures the proposed frequency offset estimator is unbiased.

Adaptive equalizers that compensate for the ISI take a relatively long time to converge, necessitating a lengthy training sequence. The convergence time is reduced using a two step technique to seed the equalizer. First, the ISI equivalent model of the channel is estimated in response to a specific short excitation sequence. Then, the estimated channel response is inverted with a novel algorithm to initialize the equalizer. It is shown that the proposed technique, while inexpensive to implement in an FPGA, can decrease the length of the required equalizer training sequence by up to 70 symbols.

It is shown that a preamble segment consisting of repeated 11-symbol Barker sequences which is well-suited to timing recovery can also be used effectively for frequency recovery and channel estimation. By performing these three functions sequentially using a single set of preamble symbols, the overall length of the preamble may be further reduced.

Table of Contents

List of Tables

List of Figures

List of Abbreviations

ADC	Analog to Digital Converter
AGC	Automatic Gain Control
ASIC	Application Specific Integrated Circuit
AWGN	Additive White Gaussian Noise
BB	Barker-Based
BPSK	Binary Phase Shift Keying
BSS	Band Selective Sampling
CAZAC	Constant Amplitude Zero Autocorrelation
CBS	Complete Band Sampling
CC	Complementary Code
CM	Cable Modem
CMTS	Cable Modem Termination System
CORDIC	COordinate Rotation DIgitial Computer
CRB	Cramer-Rao Bound
DSP	Digital Signal Processing
DOCSIS	Data Over Cable Service Interface Specification
FIR	Finite Impulse Response
FPGA	Field Programmable Gate Array
IF	Intermediate Frequency
IL	Impulse-Like
ISI	InterSymbol Interference
LMS	Least Mean Squares
LUT	Look Up Table
MAC	Media Access Control
MER	Modulation Error Ratio

ML	Maximum Likelihood
MSE	Mean Squared Error
MSO	Multiple System Operator
MVU	Minimum Variance Unbiased
NCO	Numerically Controlled Oscillator
PD	Peak Distortion
PM	Post-Main
PPM	Pre-and-Post-Main
QAM	Quadrature Amplitude Modulation
QPSK	Quadrature Phase Shift Keying
RAM	Random Access Memory
RF	Radio Frequency
RLS	Recursive Least Squares
RMS	Root Mean Square
RV	Random Variable
S-CDMA	Synchronous Code Division Multiple Access
SNR	Signal to Noise Ratio
SRRC	Square Root Raised Cosine
TDMA	Time Division Multiple Access
ZF	Zero Forcing

1. Introduction

1.1 Motivation

1.1.1 The Cable Industry

In recent years, cable television providers around the world have been extending the use of their networks in order to provide telephone and internet services to customers in addition to cable television. Such cable companies are commonly referred to as multiple system operators (MSOs). At the same time, many telephone companies have diversified into the digital television and internet businesses, placing the MSOs and telephone companies in direct competition.

The original cable networks were constructed in the United States, beginning in the late 1940s [1]. Originally, these were exclusively one-way networks, used to distribute analog television signals from a central cable office (headend) to a multitude of users. Under this traditional broadcast model, the flow of information was unidirectional; the end users had no need to transmit data back to the headend.

However, in the present day, users of the cable network demand ever higher network speeds in order to take advantage of a variety of bandwidth-intensive applications such as video-on-demand, online gaming, and videoconferencing. By nature, interactive applications such as these require each user to transmit data throughout the network, necessitating a network capable of supporting two-way traffic. The widespread usage of these types of interactive applications, coupled with the competition provided by the telephone companies, is driving many cable MSOs to significantly upgrade the capabilities of their networks.
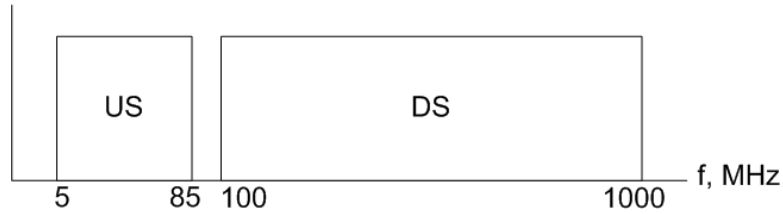
Figure 1.1 A typical frequency partitioning of signals in DOCSIS networks.

Modern cable networks are structured so as to permit simultaneous communication in two directions: from the headend to the end users (the downstream, or forward path) and from the end users back to the headend (the upstream, or return path). To support this full-duplex communication scheme, the frequency spectrum on the cable is partitioned into two distinct regions. Upstream transmissions are allocated to the lower frequency region (typically 5-85MHz), while downstream transmissions are allocated to the higher frequency band (˜100MHz - 1GHz) [2], as illustrated in Figure 1.1.

The bidirectional communication system mentioned above is governed by the Data Over Cable Service Interface Specification (DOCSIS). The DOCSIS standard, which is issued by a non-partisan organization known as CableLabs, aims to promote interoperability among the various data over cable networks. The original version of the DOCSIS standard was released in 1997 [3]. Since 1997, data throughput requirements for the cable network have continued to increase rapidly. To keep up with this demand, a number of upgraded versions of the DOCSIS standard have been released, as highlighted in Table 1.1. The most recent version of the DOCSIS standard is DOCSIS 3.0, officially released in August 2006 [2].

Table 1.1 A listing of versions of the DOCSIS standard and their release dates.

DOCSIS Version	Release Date
1.0	1997
1.1	2001
2.0	2002
3.0	2006
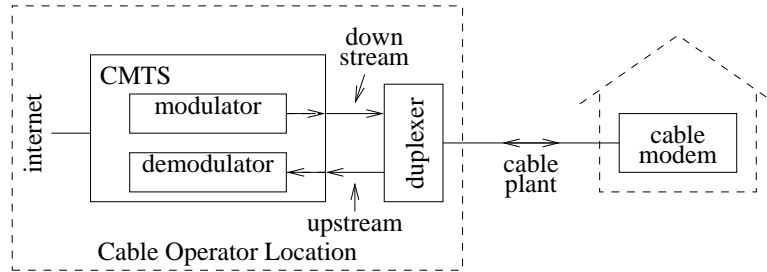
Figure 1.2 A high-level overview of the devices in a DOCSIS network.

Throughout the evolution of the DOCSIS standard over the years since the release of DOCSIS 1.0, there have been numerous changes to both the upstream and downstream transmission formats. However, by far the greater of the changes have been to the upstream transmission scheme, reflecting the huge increase in demand for upstream bandwidth. In order to provide appropriate levels of throughput and performance for various upstream applications, the DOCSIS standard is extremely flexible. A large number of parameters for upstream transmission are dynamically specified and can be modified for each upstream packet transmission. These parameters include: symbol rate, constellation type, payload size, multiple access technique, and level of error control coding, to name just a few.

As seen in Figure 1.2, there are two main types of devices which communicate over a DOCSIS network. The device communicating from the headend side of the network is known as the Cable Modem Termination System (CMTS). At the other end of the network are a large number of user terminals known as Cable Modems (CM). The CMTS is essentially the mastermind of the network, responsible for setting the upstream transmission parameters for every CM in the system, as well as allocating, monitoring, and coordinating all of the network traffic in both directions. This task is particularly onerous in the upstream direction, given that the demodulator in the CMTS must be capable of properly receiving signals from a large number of CMs, many of which may be transmitting over severely non-ideal channels [4].

In order to take advantage of the higher speeds and new features allowed by DOCSIS 3.0, the existing CMTSs and CMs in the networks must be replaced with

3

newer DOCSIS 3.0-compliant models. To date, DOCSIS 3.0 has been deployed in a relatively small number of communities across North America. Thus, the development and sale of DOCSIS 3.0-compliant CMTSs and CMs may present a significant business opportunity for cable equipment vendors.

1.1.2 FPGAs

To date, upstream demodulators used in commercially-deployed CMTS systems have typically been implemented with application-specific integrated circuits (ASICs). While ASICs tend to provide a very high level of performance, they do suffer from a number of downsides.

- High non-recurring engineering design costs: In order to manufacture an ASIC, an extremely expensive set of masks must first be produced for the use during the lithographic fabrication process [5]. The high cost of this initial fabrication means that ASICs are not generally commercially viable for lower volume applications.

- Fixed design: Once an ASIC has been designed and fabricated, its structure or function may not be changed. Even the smallest functionality change will require the production of a completely new set of lithographic masks.

- Time to market: Due to the high complexity of the design and fabrication of ASICs, ASIC designs generally take a relatively long time to complete. This time to market is further lengthened by the fact that ASIC designs must undergo an arduous testing process prior to fabrication. Since ASICs may not be modified in any way after fabrication, each ASIC design must be painstakingly tested prior to the final tape out.

To get around these weaknesses, some cable equipment vendors are considering field programmable gate arrays (FPGAs) as an alternative to ASICs for the implementation of an upstream DOCSIS demodulator. FPGAs are integrated circuits whose

internal structure may be modified after fabrication through a simple programming process. This ability to reconfigure the functionality of the device in the field serves to reduce both design times and time to market, thereby providing advantages over the traditional ASIC-based approach.

An FPGA contains a finite number of discrete logic components which may be connected together in various ways in order to produce arbitrary behavior. The amount of logic components contained in a single FPGA has increased dramatically over the past few years. As a result, FPGAs now have the logic capacity to fulfill the needs of many complex applications that could previously only be achieved through the use of ASICs. Consequently, worldwide usage of FPGAs has been steadily increasing since the introduction of the first commercial FPGA by Xilinx in 1985 [6]. By far the two largest FPGA manufacturers are Xilinx and Altera.

In addition to generic look-up tables and flip flops, modern FPGAs offer a number of specialized blocks tailored to specific applications. For example, digital signal processing (DSP) blocks allow for high-speed multiplication and accumulation of digital inputs. Dedicated random access memory (RAM) inside the FPGA allows for easy storage and retrieval of data. Some FPGAs even provide such features as high-speed serial transceivers and built-in PowerPC processors.

1.2 FPGA-Based DOCSIS Upstream Demodulator

The high-level goal of this research is to work towards establishing the feasibility of implementing a DOCSIS 3.0 upstream demodulator in an FPGA. An investigation into FPGA-based DOCSIS 3.0 upstream demodulators is desirable for a number of reasons:

- The lower development cost of an FPGA-based solution as compared to an ASIC-based solution could lower barriers to entry into the CMTS market, providing smaller companies with a chance to compete.

- The field-reconfigurability of FPGAs is extremely valuable in a frequently-

changing environment such as the cable industry. For example, should a new version of the DOCSIS standard be released in a few years, FPGA-based CMTS systems could potentially be reconfigured to conform to the new standard through a firmware upgrade. On the other hand, systems which rely on ASICs would need to be completely replaced.

- Despite the recent increases in FPGA capacity, FPGAs are typically limited in terms of the available logic resources when compared to ASICs [7], especially in terms of dedicated multiplier circuits. Many well-known receiver algorithms require a large number of multiplications. Consequently, these algorithms are often not optimal for use in an FPGA and new algorithms which conserve multipliers may be required. For this reason, the design and implementation of communications circuits in FPGAs is an intellectually stimulating task.

1.2.1 Problem Statement

As will be discussed in detail in Section 2.1.2, upstream packets in a cable network are typically corrupted by a number of transmitter-specific impairments. These may include timing error, carrier frequency and phase error, and channel micro-reflections (echoes) [8]. In order for a demodulator to provide adequate performance, it is necessary to estimate and correct for these impairments on a packet-by-packet basis.

Digital demodulators are generally structured in a manner similar to that of Figure 1.3. Note that this high-level structure is not particularly unique; many examples of similar structures can be found in the open literature [9]. As shown in the figure, the demodulator contains a number of synchronization blocks which attempt to compensate for the impairments present in the input signal. In general, the performance and cost of a digital demodulator significantly depends upon the quality of these synchronization blocks [10]. As a consequence, the design of high-performance, low complexity digital synchronization techniques has been an active research topic in recent years [11], [12], [13], [14].

The research discussed in this thesis was centered around the design of synchro-
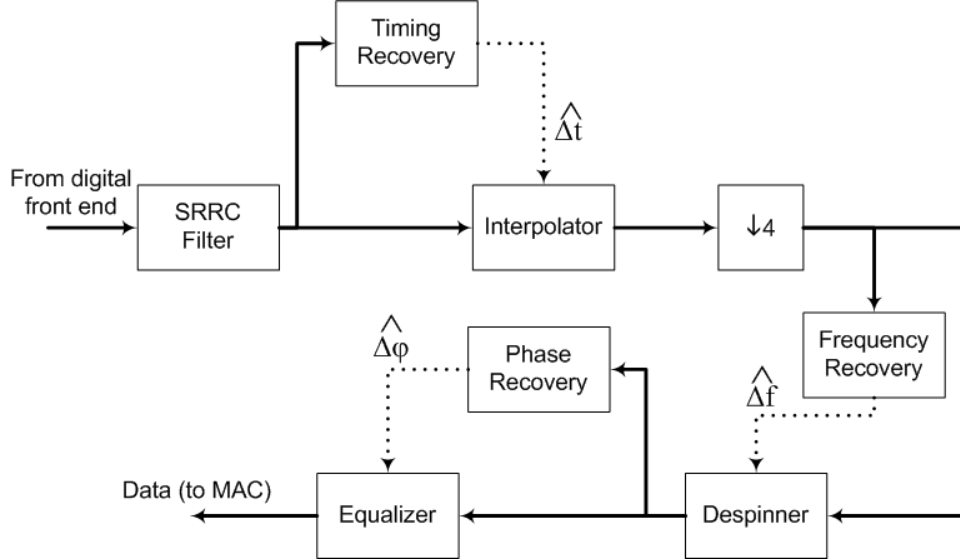
Figure 1.3 A high-level block diagram of a digital demodulator.

nization algorithms for DOCSIS upstream channels which are suitable for FPGA-based implementation. Specifically, the aim of the research was to solve two key synchronization problems which are prerequisites for an implementation of a DOCSIS upstream demodulator:

- Frequency recovery: Many frequency estimation algorithms have been presented in the literature over the past half century, including [15], [16], [17], [18]. These references are discussed in detail in Chapter 4. However, the suitability of these algorithms for the DOCSIS upstream is questionable, as they were not specifically designed to operate in channels with significant intersymbol interference (ISI). This research aimed to develop a new frequency offset estimator which is economical to implement in an FPGA and is capable of operating reliably in the presence of DOCSIS channel echoes.

- Equalization: In order to compensate for the ISI caused by echoes in the cable plant, an equalizer is required in a DOCSIS upstream demodulator. This equalizer initially needs to be trained, which is typically a time-consuming and computationally expensive task, as discussed in [19], [20], [21], which are general primers on equalization theory. In order to maximize the data throughput of

7

the channel, it is desirable for this training process to be as short as possible. The goal of this research is to develop a fast-converging equalization scheme for DOCSIS channels which can be inexpensively implemented in an FPGA.

1.2.2   Organization of Thesis and Main Contributions

The remainder of the thesis is organized as follows. Background material which is intended to improve the comprehensibility of the thesis as a whole is contained in Chapters 2 and 3. More specifically, Chapter 2 provides an in-depth look at the operation and modeling of DOCSIS upstream channels. Next, the proposed demodulator architecture is outlined in Chapter 3.

Frequency recovery for DOCSIS upstream channels is discussed in Chapter 4. This chapter contains two main contributions. The first is a novel high-performance frequency recovery algorithm which has been derived from first principles. The structure of this algorithm is well-suited to a cost-effective FPGA-based implementation. The second main contribution of this chapter is a rule which may be used to predict whether a given frequency offset estimator will be unbiased in the presence of ISI. For applications where unbiased estimation is required, this rule places a restriction on the structure of a frequency offset estimator and the preamble sequence upon which it operates. It is shown that the proposed frequency offset estimator can be made unbiased for a wide range of preamble sequences.

Chapter 5 then addresses the problem of DOCSIS upstream equalization. The main contribution of this chapter is a method for reducing the convergence time of an adaptive equalizer for DOCSIS upstream channels. The method is comprised of two parts. First, the ISI caused by micro-reflections in the upstream channel is modeled as an equivalent filter. By observing the distortion caused by the channel to a known excitation sequence, the equivalent filter's impulse response is estimated. Next, the impulse response is crudely inverted in order to initialize the coefficients of the adaptive equalizer. It is shown that this technique can decrease the length of the required training sequence for the adaptive equalizer by up to 70 symbols.

Finally, Chapter 6, which concludes the thesis, presents a detailed summary of the research contributions.

2. Upstream Channel Operation

2.1 Upstream Physical Layer

The design of a DOCSIS upstream receiver is complicated by the many impairments present in typical upstream signals. In order to understand the synchronization algorithms which are discussed in this thesis, it is first necessary to understand these impairments and the effect which they have upon the signal presented to the upstream demodulator. Accordingly, this section presents background material related to the physical layer of DOCSIS upstream channels.

2.1.1 Basic QAM Theory

As specified in the DOCSIS standard, data is transferred across upstream cable channels using Quadrature Amplitude Modulation (QAM). QAM is a well-known communication technique whereby the magnitudes of two sinusoidal carriers may be varied independently to convey information. The carriers are chosen to be $\pi/2$ radians out of phase, which guarantees orthogonality and prevents the carriers from interfering with each other. Figure 2.1 illustrates the complete structure of a QAM modulator/transmitter.

In a QAM modulator, incoming binary data bits are encoded into symbols in a fashion known to both transmitter and receiver. Such an encoding rule maps a finite integer k binary digits into one of 2^k symbols in a manner prescribed by the standard. The rate at which the symbol encoder accepts blocks of k binary digits and converts them into symbols is referred to as the symbol rate. For a digital QAM system, each symbol is a 2-tuple (a_I, a_Q), where each of the components is used to amplitude
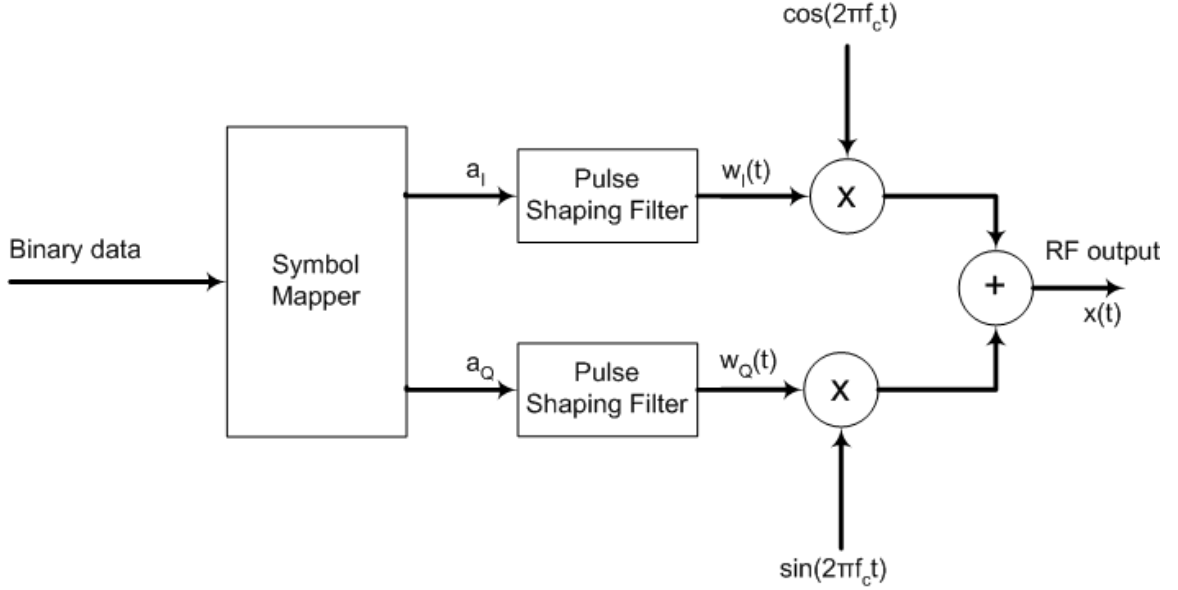
Figure 2.1 Block diagram of a basic QAM modulator.

modulate one of the quadrature carriers. By plotting all of the 2^k possible symbols specified by the encoding rule on a 2-dimensional plane, a visual representation - typically called a constellation diagram - of the encoding rule may be obtained. An example constellation diagram for a 16-QAM encoding rule is shown in Figure 2.2.

For each symbol generated by the symbol mapper, two pulses are generated with weights specified by the values of a_I and a_Q. Since bandwidth is a precious resource in modern communication systems, the resulting sequences of pulses are passed through a low pass pulse shaping filter in order to limit the bandwidth consumed by the transmission. The filtered signals may be written as the summation of a number of scaled and delayed versions of the filter's impulse response as follows:

$$w_I(t) = \sum_{k=-\infty}^{\infty} a_{Ik} h_t(t - kT) \tag{2.1}$$

$$w_Q(t) = \sum_{k=-\infty}^{\infty} a_{Qk} h_t(t - kT) \tag{2.2}$$

where the impulse response of the pulse shaping filter is $h_t(t)$ and the symbol period is T, which has units of seconds per symbol.
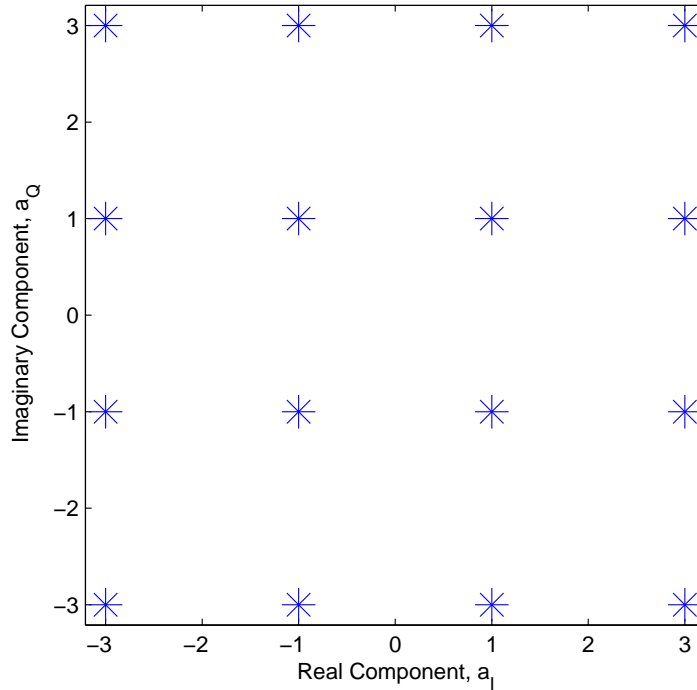
Figure 2.2   Constellation diagram for 16-QAM modulation.

At this point, a brief digression is advisable in order to clarify one key matter. The term 'symbol' is a frequent source of confusion when digital communication systems are discussed. Some sources define a symbol as the baseband continuous-time waveform which is generated by filtering each output pulse from the symbol mapper. Others use the term 'symbol' to mean a 2-tuple or a complex number. In this document, the term symbol refers to a complex number which represents the magnitudes of the pulses from the symbol mapper, i.e. $a_I + ja_Q$. For an M-QAM system, the symbol mapper's encoding rule defines M possible symbols, each of which is represented by a complex number. For example, a 4-QAM quadrature phase shift keying (QPSK) system defines the following four symbols: $E_s e^{j\pi/4}$, $E_s e^{j3\pi/4}$, $E_s e^{-j3\pi/4}$, and $E_s e^{-j\pi/4}$, where E_s is a constant which represents the average symbol energy.

Returning to the modulator description, the outputs of the pulse shaping filter are used to modulate the aforementioned pair of sinusoidal carriers. The two modulated

carriers are then added together. The result is a radio frequency (RF) signal which is suitable for transmission across the cable channel. The transmitted RF signal, $x(t)$, may be represented mathematically as follows:

$$x(t) = w_I(t)\cos(2\pi f_c t) + w_Q(t)\sin(2\pi f_c t) \tag{2.3}$$

It is mathematically convenient to express the baseband signal using complex numbers: $x_b(t) = w_I(t) - jw_Q(t)$. Then, equation (2.3) may be written in terms of the complex baseband signal multiplied by a complex exponential carrier as follows:

$$
\begin{aligned}
x(t) &= \Re[x_b(t) \cdot e^{2\pi f_c t}] \\
&= \Re[(w_I(t) - jw_Q(t)) \cdot e^{2\pi f_c t}] \tag{2.4}
\end{aligned}
$$

The structure of a circuit which demodulates the QAM transmission and recovers the original binary data is shown in Figure 2.3. For now, it shall be assumed that the input signal to the demodulator $y(t)$ is exactly equal to $x(t)$, which is the transmitter's output. As shown in the figure, the first step in demodulating the received signal is to downconvert the RF signal to baseband by multiplying it with two quadrature carriers which are generated in the receiver:

$$
\begin{aligned}
v_I(t) &= y(t)2\cos(2\pi f_c t) \\
&= 2[w_I(t)\cos(2\pi f_c t)\cos(2\pi f_c t) + w_Q(t)\sin(2\pi f_c t)\cos(2\pi f_c t)] \\
&= w_I(t)[\cos(4\pi f_c t) + \cos(0)] + w_Q(t)[\sin(4\pi f_c t) + \sin(0)] \\
&= w_I(t) + w_I(t)\cos(4\pi f_c t) + w_Q(t)\sin(4\pi f_c t) \tag{2.5}
\end{aligned}
$$

$$
\begin{aligned}
v_Q(t) &= y(t)2\sin(2\pi f_c t) \\
&= 2[w_I(t)\cos(2\pi f_c t)\sin(2\pi f_c t) + w_Q(t)\sin(2\pi f_c t)\sin(2\pi f_c t)] \\
&= w_I(t)[\sin(4\pi f_c t) + \sin(0)] + w_Q(t)[-\cos(4\pi f_c t) + \cos(0)] \\
&= w_Q(t) - w_Q(t)\cos(4\pi f_c t) + w_I(t)\sin(4\pi f_c t) \tag{2.6}
\end{aligned}
$$

As can be seen in equations (2.5) and (2.6), the process of downconverting the received signal to baseband also produces signal components at double the carrier frequency.

13
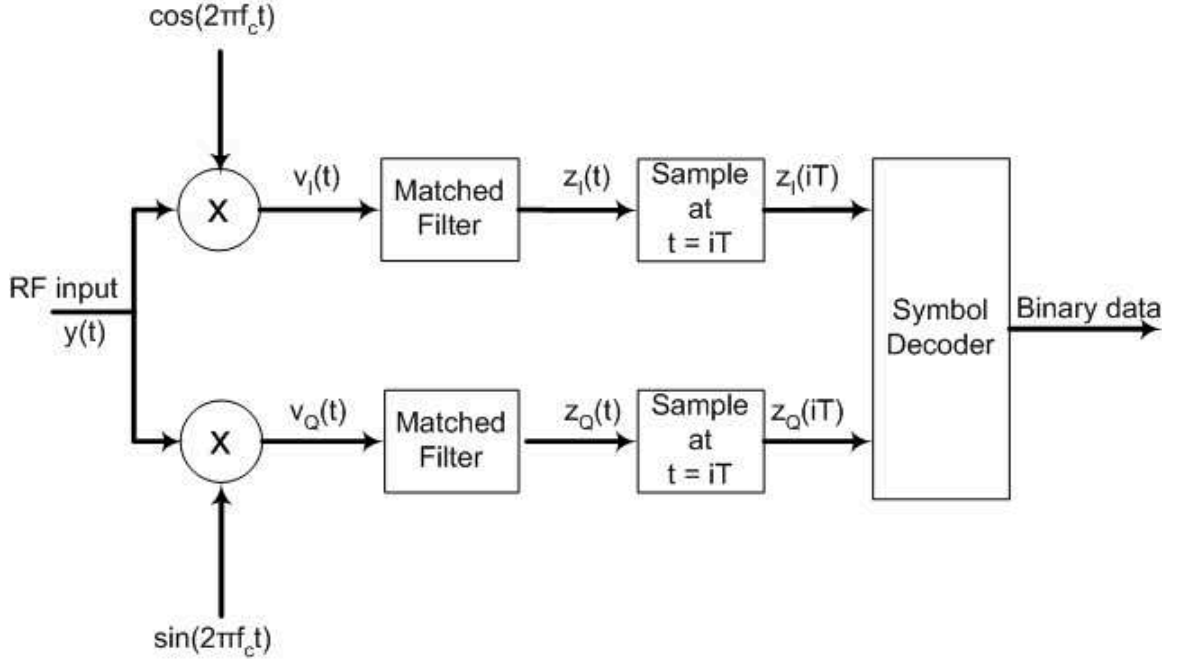
Figure 2.3   Block diagram of a basic QAM demodulator.

In order to remove these unwanted double frequency components, a low pass filter is applied. It is well-known [22] that if the received signal is corrupted with additive white Gaussian noise, the maximum signal to noise ratio is obtained if the receiver's low pass filter has an impulse response that is the time-reversed version of the transmitter's pulse shaping filter. In practice, these two filters are generally identical, as the impulse response of the transmitter's filter usually has even symmetry. After the application of the matched filter, the signals at the receiver may be written as follows:

$$
\begin{aligned}
z_I(t) &= v_I(t) * h_r(t) \\
&= w_I(t) * h_r(t) \\
&= \sum_{k=-\infty}^{\infty} a_{Ik} g(t - kT) \tag{2.7}
\end{aligned}
$$

$$
\begin{aligned}
z_Q(t) &= v_Q(t) * h_r(t) \\
&= w_Q(t) * h_r(t) \\
&= \sum_{k=-\infty}^{\infty} a_{Qk} g(t - kT) \tag{2.8}
\end{aligned}
$$

14

where $h_r(t)$ is the impulse response of the receiver filter and $g(t)$ is the combined impulse response of the transmitter and receiver filters.

Assuming for the moment that the transmitted symbols do not interfere with each other, it is possible to recover the ith symbol by sampling $z_I(t)$ and $z_Q(t)$ at the symbol time $t = iT$. With the symbol values recovered, it is a simple matter to pass these values through a symbol decoder which performs the complementary operation to that of the transmitter's symbol encoder to obtain the original k binary information bits.

While bandlimiting the transmitted QAM signal through the application of a low pass filter is beneficial in terms of reducing the bandwidth consumed by the transmission, this process also has a downside: each pulse is spread out in time. When the duration of each pulse is increased beyond the symbol period, it becomes possible for the symbols to interfere with one another. This type of interference between symbols is commonly known as intersymbol interference (ISI).

Fortunately, it is possible to design the bandlimiting filter in order to prevent ISI under ideal conditions. In order to do so, the combined impulse response of the transmitter and receiver filters must meet the well-known Nyquist criterion. Practically speaking, this means that the combined impulse response of the pulse shaping and matched filters, which is denoted $g(t)$, must be equal to zero at all multiples of the symbol period:

$$g(kT) = \begin{cases} 1 & \text{if } k = 0 \\ 0 & \text{if } k \neq 0 \end{cases} \tag{2.9}$$

Figures 2.4 and 2.5 provide a visual representation of the Nyquist criterion. In these plots, a filter impulse response is shown with a solid line. Since the input to this filter is a series of impulses at the symbol rate, the output will be the summation of multiple shifted copies of the filter's impulse response. To illustrate this fact, two copies of the filter's impulse response, shifted by $+1$ and -1 symbol intervals are shown using dashed lines. For all three responses, the samples which would be obtained by an ideal receiver at $t = iT$ are highlighted using asterisks.
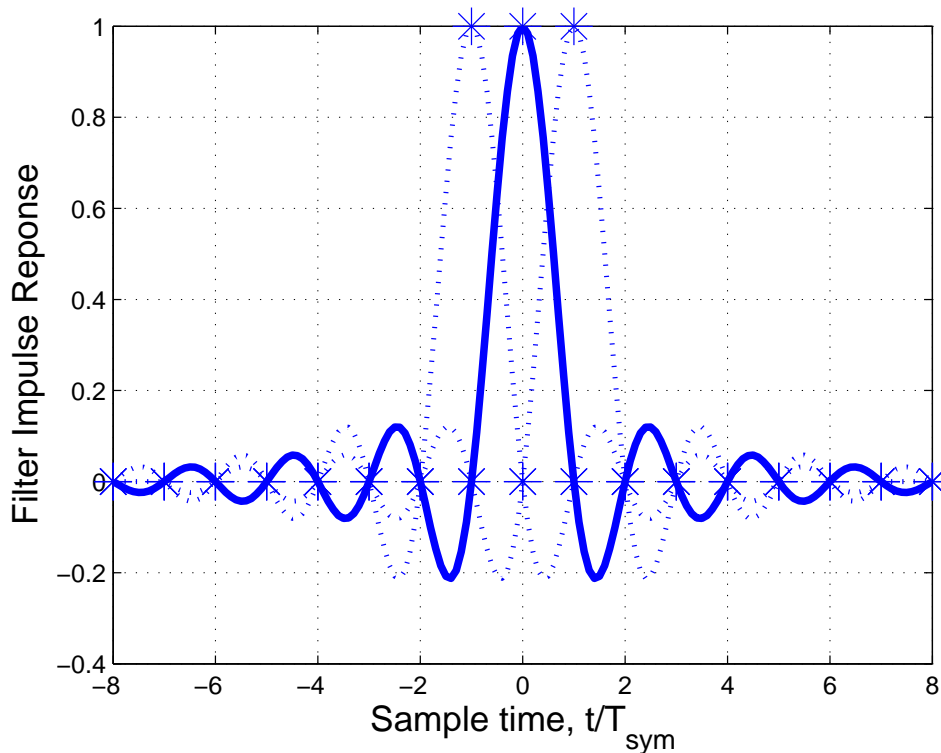
Figure 2.4   Graphical representation of a filter meeting the Nyquist criterion.

In Figure 2.4, it is clear that the samples seen by a properly-synchronized receiver contain contributions from only one symbol at a time, indicating that the Nyquist criterion has been met. In contrast, the filter of Figure 2.5 does not achieve the Nyquist criterion. Samples taken from the filter's output at the correct symbol times contain contributions not only from the current symbol, but also previous and future symbols. This phenomenon, which is known as ISI, can significantly degrade the performance of a communication system.

The filter of Figure 2.4 is actually a very famous and widely-used filter. This filter, which is known as a raised-cosine filter because its magnitude response has a cosine shaped transition band, is used as the pulse shaping filter for DOCSIS upstream communication. The impulse response of a raised cosine filter has the form:

$$g(t) = \frac{\sin(\pi t/T)}{\pi t/T} \frac{\cos(\pi \alpha t/T)}{1 - 4\alpha^2 t^2/T^2} \tag{2.10}$$

where $0 \leq \alpha \leq 1$ is a parameter which defines the transition bandwidth of the filter.
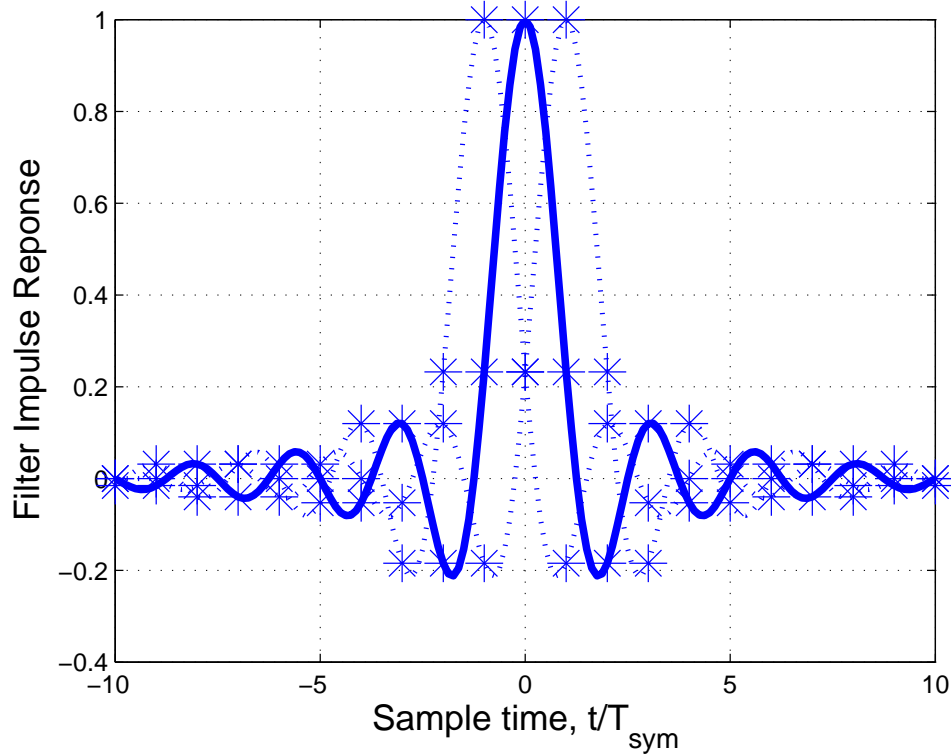
Figure 2.5 Graphical representation of a filter failing the Nyquist criterion.

When raised cosine filters are used in communication systems, it is common to split the filter equally between the transmitter and receiver. In this case, the so-called square root raised cosine (SRRC) filters have the following impulse response:

$$
g(t) = \begin{cases} 1 - \alpha + 4\dfrac{\alpha}{\pi} & , \quad t = 0 \\[2ex] \dfrac{\alpha}{\sqrt{2}}\left[\left(1 + \dfrac{2}{\pi}\right)\sin\left(\dfrac{\pi}{4\alpha}\right) + \left(1 - \dfrac{2}{\pi}\right)\cos\left(\dfrac{\pi}{4\alpha}\right)\right] & , \quad t = \pm\dfrac{T}{4\alpha} \\[3ex] \dfrac{\sin\left[\pi\dfrac{t}{T}\left(1 - \alpha\right)\right] + 4\alpha\dfrac{t}{T}\cos\left[\pi\dfrac{t}{T}\left(1 + \alpha\right)\right]}{\pi\dfrac{t}{T}\left[1 - \left(4\alpha\dfrac{t}{T}\right)^2\right]} & , \quad \text{otherwise} \end{cases}
$$

(2.11)

DOCSIS upstream channels employ SRRC filters with $\alpha = 0.25$ in both the transmitter and receiver.

Having covered the basic theory of QAM communication, channel impairments present in the upstream cable channel which complicate the task of the receiver are

17
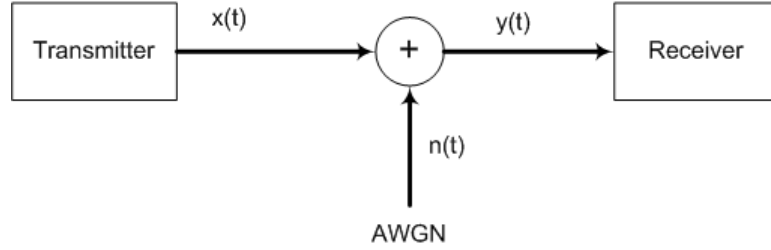
Figure 2.6   Model of AWGN channel.

addressed next.

2.1.2   Channel Impairments

As mentioned in the introduction, the portion of the cable spectrum which may be allocated to DOCSIS upstream channels is 5-85 MHz. Unfortunately, this is typically a fairly challenging frequency range in which to operate, due to the large number of frequency-dependent impairments present in the cable plant within the allocated band. Some of the impairments faced by a demodulator operating in an upstream cable channel will be discussed in the following sections.

Additive White Gaussian Noise

Additive White Gaussian Noise (AWGN) is an impairment which is common to all communications systems. It arises from a number of sources, the most prominent of which is Johnson noise [23] generated inside the electrical components inside the receiver. Another common source of AWGN in cable channels is spurious transmissions from adjacent channels. As the name implies, the effect of AWGN on the transmitted signal in the cable channel is additive, as illustrated in Figure 2.6.

Taking AWGN into account, the received signal at the receiver input may be written as:

$$
\begin{aligned}
y(t) &= x(t) + n(t) \\
&= w_I(t)\cos(2\pi f_c t) - w_Q(t)\sin(2\pi f_c t) + n(t) \quad\quad (2.12)
\end{aligned}
$$

18

The AWGN process $n(t)$ is modeled as having an amplitude with a Gaussian probability density function and a white frequency spectrum: ie,

$$f_n(a) = \frac{1}{\sqrt{2\pi\sigma^2}} e^{\left(-\frac{(a-\mu)^2}{2\sigma^2}\right)} \tag{2.13}$$

$$N(f) = \begin{cases} 1 & f \neq 0 \\ 0 & f = 0 \end{cases} \tag{2.14}$$

where a is the amplitude of $n(t)$ at an arbitrary time $t = t_o$.

While the bandwidth of the AWGN may not be strictly infinite as (2.14) implies, this discrepancy is inconsequential, given that the digital receiver applies a low pass filter to the received signal. The bandwidth of the AWGN is much greater than the bandwidth of the filter, so the noise process $n(t)$ appears to have infinite bandwidth as far as the receiver is concerned.

The effects of AWGN on digital systems have been investigated thoroughly and are presented in a number of well-known communications textbooks, including [24] and [25]. In fact, it is well-known [25] that the most fundamental limiting factor on the performance of a digital communication system is the signal to noise ratio, defined as the average energy per symbol divided by the power spectral density of the noise, i.e. E_s/N_o. For DOCSIS upstream channels, the levels of the received signals in combination with the operating temperature of the receiver ensures $E_s/N_o > 25\text{dB}$ [2].

It is important to keep the effect of noise in mind when designing synchronization algorithms for communication receivers. AWGN degrades the performance of a communications receiver by adding a degree of uncertainty to the received signal. This uncertainty in the received signal will be translated into randomness in the parameter estimate. Reducing this randomness, measured by the variance of the estimates, is one of the major goals for the design of a synchronization algorithm. The Cramer-Rao lower bound (CRB) [26] specifies the lowest possible variance for a circuit which generates estimates of a parameter θ based on an observation vector x:

$$\text{var}(\theta) = \frac{-1}{E\left[\frac{\delta^2}{\delta\theta^2}\ln(f(x;\theta))\right]} \tag{2.15}$$

where $f(x; \theta)$ is the likelihood function corresponding to observervations x and parameter θ. When a synchronization algorithm has been designed, it is customary to compare its variance to the limit specified by the CRB.

Timing Offset

Timing offset refers to error in the sampling time of the digital receiver. As discussed in Section 2.1.1 and shown in Figure 2.3, once the receiver has downconverted and filtered the incoming signal, it must sample the filtered signal at a time of precisely $t = iT$ in order to perfectly recover the transmitted symbol. In a practical system, the receiver and transmitter operate using independent oscillators which are not synchronized. Therefore, the phase and frequency of these oscillators will generally not be identical. In effect, the mismatch causes the receiver to sample the filtered signal at $t = iT' + \Delta t$, where $T' \neq T$ reflects an incorrect sampling clock frequency and Δt reflects an incorrect sampling clock phase.

The Nyquist criterion guarantees that the receiver can recover the transmitted symbols free of ISI provided that the signal is sampled at exactly $t = iT$. However, if the receiver instead samples the signal at an incorrect time $t = iT' + \Delta t$, ISI will result. This ISI will increase the probability of symbol errors by making it more difficult for the receiver to distinguish between the possible transmitted symbols. A useful tool for visualizing the harmful effects of ISI is the 'eye diagram', which overlays the receiver output waveform $z_I(t)$ or $z_Q(t)$ for a large number of symbol periods. An example eye diagram for a QPSK system is shown in Figure 2.7. Notice that the separation between the large clusters of waveforms is greatest at the correct symbol time, which is indicated by a dotted vertical line. At incorrect sampling times the eye is partially closed, which reduces the system's noise tolerance.

It is very unlikely that a digital receiver will sample the continuous-time signal at the correct symbol instants. The typical solution to this problem in modern receivers is to design a circuit which inspects the sampled values and estimates the error in the sampling time. Such a circuit is referred to as a timing synchronizer or timing
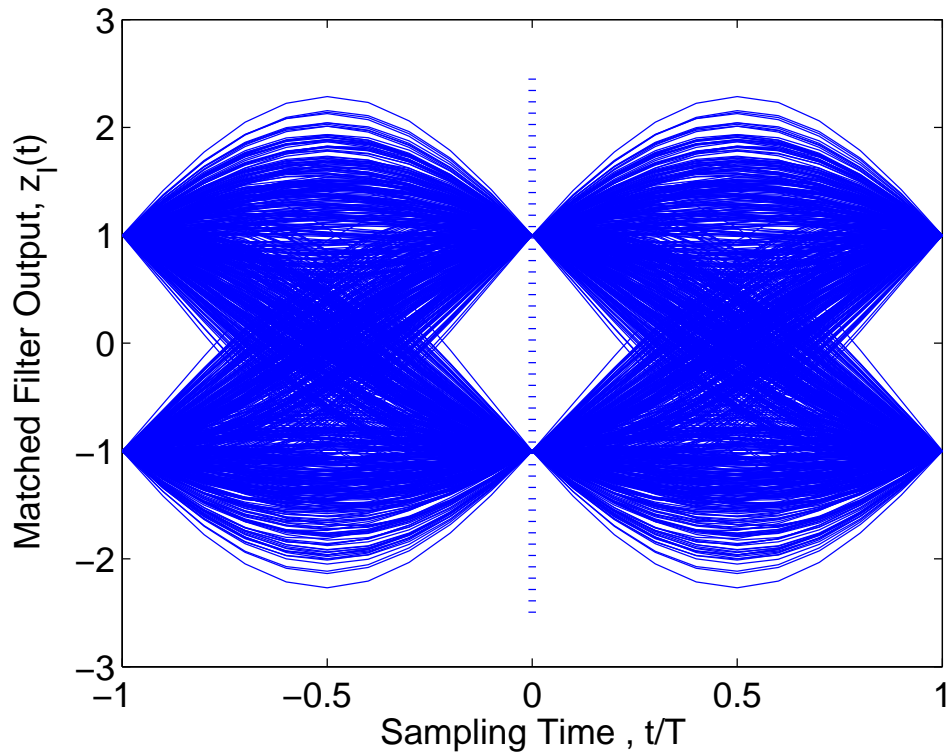
Figure 2.7　Eye diagram for QPSK system with $\alpha = .1$.

recovery circuit. The timing error estimate is then passed to a digital interpolation filter which processes the incoming samples to effectively resample the underlying continuous-time signal at the correct sampling instants.

Frequency and Phase Offset

Another potential source of mismatch between the transmitter and receiver in a digital communication system lies in the sinusoidal carriers used for upconversion and downconversion in the transmitter and receiver respectively. Since these carriers are generated from independent oscillators, there is some degree of disparity in their frequency and phase. Mathematically, we can model the effect of this frequency and phase offset by changing the arguments to the sinusoidal functions in the receiver from $2\pi f_c t$ to $2\pi (f_c + \Delta f)t + \phi_o$. Using this model, the effect of phase and frequency

offset on the receiver's downconversion process may be investigated:

$$
\begin{aligned}
v_I(t) &= y(t)2\cos(2\pi(f_c + \Delta f)t + \phi_o) \\
&= 2[w_I(t)\cos(2\pi f_c t)\cos(2\pi(f_c + \Delta f)t + \phi_o) \\
&\quad + w_Q(t)\sin(2\pi f_c t)\cos(2\pi(f_c + \Delta f)t + \phi_o)] \\
&= w_I(t)\cos(2\pi\Delta f t + \phi_o) - w_Q(t)\sin(2\pi\Delta f t + \phi_o) \quad (2.16)
\end{aligned}
$$

$$
\begin{aligned}
v_Q(t) &= y(t)2\sin(2\pi(f_c + \Delta f)t + \phi_o) \\
&= 2[w_I(t)\cos(2\pi f_c t)\sin(2\pi(f_c + \Delta f)t + \phi_o) \\
&\quad + w_Q(t)\sin(2\pi f_c t)\sin(2\pi(f_c + \Delta f)t + \phi_o)] \\
&= w_Q(t)\cos(2\pi\Delta f t + \phi_o) + w_I(t)\sin(2\pi\Delta f t + \phi_o) \quad (2.17)
\end{aligned}
$$

Note that the double frequency components have been omitted from the final step in equations (2.16) and (2.17) due to the fact that they will be immediately removed by the receiver's matched filter. Clearly, frequency and phase offset cause the received constellation points to rotate. In the case of phase offset, there is a single initial rotation of ϕ_o radians, whereas frequency offset causes the constellation to spin at a constant rate of $2\pi\Delta f T$ radians per symbol. These two effects may be seen in Figure 2.8, which shows the received constellation points for 1000 transmitted QPSK symbols with a phase offset of $\pi/8$ radians and a frequency offset of $10^{-4} * 2\pi$ radians per symbol.

It is apparent from Figure 2.8 that frequency and phase offset complicate the task of the receiver, as the modulation scheme relies upon the angle of the received constellation points to convey significant information. In order to make correct decisions, the receiver must be able to estimate the phase and frequency offset so that it may compensate for them by performing a derotation internally. Consequently, the design and analysis of a frequency offset estimator for DOCSIS upstream channels is one of the major goals of this thesis.
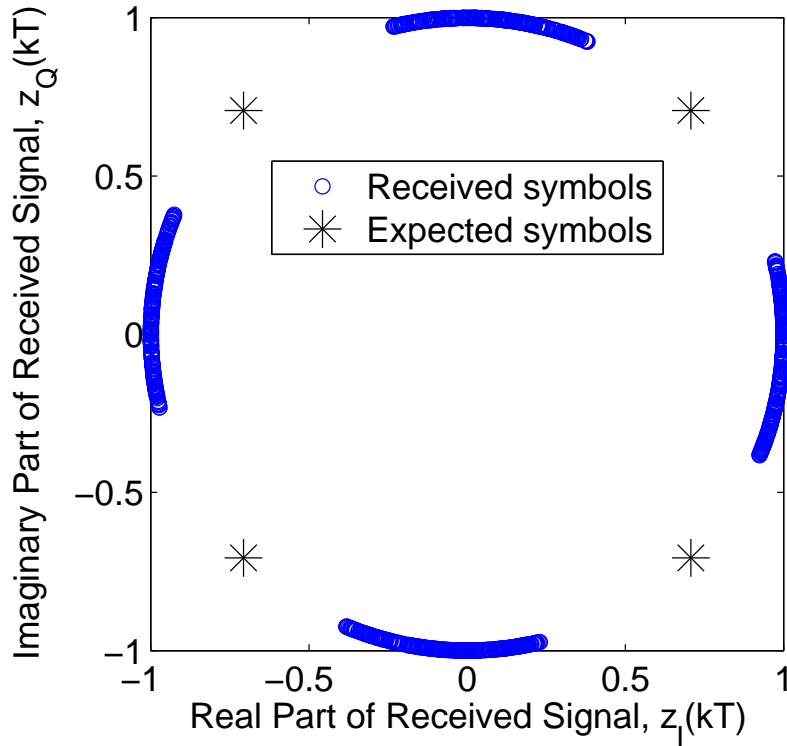
Figure 2.8 Received constellation points for 1000 QPSK symbols with $\Delta f = 10^{-4}$ and $\phi_o = \pi/8$.

Channel Echoes

The design of a DOCSIS-based cable network is such that many CMs are connected to the same physical cable network which eventually connects back to the headend. Consequently, when a CM transmits on an upstream channel, its signal travels across the network not only to the headend, but also to a potentially large number of CMs. Given that the signal is reaching such a large number of devices, there is a relatively high probability that some of the devices may not be perfectly impedance-matched to the channel. The result of such a mismatch is that a portion of the transmitted signal will be reflected back onto the cable and eventually to each of the connected devices. Due to this phenomenon, the CMTS will not receive just a single copy of the transmitted signal. Rather, it will receive multiple delayed copies of the transmitted signal, each having different attenuation values and phase shifts. These reflected
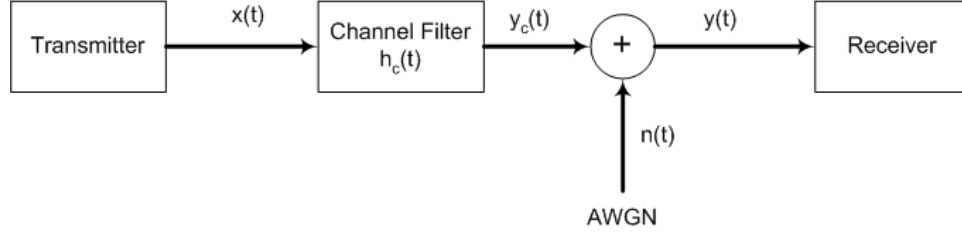
Figure 2.9 Linear filter channel model used to represent effect of echoes.

signals are known as echoes or micro-reflections.

The effect of echoes on the signal received by a digital demodulator may be modeled as the application of a linear filter $h_c(t)$ to the transmitted signal, as shown in Figure 2.9. Note that in the model, the channel filter is applied prior to the addition of AWGN.

When the distorted signal is processed at baseband inside the receiver, the continuous time channel filter may be modeled as an equivalent complex baseband filter operating at the symbol rate. The coefficients of this filter may be determined for a specific set of echoes by summing delayed and shifted copies of the combined impulse responses of the transmitter and receiver shaping filters in order to generate an overall impulse response. The linear filter coefficients may then be determined by sampling the overall impulse response at the symbol rate, as shown in Figure 2.10.

To generate Figure 2.10, a single echo with an attenuation of 10dBc, a delay of $0.5T$ seconds, and a phase rotation of π radians has been applied to the signal. When the echo-laden signal is sampled at the symbol rate, the samples indicated by large dots are obtained. These samples determine the equivalent channel impulse response for this scenario, which turns out to be: $-.001z^4 + .0129z^3 - .0274z^2 + .0587z^1 + .8016 - .1984z^{-1} + .0587z^{-2} - .0274z^{-3} + .0129z^{-4}$. Notice that the Nyquist ISI criterion is not fulfilled when the echoes are present, highlighting the fact that the typical effect of channel echoes is to add ISI to the signal. A constellation plot illustrating the impact of this ISI may be seen in Figure 2.11.

The echo characteristics of the DOCSIS upstream channel are unique to each
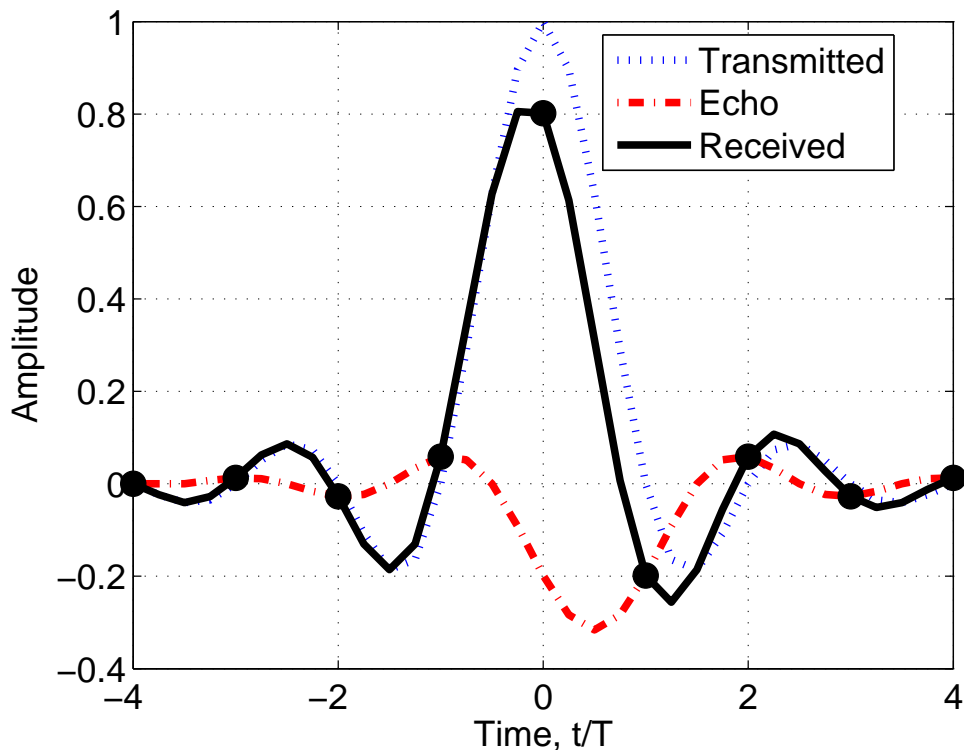
Figure 2.10 Effect of an echo on received baseband signal.

individual user. Additionally, new CMs are occasionally connected to the network, while old CMs are periodically removed from the network. Each of these changes will naturally cause the echoes present in the DOCSIS upstream channel to change over time.

In this thesis, a channel model based on the DOCSIS standard [2] will be used. The model allows for up to three echoes, with specifications as shown in Table 2.1 below:

Table 2.1 Echo channel model.

Relative Amplitude (dBc)	Echo Delay (sym)	Echo Phase (rad)
-10	Uniform $(0 \to 2.5)$	Uniform $(0 \to 2\pi)$
-20	Uniform $(0 \to 5)$	Uniform $(0 \to 2\pi)$
-30	Uniform $(0 \to 7.5)$	Uniform $(0 \to 2\pi)$

In order for the upstream demodulator to properly recover the transmitted sym-
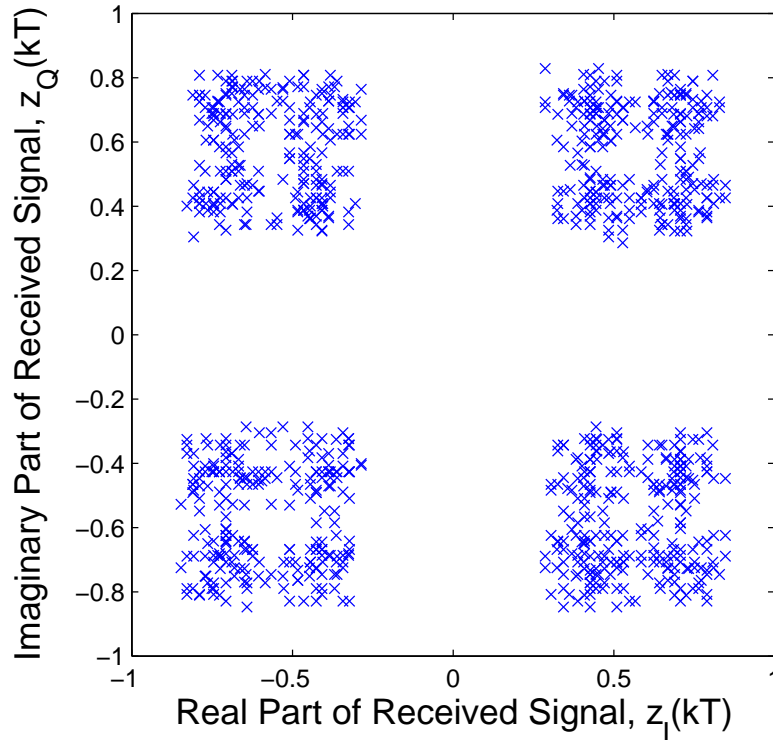
Figure 2.11 ISI seen in QPSK constellation due to echo.

bols, it is necessary to remove some of the ISI from the received signal. Since the characteristics of the upstream channel are not known a priori, it is necessary for the demodulator to detect and compensate for the ISI on the fly. An adaptive equalizer is particularly well-suited for this task, as will be discussed in Chapter 5.

2.2 MAC Layer Control

2.2.1 Overview

The overall network management for upstream DOCSIS channels is performed by the media access control (MAC) layer of the CMTS. Although the detailed operation of the MAC is outside the scope of this research, an overview of the basic principles involved in the control of upstream channels is useful to provide context for the remainder of the document.

In order to allow multiple users to transmit data to the headend via a single up-stream channel, recent versions of the DOCSIS standard permit two multiple access schemes: time division multiple access (TDMA) and synchronous code division multiple access (S-CDMA). Each upstream channel in a cable network must be using one of these two multiple access schemes. Note that it is possible for these two schemes to coexist on separate upstream channels within the same cable network. In TDMA mode, the entire channel is allocated to a single user for a period of time. The users take turns transmitting short bursts of data across the channel. In contrast, S-CDMA mode allows multiple users to transmit data over the channel simultaneously using orthogonal codes. The orthogonality of these codes ideally permits the CMTS to correctly recover each of the transmitted data streams without any cross-user interference.

The goal of the present research is to develop synchronization algorithms for the DOCSIS TDMA mode. Consequently, the remainder of this thesis will exclusively focus on TDMA.

Each TDMA upstream channel is broken up into a sequence of timeslots by the CMTS MAC. These timeslots, each of which corresponds to an upstream transmission opportunity, are called minislots in the standard. The minislots are synchronized to an extremely accurate 10.24MHz reference clock stored in the headend. The CMTS keeps a count of the number of reference clock edges in a reference counter and periodically transmits this count value to the CMs in a synchronization message via a downstream channel. Like the CMTS, each CM contains a 10.24MHz clock that drives its own reference counter. The value of this local reference counter is updated to match the value transmitted by the CMTS reference counter to correct for drift caused by differences between the two 10.24MHz clocks. This allows each CM within the network to maintain a relatively accurate timebase.

The CMTS MAC layer is responsible for scheduling minislots on the upstream channels and allocating these minislots to the individual CMs. In doing so, the MAC layer attempts to maximize network throughput and minimize the latency experienced
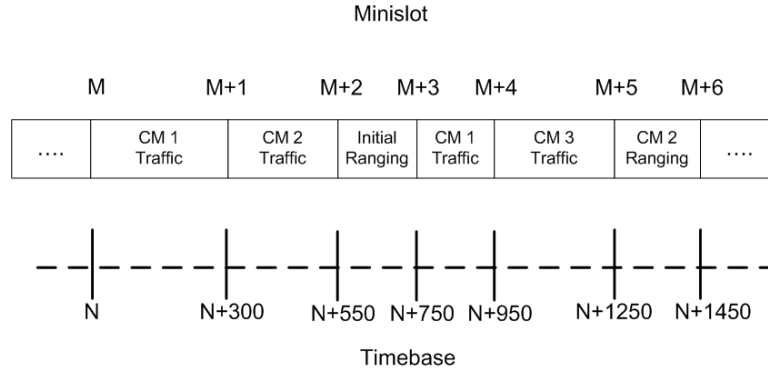
Figure 2.12 An example of upstream bandwidth allocation using minislots.

by each user while ensuring an equitable distribution of network resources. Although the the design of such a scheduling algorithm is clearly a difficult and important problem, it is not of interest in the present document. Once the MAC layer has decided upon the allocation of some number of minislots for an upstream channel, it broadcasts a bandwidth map message to all of the CMs via a downstream channel in order to inform the CMs of this allocation. Figure 2.12 provides an example of a simple bandwidth allocation. Note that all of the minislots in the figure are defined based on the value contained in the CMTS reference clock counter, which holds a value of N at the start-time of minislot M.

As suggested in Figure 2.12, there are two main types of packets which are transmitted across DOCSIS upstream channels: ranging packets and traffic mode packets. These two packet types will be discussed in detail in Sections 2.2.2 and 2.2.3.

2.2.2 Ranging Mode

As discussed in Section 2.1.2, there are a large number potential impairments which complicate the use of DOCSIS upstream channels. Fortunately, the CMs have the capacity to correct many of these if given proper instruction by the CMTS. The purpose of ranging mode is to allow the CMTS to measure certain parameters in a controlled environment and to verify that the transmissions from a given CM may be acceptably received. A CM must enter ranging mode upon initially connecting to
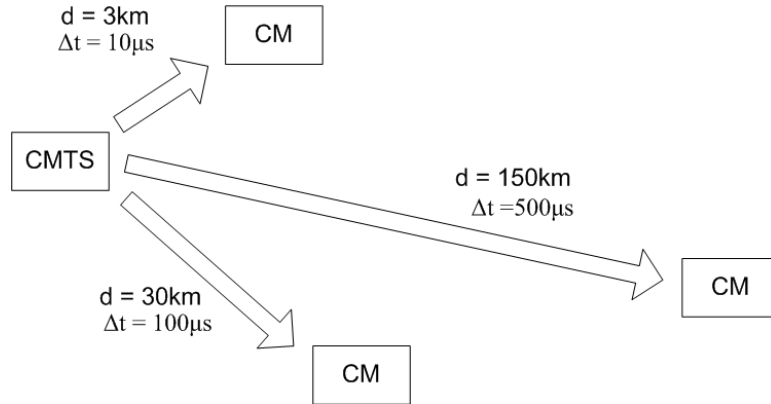
Figure 2.13 A spatial distribution of CMs can result in a large variation in message transit times.

the network. Thereafter, each CM will be periodically instructed by the CMTS to re-range in order to ensure the reliability of the upstream channel. Typically, each modem is re-ranged every one to two minutes.

The most important of the transmission parameters which must be measured in ranging mode is the timing offset of a CM. As discussed in Section 2.2.1, each CM attempts to use the information received from synchronization messages on a downstream channel to correct the local reference counter. Unfortunately, this system does not work perfectly since the CMs are spread out over a geographical area of up to 150 kilometres. Given this wide spatial distribution of CMs, a synchronization message containing the same timestamp can arrive at two different CMs at significantly different times, as shown in Figure 2.13.

Due to this phenomenon, the transmission of synchronization messages alone is not enough to ensure the CMs are able to time their transmissions to arrive at the CMTS at precisely the start of the appropriate minislots. Ranging packets are used to measure the transit time prior to allowing a CM to enter traffic mode and begin transmitting 'real' data. In order to do so, the CMTS allocates a number of minislots for ranging opportunities, during which CMs attempt to transmit a known packet at a known time. The measured transit time is then sent to the CM via a downstream transmission. When allocating minislots, the CMTS ensures that ranging minislots
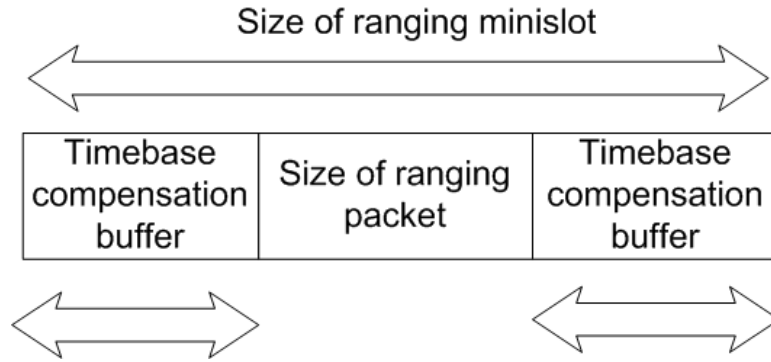
Figure 2.14 Ranging minislots provide a buffer to allow for CM timebase variability.

are much larger than is strictly necessary to transmit the necessary ranging packet, as seen in Figure 2.14. This ensures that a transmission from a CM with an incorrect timebase will not overlap into the next minislot and interfere with another user's transmission. By searching through the ranging packet for a specific pattern, the CMTS is able to deduce the propagation delay of the ranging CM.

In addition to timing recovery, a number of other important transmission parameters are generally optimized by the CMTS during ranging:

Frequency offset: As discussed in Section 2.1.2, a frequency offset causes the received constellation to spin, making the demodulator's task much more difficult. It is desirable to reduce the frequency offset associated with each CM, especially when higher order QAM constellations are to be used. The CMTS measures the frequency offset for each ranging packet and instructs the transmitting CM to adjust its carrier frequency in order to minimize the frequency offset in future packets.

Transmit power: In order to keep the network running smoothly, it is desirable for the power level received by the CMTS to be relatively consistent between CMs. Transmit power is measured during a ranging packet so that the power of the transmitting CM may be adjusted as necessary to achieve this goal.

Channel echoes: As mentioned in Section 2.1.2, echoes are often present on DOC-
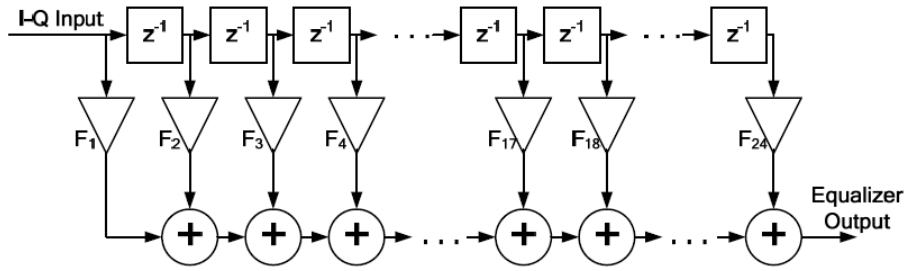
Figure 2.15 Structure of pre-equalizer in DOCSIS upstream transmitter.

SIS upstream channels. These echoes produce ISI, complicating the demodu-
lation process. Although it is possible to remove the ISI in the demodulator
through the use of an adaptive equalizer, the process of adapting the equalizer
coefficients requires the transmission of a large number of symbols, which would
add a great deal of overhead to each upstream packet. The solution presented
in the DOCSIS standard is to place a pre-equalizer in the CM and allow the
CMTS to determine the coefficients of this equalizer. The equalizer in the CM
has a linear structure, as shown in Figure 2.15. Each ranging packet contains
the necessary overhead for the CMTS to determine the equalizer coefficients
necessary to cancel the unique ISI produced by the channel from the transmit-
ting CM to the CMTS. Using these coefficients, each CM is able to pre-equalize
its transmissions in order to cancel the channel ISI so that the signal reaching
the CMTS is ideally ISI-free.

After each ranging packet, the CMTS will send a ranging response packet back to
the CM on a downstream channel. The ranging response packet contains information
regarding all of the estimated parameters discussed above. Additionally, the response
will indicate whether further ranging is necessary. If the ranging packet was received
successfully and the CM is matched to the channel acceptably well, the CM is reg-
istered with the CMTS and instructed to exit ranging mode and enter traffic mode.
Alternatively, if the ranging packet was not received sufficiently well or if any of the
transmitter parameters discussed above require significant adjustment, the CM is re-

quired to update its parameters and send another ranging packet in an appropriate minislot.

2.2.3 Traffic Mode

In traffic mode, a CM uses upstream bandwidth in order to transmit 'real' data. In this mode, transmissions are relatively free of impairments, since the CMs are re-ranged often enough to ensure that is the case. Thus, it is unnecessary for the CMTS to measure and correct transmitter inaccuracies in traffic mode. As a result, there is typically much less overhead in traffic mode packets than ranging packets.

The overall goal of the CMTS is to maximize the amount of data flowing through the upstream channels in order to provide the highest possible level of service to users of the cable network. In order to achieve this goal, the DOCSIS MAC is responsible for defining and allocating minislots to individual CMs in response to bandwidth requests. For each individual minislot allocation, the MAC must also select appropriate physical layer transmission parameters, including the constellation, error control coding parameters, and interleaving parameters. These parameters must be selected on a per-user basis in order to optimize the throughput of each minislot. Once again, the algorithms which the MAC uses to complete this scheduling and parameter selection task are intriguing and complex, but not directly relevant to the current discussion.

Over time, the timing offset, frequency offset, channel echoes, and received power corresponding to each CM may slowly change, causing degradations to traffic mode performance. To combat this phenomenon, the CMTS periodically sends the modems back into ranging mode to resynchronize. Additionally, the CMTS continues to monitor each of the synchronization parameters during traffic mode. In the event that any of these parameters deviates beyond an acceptable tolerance level, the CMTS instructs the CM in question to return to ranging mode in order to re-measure and then re-optimize the transmission parameters.

This research is focused on synchronization algorithms for the TDMA DOCSIS upstream channel, so the remainder of the document will concentrate on ranging

mode packets.

3. Demodulator Architecture

3.1 High-Level Architecture

The general structure of the proposed CMTS upstream receiver is shown in Figure 3.1. As shown in the figure, the input RF signal is first passed to an analog front end module, which bandlimits the incoming signal. The signal is then digitized through the use of an analog to digital converter (ADC) and passed to an FPGA for processing. Inside the FPGA, the sampled signal is first passed to a digital front end, which downconverts and downsamples the signal to reduce the computational burden on the digital demodulator. The output of the digital front end, which is a complex baseband signal, is sent to the digital demodulator. The demodulator recovers the data and passes the results to the MAC. Note that the demodulator and both front ends are controlled by tuning and channel information from the MAC layer.

The functionality and design of the analog and digital front end blocks will be briefly discussed prior to a more detailed overview of the structure of the digital demodulator, which is the focus of this research.
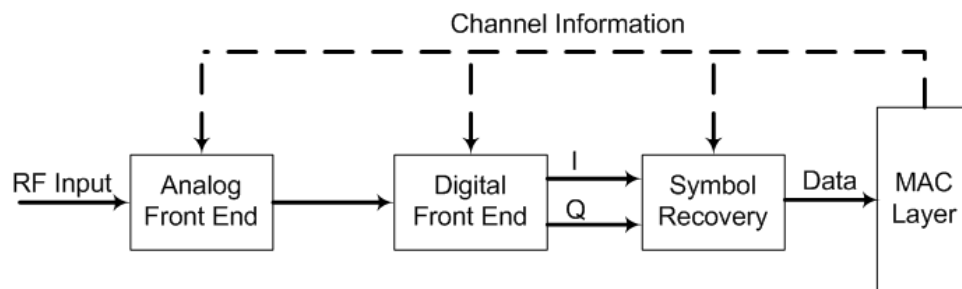
Figure 3.1 High level structure of upstream demodulator.

Figure 3.2   Block diagram of complete band sampling analog front end.

3.1.1   Analog Front End

The goal of the analog front end is to generate an accurate and high-resolution digital representation of the incoming analog signal. In order to do so, any frequency components in the input signal which are outside the valid DOCSIS upstream band of 5-85MHz must first be removed with a bandpass filter. However, the design of the remainder of the analog front end is not so straightforward. Two potential structures, each of which has some compelling advantages, will be considered.

The first option is to sample the entire upstream frequency band using a very high-speed and high-resolution ADC. The analog front end for this technique, which will be referred to as 'complete band sampling' (CBS), is depicted in Figure 3.2.

The main advantage of the CBS design is seen when multiple demodulators are placed in a single FPGA. In such a scenario, only one analog front end is necessary since the sampled signal simultaneously contains all of the upstream channels. Additionally, this design uses a minimum amount of analog RF circuitry, which may be beneficial from a reliability standpoint, given the unit-to-unit variability associated with analog circuits.

The downside to the CBS structure is that it requires a very high quality ADC. In order to sample the entire 5-85MHz frequency spectrum without any aliasing issues, the sampling frequency must be at least $85\text{MHz} * 2 = 170\text{MHz}$. Additionally, there may be significant variability in power between upstream channels, making some of the lower-powered channels more difficult to receive. To combat this problem, the ADC must provide a very high quality output signal, which necessitates an expensive ADC.
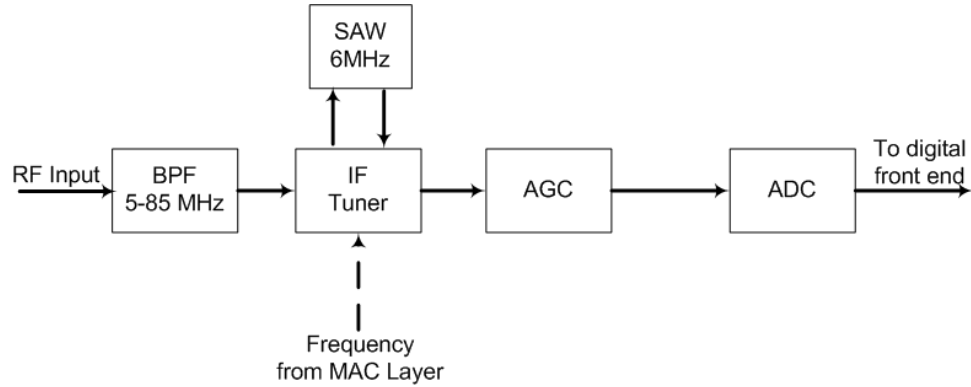
Figure 3.3   Block diagram of band-selective sampling analog front end.

A second option for the design of the analog front end is to sample only a small portion of the upstream frequency band. In order to use this approach, which will be referred to as 'band-selective sampling' (BSS), additional filters must be used to bandlimit the analog signal prior to the analog-to-digital conversion process in such a way that the channel of interest is retained. One typical method for bandlimiting the analog signal utilizes an intermediate frequency (IF) tuner, as shown in Figure 3.3. The IF tuner mixes the desired channel to a specific intermediate frequency (commonly 44MHz) and then applies a narrowband filter to the IF signal. The filter is selected to be just slightly wider than the widest possible input channel, likely around 6MHz in the case of DOCSIS upstream channels. The narrowband output from the filter is passed to an ADC and then to the FPGA.

Compared to the CBS model, the ADC in a BSS architecture can use a much lower sampling frequency for its ADC without experiencing any aliasing. Also, since the output of the IF tuner is a narrowband signal containing only one upstream channel, it is possible to apply AGC to only the channel of interest, meaning that the full resolution of the ADC is used to represent the desired channel. Thus, less resolution is needed in the ADC for BSS than in CBS, where the AGC is unable to perform scaling on a single channel. Due to the less stringent ADC requirements, it is expected that the hardware cost of a BSS front end would be significantly less than that of a CBS front end. However, since the CBS samples only a single upstream
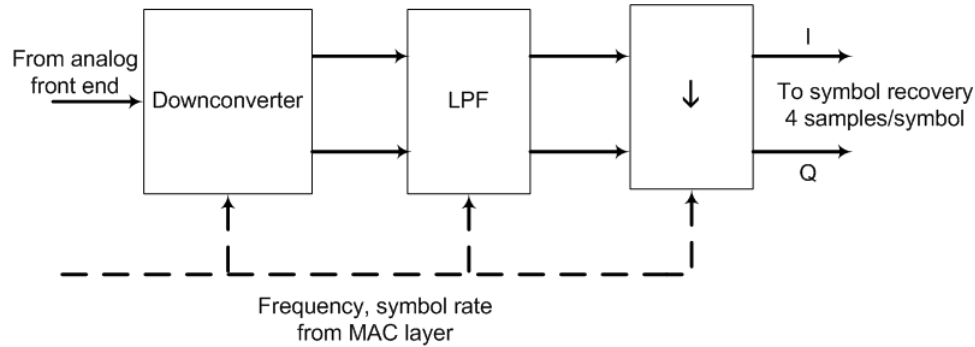
Figure 3.4 Block diagram of digital front end for upstream demodulator.

channel, it is necessary to use one BSS for each demodulator.

3.1.2 Digital Front End

Regardless of which analog front end architecture is used, the input to the FPGA will be sampled at a rate which is significantly higher than the symbol rate of the upstream channel of interest. For the symbol recovery block to do its job efficiently, the sampling rate of the digital signal should be reduced to be two, three, or four times the symbol rate of the upstream channel in question. The symbol recovery design discussed in this thesis operates using four samples per symbol. Also, the symbol recovery circuit operates on the complex baseband equivalent of the upstream channel. Thus, it is necessary for the digital front end to downconvert the input signal to baseband.

Conceptually, the structure of the digital front end is illustrated in Figure 3.4. Note that input from the MAC is necessary in order for the digital front end to know what frequency to mix the incoming signal with and also to know by what factor the baseband signal should be downsampled. In order to prevent aliasing, a low pass filter must be applied to the downconverted signal prior to downsampling. Polyphase finite impulse response (FIR) filters are a good choice for this purpose, as they are relatively inexpensive to implement in modern FPGAs.

Recent developments in digital signal processing suggest that the digital front

37

end could be constructed more economically using a fast-Fourier-transform-based structure, rather than that of Figure 3.4. However, the detailed design of the digital front end is outside the scope of this document.

3.1.3 Symbol Recovery

The symbol recovery module accepts a complex baseband input signal from the digital front end and recovers the symbols transmitted on the upstream channel by the CM. In order to demodulate the upstream transmission, the symbol recovery module must first filter the incoming signal with a filter that is matched to the transmitter's pulse shaping filter. For DOCSIS upstream channels, the transmitter's pulse shaping filter is specified as having a SRRC impulse response with $\alpha = 0.25$.

As discussed in Section 2.1.2, there are a number of impairments present in the DOCSIS upstream channel which, left uncorrected, will significantly hinder the performance of the symbol recovery circuit. Thus, prior to making a decision regarding which symbols have been transmitted, the demodulator must first attempt to synchronize with the transmitter in order to compensate for impairments in the filtered signal. In order to facilitate this synchronization, a known sequence of symbols is transmitted at the beginning of each upstream packet, as shown in Figure 3.8. These symbols, collectively referred to as the preamble, are selected by the CMTS so as to permit the best possible impairment correction performance.

The design of the synchronization circuits used for impairment detection and correction is one of the main challenges in the design of a DOCSIS upstream receiver. In general, there are two main categories of synchronization algorithms: feedback systems and feedforward systems.

Feedback Synchronizers

In feedback synchronizers, the incoming signal is passed into a parameterized compensation device, the purpose of which is to adjust the signal in order to compensate for errors in the parameter of interest (timing, frequency, or phase). The output of the
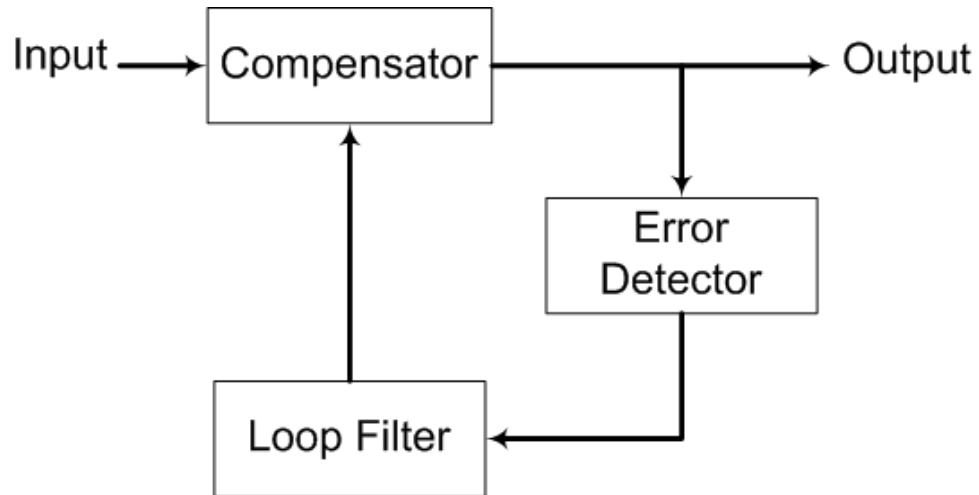
Figure 3.5   Typical structure of a feedback synchronizer.

compensator is passed to an error detection block, which indicates the approximate magnitude of the error remaining in the compensated signal, as shown in Figure 3.5. This error signal is passed through a loop filter in order to reduce jitter, then fed back to the parameterized compensator. Over time, if the loop is working correctly, the error in the compensator's output should approach zero.

Note that a synchronization circuit operating in feedback mode does not actually estimate the error in the parameter as seen at the demodulator input. Rather, the error in the compensated output is detected. When the error at the output of the compensator is large, feedback synchronization circuits tend to suffer from nonlinearity issues. To prevent the nonlinearity of the estimator from having an adverse effect on the convergence of a feedback estimator, the loop gain must be made small. The result is that feedback estimators can be relatively slow to converge. While this is not a problem for systems utilizing continuous transmission such as DOCSIS downstream channels, it is not ideal for burst channels, such as those used for DOCSIS upstream communication [9].

Feedforward synchronizers

The typical structure of a feedforward estimator is shown in Figure 3.6. As shown in the figure, the estimation portion of a feedforward synchronizer operates on the
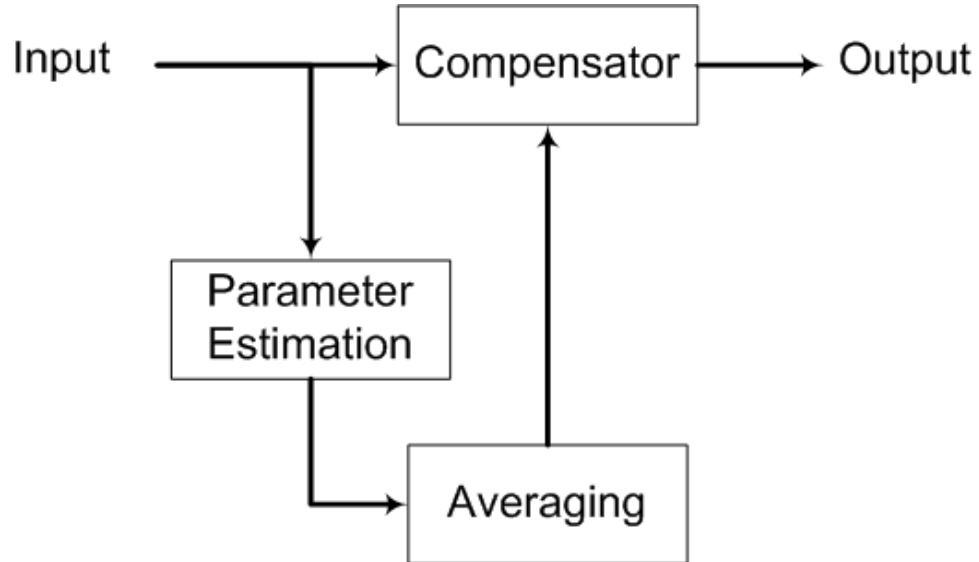
Figure 3.6 Typical structure of a feedforward synchronizer.

input signal, rather than the output of the compensator. In contrast to a feedback estimator, the estimation module in a feedforward configuration is responsible for estimating the overall value of the parameter at the synchronizer's input. This information is then passed on to the compensation block.

Since stability is not a concern in feedforward systems, feedforward synchronizers are able to avoid the loop gain and nonlinearity issues faced by feedback synchronizers. The result is that feedforward synchronizers tend to converge more quickly than do feedback synchronizers. Due to this faster convergence, feedforward synchronizers are well-suited to burst applications, such as DOCSIS upstream channels.

It has been shown in [13] that feedback circuits can be used effectively in a DOCSIS upstream demodulator. However, the current research focuses on feedforward techniques, as they are a natural fit for DOCSIS upstream channels. The overall structure of the proposed symbol recovery module is shown in Figure 3.7.

In the most straightforward implementation, the preamble symbols are broken up into four distinct blocks, each of which is used by one of the impairment-correcting circuits:
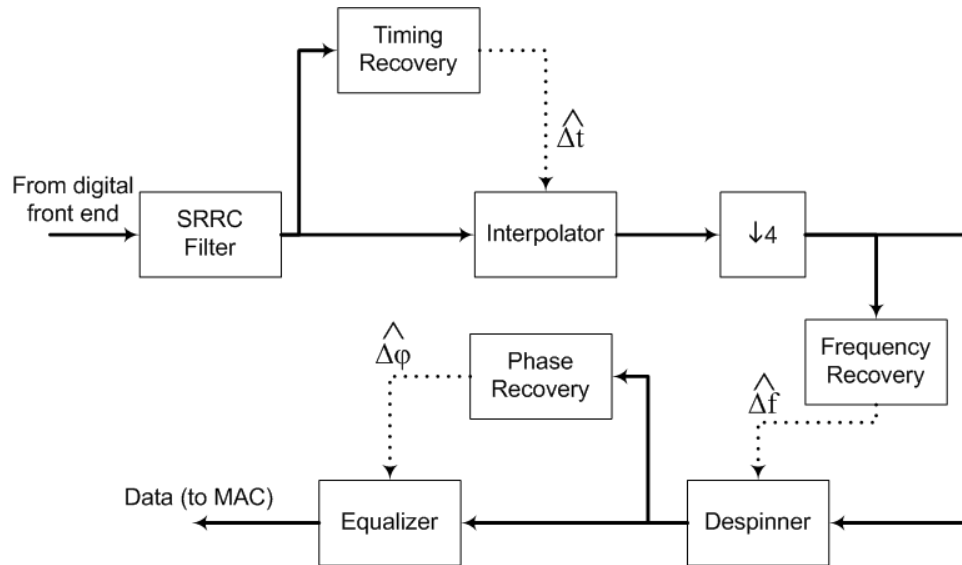
Figure 3.7 High level block diagram of symbol recovery module.
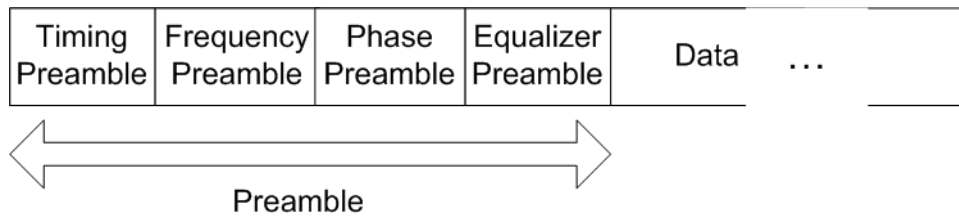
Figure 3.8 The structure of an upstream packet.

The general signal flow through the symbol recovery module is:

1. Using the preamble symbols, the symbol recovery module first estimates the timing error in the upstream transmission. Using an interpolator and down-sampler, the effective sampling times of the digital signal are modified so that the demodulator has access to samples corresponding to the correct symbol times.

2. Next, the frequency recovery module acts on the downsampled signal in order to estimate any carrier frequency offset which may be present in the channel using a specialized frequency recovery preamble. The estimated carrier frequency error is removed from the signal by a despinner.

41

3. A third portion of the preamble is used by the phase recovery circuit in order to detect a rotation of the constellation by a fixed angle. The resulting phase error estimate is passed to a derotator inside the equalizer for correction.

4. The fourth and final section of the preamble is a training sequence for an equalizer. Using this preamble, the equalizer applies an adaptive algorithm to determine a set of filter coefficients which is able to compensate for the micro-reflections present in the upstream channel.

Note that the timing, frequency, and phase estimators operate only during the preamble portion of the packet. Once an estimate of the relevant parameter has been obtained from the preamble symbols, an appropriate correction is applied for the remainder of the packet. In contrast, the equalizer is able to continually adapt its taps throughout the entire packet.

One common metric used to analyze the performance of a demodulator is Modulation Error Ratio (MER), which measures the amount of error in the received constellation points after the demodulator has attempted to compensate for the impairments. Mathematically, MER is defined as follows:

$$\text{MER(dB)} = 10 * \log_{10}\left(\frac{E_s}{\frac{1}{N}\sum_{j=1}^{N}|e_j|^2}\right) \tag{3.1}$$

where E_s is the average symbol energy and e_j is the error in the jth received symbol.

The choice of a preamble for each of the impairment estimation circuits can have a significant impact on the performance of each of the circuits. Certain patterns of preamble symbols can be used to maximize the probability of accurate estimates. The length of the sequence used to estimate the transmission impairments present in the upstream channel will also affect the performance of the impairment estimators. Longer preamble sequences permit more accurate estimates, but are less efficient from a data throughput point of view. Additionally, it is desirable if the same preamble can be used for multiple synchronization functions simultaneously. This would allow the overall preamble sequence to be shortened, increasing the efficiency of the channel.

Given these considerations, the selection of an appropriate preamble sequence will be one of the major topics of this document.

The remaining chapters of this thesis will develop novel frequency recovery, phase recovery, and equalization circuits that use modest amounts of FPGA resources, yet perform at near optimum levels.

4. Frequency and Phase Recovery

4.1 Introduction

As discussed in Section 2.1.2, frequency and phase differences between the carriers used for upconversion and downconversion cause the received constellation to spin and rotate, respectively. Any unexpected rotation is problematic in QAM systems, as the transmitted data is encoded in both the amplitude and phase of the sinusoidal carrier. Thus, in order to reliably recover the transmitted symbols, it is necessary to estimate and correct these offsets. This chapter discusses the design of the circuits which perform this task, known as the frequency and phase recovery modules.

As previously seen in Figure 3.7, the frequency recovery circuit operates upon the downsampled output of the timing recovery interpolator. Assuming that the timing recovery circuit is working correctly, the digital signal presented to the frequency recovery circuit has exactly one sample per symbol, with the sample being taken at the correct sampling time. Ignoring any potential ISI for the time being, the input signal to the frequency recovery module during the preamble portion of the packet may be written as follows:

$$y_f[n] = a_n e^{j(\Delta \omega n + \phi_o)} + \eta[n] \ ; \qquad 0 \le n \le N - 1 \tag{4.1}$$

where a_n is the complex transmitted symbol chosen from a unit-energy QPSK constellation, $\Delta \omega$ is the frequency offset, and ϕ_o is the phase offset. During the preamble, it is possible for the receiver to remove the angle modulation on this complex sinusoid by multiplying with the complex conjugate of the transmitted symbol, a_n^*, which

reduces the expression to:

$$y_u[n] = e^{j(\Delta\omega n + \phi_o)} + \eta_r[n] \quad ; \quad 0 \le n \le N - 1 \tag{4.2}$$

where $\eta_r[n]$ is a rotated version of the noise and has the same statistics as $\eta[n]$, which are a mean of 0 and a variance of σ^2.

For the reasons discussed in Section 3.1.3, the frequency and phase estimators are restricted to the use of data-aided feedforward algorithms in this research.

4.2 Performance Limits

Before proceeding with the development of the frequency and phase recovery algorithms, the performance limits for such algorithms are investigated. These limits, in the form of CRBs, will provide a reference point against which the proposed algorithms may be evaluated.

In order to find the CRB for a random vector of N_p parameters $p = [p_0 \, p_1 \ldots p_{N_p-1}]$ to be estimated, the Fisher information matrix, denoted $I(p)$, must first be calculated. The entries of $I(p)$ are determined by taking the expectation of partial derivatives of the log-likelihood function as follows:

$$[I(p)]_{ij} = E\left[-\frac{\partial^2 \ln f_y(y;p)}{\partial p_i \partial p_j}\right] \tag{4.3}$$

The CRB on the variance of each parameter p_i may be read from a diagonal entry of the inverse of the Fisher information matrix:

$$\text{var}(\widehat{p_i}) \ge [I^{-1}(p)]_{ii} \tag{4.4}$$

From equation (4.2), it is clear that $y_u[n]$ is a complex Gaussian random variable with a mean of $e^{j(\Delta\omega n + \phi_o)}$ and a variance of σ^2. Since the noise $\eta_r[n]$ is independent of $\eta_r[k]$ if $k \ne n$, the likelihood function for $y_u = [\, y_u[0], \, y_u[1], \, \ldots \, y_u[N-1] \,]$ may be expressed as:

$$f_{y_u}(y_u; \Delta\omega, \phi_o) = \left(\frac{1}{\pi\sigma^2}\right)^N e^{\frac{-1}{\sigma^2}\sum_{n=0}^{N-1}\left|y_u[n]-e^{j(\Delta\omega n+\phi_o)}\right|^2} \tag{4.5}$$

45

and the log-likelihood function is given by:

$$\Lambda_{y_u}(y_u) \;=\; \ln(f_{y_u}(y_u; \Delta\omega, \phi_o)) = \ln\left(\frac{1}{\pi\sigma^2}\right)^N - \frac{1}{\sigma^2}\sum_{n=0}^{N-1}\left|y_u[n] - e^{j(\Delta\omega n + \phi_o)}\right|^2$$

$$\;=\; \ln\left(\frac{1}{\pi\sigma^2}\right)^N -$$

$$\frac{1}{\sigma^2}\sum_{n=0}^{N-1}\left(y_u[n]y_u[n]^* - y_u[n]e^{-j(\Delta\omega n + \phi_o)} - y_u[n]^*e^{j(\Delta\omega n + \phi_o)} + 1\right) \quad (4.6)$$

Next, finding the required second partial derivatives of the log-likelihood function:

$$\frac{\partial \Lambda_{y_u}(y_u)}{\partial \Delta\omega} = \frac{-1}{\sigma^2}\sum_{n=0}^{N-1}\left(y_u[n]e^{-j(\Delta\omega n + \phi_o)}(jn) - y_u[n]^*e^{j(\Delta\omega n + \phi_o)}(jn)\right) \quad (4.7)$$

$$\frac{\partial \Lambda_{y_u}(y_u)}{\partial \phi_0} = \frac{-1}{\sigma^2}\sum_{n=0}^{N-1}\left(jy_u[n]e^{-j(\Delta\omega n + \phi_o)} - jy_u[n]^*e^{j(\Delta\omega n + \phi_o)}\right) \quad (4.8)$$

$$\frac{\partial^2 \Lambda_{y_u}(y_u)}{\partial \Delta\omega^2} = \frac{-1}{\sigma^2}\sum_{n=0}^{N-1}\left(n^2 y_u[n]e^{-j(\Delta\omega n + \phi_o)} + n^2 y_u[n]^*e^{j(\Delta\omega n + \phi_o)}\right) \quad (4.9)$$

$$\frac{\partial^2 \Lambda_{y_u}(y_u)}{\partial \Delta\omega \partial \phi_0} = \frac{-1}{\sigma^2}\sum_{n=0}^{N-1}\left(n y_u[n]e^{-j(\Delta\omega n + \phi_o)} + n y_u[n]^*e^{j(\Delta\omega n + \phi_o)}\right) \quad (4.10)$$

$$\frac{\partial^2 \Lambda_{y_u}(y_u)}{\partial \phi_0^2} = \frac{-1}{\sigma^2}\sum_{n=0}^{N-1}\left(y_u[n]e^{-j(\Delta\omega n + \phi_o)} + y_u[n]^*e^{j(\Delta\omega n + \phi_o)}\right) \quad (4.11)$$

Substituting the right hand side of equation (4.2) for $y_u[n]$ in equations (4.9), (4.10), and (4.11), then taking the expectation yields:

$$E\left[-\frac{\partial^2 \Lambda_{y_u}(y_u)}{\partial \Delta\omega^2}\right] \;=\; \frac{1}{\sigma^2}\sum_{n=0}^{N-1}\left(n^2 e^{j(\Delta\omega n + \phi_o)}e^{-j(\Delta\omega n + \phi_o)} + n^2 e^{-j(\Delta\omega n + \phi_o)}e^{j(\Delta\omega n + \phi_o)}\right)$$

$$\;=\; \frac{2}{\sigma^2}\sum_{n=0}^{N-1}n^2 \quad (4.12)$$

$$E\left[-\frac{\partial^2 \Lambda_{y_u}(y_u)}{\partial \Delta\omega \partial \phi_o}\right] \;=\; \frac{1}{\sigma^2}\sum_{n=0}^{N-1}\left(n e^{j(\Delta\omega n + \phi_o)}e^{-j(\Delta\omega n + \phi_o)} + n e^{-j(\Delta\omega n + \phi_o)}e^{j(\Delta\omega n + \phi_o)}\right)$$

$$\;=\; \frac{2}{\sigma^2}\sum_{n=0}^{N-1}n \quad (4.13)$$

$$E\left[-\frac{\partial^2 \Lambda_{y_u}(y_u)}{\partial \phi_o^2}\right] \;=\; \frac{1}{\sigma^2} \sum_{n=0}^{N-1} \left(e^{j(\Delta\omega n+\phi_o)}e^{-j(\Delta\omega n+\phi_o)} + e^{-j(\Delta\omega n+\phi_o)}e^{j(\Delta\omega n+\phi_o)}\right)$$

$$=\; \frac{2}{\sigma^2} \sum_{n=0}^{N-1} 1 \tag{4.14}$$

The expressions above can be simplified using the identities

$$\sum_{n=0}^{N-1} n = \frac{(N-1)N}{2} \tag{4.15}$$

$$\sum_{n=0}^{N-1} n^2 = \frac{(N-1)N(2N-1)}{6} \tag{4.16}$$

with the result:

$$E\left[-\frac{\partial^2 \Lambda_{y_u}(y_u)}{\partial \Delta\omega^2}\right] \;=\; \frac{(N-1)N(2N-1)}{3\sigma^2} \tag{4.17}$$

$$E\left[-\frac{\partial^2 \Lambda_{y_u}(y_u)}{\partial \Delta\omega \partial \phi_o}\right] \;=\; \frac{(N-1)N}{\sigma^2} \tag{4.18}$$

$$E\left[-\frac{\partial^2 \Lambda_{y_u}(y_u)}{\partial \phi_o^2}\right] \;=\; \frac{2N}{\sigma^2} \tag{4.19}$$

Thus, the Fisher information matrix is:

$$[I(p)] = \begin{bmatrix} \dfrac{(N-1)(N)(2N-1)}{3\sigma^2} & \dfrac{(N-1)(N)}{\sigma^2} \\[3mm] \dfrac{(N-1)(N)}{\sigma^2} & \dfrac{2N}{\sigma^2} \end{bmatrix} \tag{4.20}$$

and its inverse is:

$$\left[I^{-1}(p)\right] = \frac{1}{\det(I(p))} \begin{bmatrix} \dfrac{2N}{\sigma^2} & \dfrac{-(N-1)(N)}{\sigma^2} \\[3mm] \dfrac{-(N-1)(N)}{\sigma^2} & \dfrac{(N-1)(N)(2N-1)}{3\sigma^2} \end{bmatrix} \tag{4.21}$$

where

$$\begin{aligned} \det(I(p)) \;&=\; \frac{2N^2(N-1)(2N-1)}{3\sigma^4} - \frac{N^2(N-1)^2}{\sigma^4} \\[2mm] &=\; \frac{1}{3\sigma^4}\left[2N^2(N-1)(2N-1) - 3N^2(N-1)^2\right] \\[2mm] &=\; \frac{N^2(N^2-1)}{3\sigma^4} \end{aligned} \tag{4.22}$$

This reduces to

$$\left[I^{-1}(p) \right] = \begin{bmatrix} \dfrac{6\sigma^2}{N(N^2 - 1)} & \dfrac{-3\sigma^2}{N(N + 1)} \\[3mm] \dfrac{-3\sigma^2}{N(N + 1)} & \dfrac{\sigma^2(2N - 1)}{N(N + 1)} \end{bmatrix}. \tag{4.23}$$

The CRBs on the variance of frequency and phase offset estimators may be read from the inverse of the Fisher information matrix. Keeping in mind that $E[|a_n|^2] = 1$ and $E[|\eta|^2] = \sigma^2$, the bounds may be expressed in terms of the signal-to-noise ratio (SNR) rather than the noise variance by using the identity $SNR = \frac{1}{\sigma^2}$.

$$\text{var}(\widehat{\Delta\omega}) \geq \left[I^{-1}(p) \right]_{11} = \frac{6\sigma^2}{N(N^2 - 1)} = \frac{6}{N(N^2 - 1)SNR} \tag{4.24}$$

$$\text{var}(\widehat{\phi_o}) \geq \left[I^{-1}(p) \right]_{22} = \frac{\sigma^2(2N - 1)}{N(N + 1)} = \frac{2N - 1}{N(N + 1)SNR} \tag{4.25}$$

4.3   Maximum Likelihood Estimators

The maximum likelihood technique is a common method for estimating a set of parameters. This technique is very popular because it offers a straightforward method of generating estimators which achieve the CRB for high SNRs and long observation sequences. For this reason, the maximum likelihood technique is a logical place to start a search for resource-efficient frequency and phase offset estimators.

As the name suggests, the maximum likelihood algorithm involves finding the parameter values which maximize the likelihood function for the given set of observations. An estimator derived in this fashion is referred to as a maximum likelihood (ML) estimator.

Since the natural logarithm function is monotonic, maximizing the log-likelihood function is equivalent to maximizing the likelihood function. Given the exponential nature of the likelihood function, the log-likelihood function is typically much easier to work with than the original likelihood function. In order to maximize the log-likelihood function, the most straightforward technique is to find the point at which the derivative of the function with respect to the parameter of interest is zero. In

the case of multiple parameters, the joint ML estimator is found by solving for the set of parameters that simultaneously set the partial derivatives with respect to each parameter equal to zero.

The application of the maximum likelihood technique to the current task of estimating the frequency and phase offsets starts with the log-likelihood function:

$$\Lambda_{y_u}(y_u) \quad = \quad \ln(f_{y_u}(y_u; \Delta\omega, \phi_o)) = \ln\left(\frac{1}{\pi\sigma^2}\right)^N - \frac{1}{\sigma^2}\sum_{n=0}^{N-1}\left|y_u[n] - e^{j(\Delta\omega n + \phi_o)}\right|^2 \quad (4.26)$$

The partial derivatives of the log-likelihood function with respect to $\Delta\omega$ and ϕ_o are given by equations (4.7) and (4.8). Setting the derivatives to 0 yields the equations:

$$0 \quad = \quad \sum_{n=0}^{N-1}\left(-n y_u[n]e^{-j(\widehat{\Delta\omega}n + \widehat{\phi_o})} + n y_u[n]^* e^{j(\widehat{\Delta\omega}n + \widehat{\phi_o})}\right) \quad\quad (4.27)$$

$$0 \quad = \quad \sum_{n=0}^{N-1}\left(-y_u[n]e^{-j(\widehat{\Delta\omega}n + \widehat{\phi_o})} + y_u[n]^* e^{j(\widehat{\Delta\omega}n + \widehat{\phi_o})}\right) \quad\quad (4.28)$$

Unfortunately, in many cases, the ML approach does not yield a simple closed-form expression for an estimator. The current problem appears to be such a case, as it is not possible to solve equations (4.27) and (4.28) for $\widehat{\Delta\omega}$ and $\widehat{\phi_o}$. If computational complexity and latency were not important considerations, it would be possible to implement a maximum likelihood estimator by exhaustively evaluating the likelihood function over the allowable parameter range. However, this type of approach is clearly impractical for a resource-constrained FPGA-based demodulator.

Alternatively, it is possible to obtain closed-form expressions for ML frequency and phase offset estimators by making certain approximations which are valid for high SNRs. The details of this derivation are outlined in Appendix A. Unfortunately, the estimators derived in this section are still too complex to implement economically in an FPGA.

When the ML technique fails to yield a convenient estimator, it is necessary to utilize alternate approaches to deriving an estimator. The design of such approaches commonly relies upon intuition and mathematical heuristics. The following sections

will individually examine the tasks of frequency offset estimation and phase offset estimation in this fashion.

4.4   Frequency Offset Estimator

4.4.1   Previous Work

The problem of estimating the carrier frequency of a burst digital signal has been well-studied over the last half-century. Rife and Boorstyn laid the groundwork for the field [27] by deriving the Cramer-Rao bounds (CRB) and maximum likelihood estimators for the estimation of the amplitude, frequency, and phase of a single tone from discrete-time observations. In [15], Tretter showed that a statistically efficient estimator of the frequency of a noisy sinusoid may be generated using linear regression techniques. An alternative CRB-achieving scheme, proposed by Kay in [16], exploits the correlation between the phase of the incoming samples. Later, Luise and Reggiannini [17] used maximum likelihood techniques to derive a cost-effective frequency recovery algorithm for high-SNR signals. One other notable estimator is that proposed by Mengali and Morelli in [18], which has the advantage of a particularly large estimation range.

The amount of published work in the area of frequency estimation specifically for DOCSIS upstream channels is relatively limited. In [28], Wang and Speidel suggested a technique based upon the measurement of the phase angle of the output of a preamble detector. Most recently, Kim et al. [12] surveyed the literature and concluded that Mengali and Morelli's technique is well-suited to the upstream channel.

Despite all of this fine work, DOCSIS upstream channels present one key issue which does not appear to have been analyzed in the literature: the effect of micro-reflections or 'echoes'. Significant ISI in the received signal due to micro-reflections tends to bias the carrier frequency estimators discussed above, reducing their suitability for use in a DOCSIS upstream receiver.

Going forward, a data-aided frequency estimation algorithm is developed that is

robust in the presence of ISI. Furthermore, the algorithm is economical to implement and can be used simultaneously with a channel estimator, while still providing a high level of performance. It is shown that this estimator remains unbiased in the presence of channel ISI for a wide range of preambles, including preambles which are suitable for sounding the channel.

4.4.2 Derivation from First Principles

Phase Noise Model

The input to the frequency recovery module, which is given by (4.29), may be expressed as the summation of a signal component and a noise component as follows:

$$y_f[n] = s[n] + \eta[n] \qquad (4.29)$$

where $s[n] = a_n e^{j(\Delta \omega n + \phi_o)}$. The task of the frequency estimation circuit is to estimate the parameter $\Delta \omega$, which causes the signal $y_f[n]$ to spin in the complex plane. Obviously, the rate of spin is proportional to the frequency offset. Taking advantage of this fact, the following frequency offset estimators attempt to determine the frequency offset by measuring the angular rotation in $y_f[n]$ during the preamble.

In order to determine the performance of such algorithms, it is necessary to understand how the additive complex noise samples $\eta[n]$ affect the angle of the received sample $y_f[n]$. For high signal to noise ratios such as the 25dB minimum on the DOCSIS upstream channel, Kay [16] suggested that the additive noise samples can be modeled as phase noise added to $y_f[n]$. It is pointed out that Kay's model is not useful in analyzing the effects of noise-induced amplitude distortion. This is not a problem in the present case, where only the angle of the noise-corrupted signal $y_f[n]$ is important.

Kay's model can be explained with the help of Figure 4.1. As shown in the figure, each noise sample may be broken down into two orthogonal components: $\eta_{\parallel}$, which is parallel to the signal component of y_f, and $\eta_{\perp}$, which is perpendicular to the signal component of y_f. Since η is complex AWGN with variance σ^2, $\eta_{\parallel}$ and $\eta_{\perp}$ are both

51
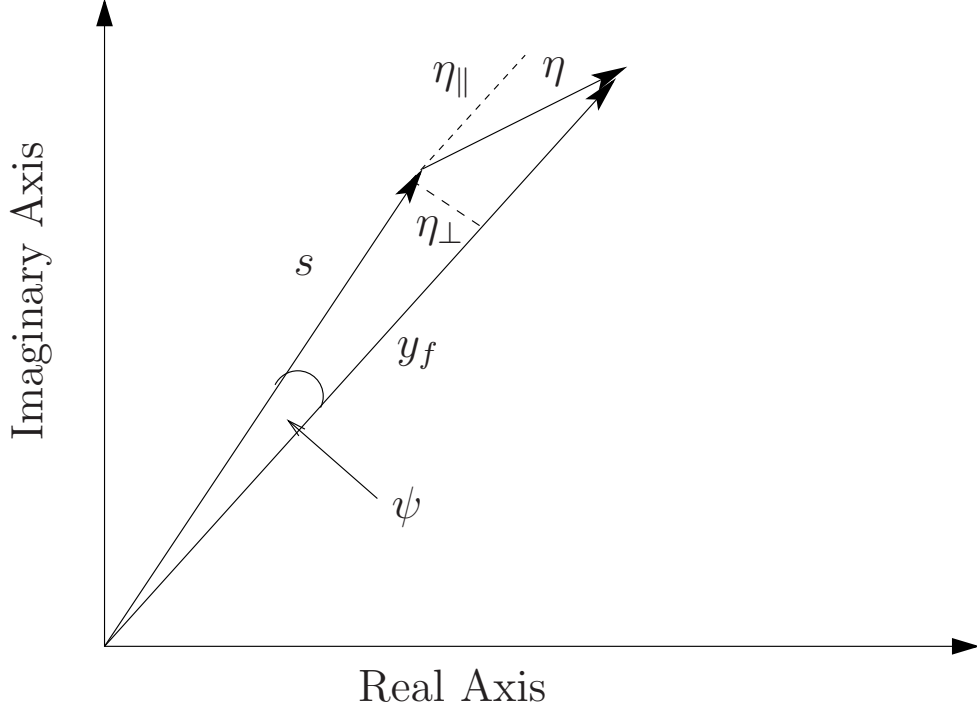
Figure 4.1 Modeling AWGN as phase noise.

Gaussian random variables with identical variances of $\sigma^2/2$. Taking advantage of the noise decomposition, the phase error, denoted as ψ, may be found using a simple trigonometric function:

$$\psi = \tan^{-1}\left(\frac{\eta_\perp}{|s|}\right) \tag{4.30}$$

For large signal to noise ratios, the magnitude of the signal component of y_f will be much larger than $\eta_\perp$, so the approximation $\tan(x) \approx x$ may be applied, yielding the result

$$\psi \approx \frac{\eta_\perp}{|s|} \quad \text{radians} \tag{4.31}$$

DOCSIS 3.0 upstream channels always use QPSK modulation for the preamble, so $|s|$ has a constant value. Thus, the variance of the phase noise ψ is equal to:

$$
\begin{aligned}
\sigma_\psi^2 &= E[(\psi - E[\psi])^2] = E\left[\left(\frac{\eta_\perp}{|s|} - E\left[\frac{\eta_\perp}{|s|}\right]\right)^2\right] \quad \text{radians}^2 \\
&= \frac{E[\eta_\perp^2]}{|s|^2} = \frac{\sigma^2}{2|s|^2} = \frac{1}{2SNR} \quad \text{radians}^2
\end{aligned}
\tag{4.32}
$$

Thus, for large SNRs, the input signal to the frequency recovery circuit may be modeled as:

$$y_p[n] = a_n e^{j(\Delta\omega n + \phi_o + \psi[n])} \tag{4.33}$$

The Estimator - Insight and Performance

Preamble-based frequency offset estimators typically operate by measuring and combining the angular differences between a set of incoming samples. Perhaps the most basic technique computes the angular difference between two successive samples. The frequency offset is then estimated as this angular difference. The heart of this simple technique is a circuit known as a differential detector. A differential detector multplies the current input sample by the complex conjugate of the previous sample. In mathematical terms, its output is:

$$y_{dd}[n] = y[n]y^*[n-1] \tag{4.34}$$

using the phase noise approximation given by (4.33) has:

$$
\begin{aligned}
y_{dd}[n] &\approx a_n e^{j(\Delta\omega n + \phi_o + \psi[n])} a_{n-1}^* e^{-j(\Delta\omega(n-1) + \phi_o + \psi[n-1])} \\
&\approx a_n a_{n-1}^* e^{j(\Delta\omega + \psi[n] - \psi[n-1])}
\end{aligned}
\tag{4.35}
$$

The phase of the output has three terms: $\Delta\omega$, $\psi[n]$, and $\psi[n-1]$. The latter two terms correspond to the phase noise. In practice, the angle of $y_{dd}[n]$ is computed through the use of either a coordinate rotation digital computer (CORDIC) inverse tangent circuit [29] or a look-up table. Neglecting any error introduced by the angle computation device, this simple estimator may be expressed as:

$$
\begin{aligned}
\widehat{\Delta\omega}_{n-1,n} = \widehat{\Delta\omega}_{\text{simple}}[n] &= \arg(y_{dd}[n]) \\
&= \arg(a_n a_{n-1}^*) + \arg(e^{j(\Delta\omega + \psi[n] - \psi[n-1])}) \\
&= \arg(a_n a_{n-1}^*) + \Delta\omega + \psi[n] - \psi[n-1] \tag{4.36}
\end{aligned}
$$

where the subscripts on $\widehat{\Delta\omega}_{n-1,n}$ indicate that the inputs to the differential detector correspond to samples $n-1$ and n. The sequence of symbol values is known during the preamble, so the contribution of $\arg(a_n a_{n-1}^*)$ can be removed. Since the sampling

rates of sequences $y[n]$ and $y_{dd}[n]$ are equal to the symbol rate, the units of the estimator given by (4.36) are radians/symbol. Keeping in mind that the phase noise $\psi[n]$ is a sequence of i.i.d. random variables with mean and variance equal to 0 and $1/(2 \cdot \text{SNR})$ respectively, it is clear that the estimator of (4.36) is unbiased and that the variance of $\widehat{\Delta\omega}_{\text{simple}}[n]$ is equal to $1/\text{SNR}$ in units of $(\text{radians/symbol})^2$.

In order to produce more precise estimates, one obvious approach is to average M estimates from the simple estimator of (4.36), yielding the following estimator:

$$
\begin{aligned}
\widehat{\Delta\omega}_{\text{avg}} &= \frac{1}{M}\sum_{n=1}^{M}\widehat{\Delta\omega}_{n-1,n} \\
&= \frac{1}{M}\sum_{n=1}^{M}(\Delta\omega + \psi[n] - \psi[n-1]) \\
&= \Delta\omega + \frac{\psi[M]}{M} - \frac{\psi[0]}{M}
\end{aligned} \tag{4.37}
$$

An alternative approach to improving the simple estimator is to use a differential detector with a larger differential delay of M samples. Such an estimator can be expressed as:

$$
\begin{aligned}
\widehat{\Delta\omega}_{n-M,n} = \widehat{\Delta\omega}_{\text{wide}} &= \frac{1}{M}\arg(y[n]y[n-M]^*) \\
&= \Delta\omega + \frac{\psi[M]}{M} - \frac{\psi[0]}{M}
\end{aligned} \tag{4.38}
$$

Interestingly, this $M-$wide differential approach yields the same result as the average of M $1-$wide differential detector outputs. The estimators of equations (4.37) and (4.38) produce the same output, so from a theoretical point of view, the $M-$wide differential and average of M $1-$wide implementations may be used interchangeably. However, from an implementation perspective, they are quite different, as discussed in Section 4.4.2.

It is apparent from (4.37) that the average of M $1-$wide estimators, $\widehat{\Delta\omega}_{\text{avg}}$, is itself an unbiased estimator that has variance $\frac{1}{M^2\text{SNR}}$, which is lower than the variance of the simple estimator by a factor of M^2. Equation (4.37) also indicates that only the phase noise at samples 0 and M corrupt the estimator's output. Since the phase noise
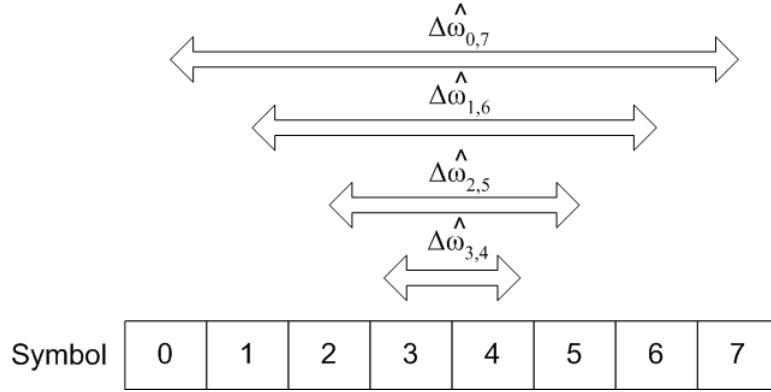
Figure 4.2   The set of independent estimators which are combined in the decreasing average-length technique.

sequence $\psi[n]$ is iid, estimators which start and end on different samples will produce independent estimates. That is, two estimators that have four different endpoints are independent.

For an N symbol preamble. it is possible to construct a set of $N/2$ (or $(N-1)/2$ for N odd) independent averaging estimators by starting and stopping the averaging on different samples. A composite estimator with lower variance can then be constructed by weighting and summing these $N/2$ or $(N-1)/2$ independent estimators. Many different sets of independent estimators can be constructed for a given preamble length. One of these possible sets of estimators for a simple eight-symbol preamble is illustrated in Figure 4.2.

The approach depicted in Figure 4.2 will be referred to as the decreasing average-length set of estimators. As shown in the figure, for the case of an eight-symbol preamble, the averaging lengths (or differential widths) for the four independent estimators are two, four, six, and eight samples. Similarly, a nine-symbol preamble yields four independent estimators of lengths three, five, seven, and nine. In either case, it is possible to construct a low-variance composite estimator by combining the outputs of the four composite estimators.

In the general case of an $N-$symbol preamble, the composite decreasing average-

length estimator is given by a weighted average of the independent estimators as follows:

$$\widehat{\Delta\omega}_{\text{decrease}} = \sum_{i=0}^{\text{floor}(N/2)-1} c_i \cdot \widehat{\Delta\omega}_{i,N-i-1} \tag{4.39}$$

where c_i is a weighting function, which may be optimized in order to minimize the variance of the combined estimator. Since each of the individual estimators is unbiased, the combined estimator will also be unbiased if the sum of the weights is equal to one.

By using a Lagrange multiplier to minimize the variance of $\widehat{\Delta\omega}_{\text{decrease}}$ subject to $\sum_{i=0}^{\text{floor}(N/2)-1} c_i = 1$, it is possible to find an optimal set of weights. First, express (4.39) in terms of the phase noise samples $\psi[n]$:

$$\widehat{\Delta\omega}_{\text{decrease}} = \Delta\omega + \sum_{i=0}^{\text{floor}(N/2)-1} c_i \cdot \left(\frac{\psi[N-i-1] - \psi[i]}{N-2i-1} \right) \tag{4.40}$$

The variance of the combined estimator is:

$$\sigma^2_{\text{decrease}} = \sum_{i=0}^{\text{floor}(N/2)-1} \frac{2c_i{}^2\sigma^2_\psi}{(N-2i-1)^2} = \frac{1}{SNR} \sum_{i=0}^{\text{floor}(N/2)-1} \frac{c_i^2}{(N-2i-1)^2} \tag{4.41}$$

Introducing a Lagrange multiplier γ, the Lagrange function may be written as:

$$\Gamma = \frac{1}{SNR} \sum_{i=0}^{\text{floor}(N/2)-1} \frac{c_i^2}{(N-2i-1)^2} + \gamma \left(\sum_{i=0}^{\text{floor}(N/2)-1} c_i - 1 \right) \tag{4.42}$$

Equating the partial derivatives of Γ to 0:

$$\begin{aligned}
\frac{\partial \Gamma}{\partial c_i} &= \frac{2c_i}{SNR(N-2i-1)^2} + \gamma = 0 \\
c_i &= \frac{-\gamma SNR(N-2i-1)^2}{2}
\end{aligned} \tag{4.43}$$

$$\begin{aligned}
\frac{\partial \Gamma}{\partial \gamma} &= \sum_{i=0}^{\text{floor}(N/2)-1} c_i - 1 = 0 \\
1 &= \sum_{i=0}^{\text{floor}(N/2)-1} c_i = \sum_{i=0}^{\text{floor}(N/2)-1} \frac{-\gamma SNR(N-2i-1)^2}{2} \\
\gamma &= \frac{-2}{SNR \sum_{i=0}^{\text{floor}(N/2)-1}(N-2i-1)^2} = \frac{-2}{SNR \cdot K}
\end{aligned} \tag{4.44}$$

where K is equal to $\sum_{i=0}^{\text{floor}(N/2)-1}(N-2i-1)^2$, which is a constant. Next, substitute (4.44) into (4.43) in order to solve for the optimal set of weights:

$$
\begin{aligned}
c_i &= \frac{-\gamma SNR(N-2i-1)^2}{2} \\
&= \frac{(N-2i-1)^2}{K}
\end{aligned}
\tag{4.45}
$$

The variance of a decreasing average-length estimator which utilizes this optimal set of weights may be found by combining equations (4.41) and (4.45):

$$
\begin{aligned}
\sigma^2_{\text{decrease}} &= \frac{1}{SNR}\sum_{i=0}^{\text{floor}(N/2)-1}\frac{c_i^2}{(N-2i-1)^2} \\
&= \frac{1}{SNR}\sum_{i=0}^{\text{floor}(N/2)-1}\frac{(N-2i-1)^4}{K^2(N-2i-1)^2} = \frac{\sum_{i=0}^{\text{floor}(N/2)-1}(N-2i-1)^2}{K^2\cdot SNR} \\
&= \frac{1}{K\cdot SNR}
\end{aligned}
\tag{4.46}
$$

Equations (4.45) and (4.46) indicate that the constant K has an important influence upon both the optimal set of weights and the variance of the optimal combined estimator. Since the upper bound of the summation includes the floor function, the value of K must be computed for both odd and even preamble lengths.

For N odd

If N is odd, $\text{floor}(N/2) = (N-1)/2$, and the upper limit of summation becomes $(N-1)/2-1$. When computing the value of K, it is helpful to make the substitution $L = N - 1$ in order to shorten the mathematical expressions:

$$
\begin{aligned}
K &= \sum_{i=0}^{(N-1)/2-1}(N-2i-1)^2 = \sum_{i=0}^{M/2-1}(L-2i)^2 \\
&= \sum_{i=0}^{M/2-1}(L^2-4Li-4i^2)
\end{aligned}
\tag{4.47}
$$

In order to simplify this expression, apply the well known equations $\sum_{i=0}^{k}i = \frac{k(k+1)}{2}$

and $\sum_{i=0}^{k} i^2 = \frac{k(k+1)(2k+1)}{6}$:

$$
\begin{aligned}
K &= L^2 \left(\frac{L}{2} \right) - \frac{4L(\frac{L}{2} - 1)(\frac{L}{2})}{2} + \frac{4(\frac{L}{2} - 1)(\frac{L}{2})(L - 1)}{6} \\
&= \frac{L^3}{2} - \frac{L^3}{2} + L^2 + \frac{L^3}{6} - \frac{2L^2}{6} - \frac{L^2}{6} + \frac{2L}{6} \\
&= \frac{L^3 + 3L^2 + 2L}{6}
\end{aligned}
\tag{4.48}
$$

Substituting $N - 1$ back into (4.48) in place of L, we have:

$$
\begin{aligned}
K &= \frac{(N - 1)^3 + 3(N - 1)^2 + 2(N - 1)}{6} \\
&= \frac{(N^3 - 3N^2 + 3N - 1) + 3(N^2 - 2N + 1) + 2N - 2}{6} \\
K &= \frac{N(N^2 - 1)}{6}
\end{aligned}
\tag{4.49}
$$

For N even

For even values of N, floor$(N/2) = N/2$, so the upper limit of the summation becomes $N/2 - 1$. Once again, the substitution $L = N - 1$ is used in order to shorten the expressions:

$$
\begin{aligned}
K &= \sum_{i=0}^{N/2-1} (N - 2i - 1)^2 = \sum_{i=0}^{(M-1)/2} (L - 2i)^2 \\
&= \sum_{i=0}^{(M-1)/2} (L^2 - 4Li - 4i^2) \\
&= L^2 \left(\frac{L+1}{2} \right) - \frac{4L(\frac{L-1}{2})(\frac{L+1}{2})}{2} + \frac{4L(\frac{L-1}{2})(\frac{L+1}{2})}{6} \\
&= \frac{L^3}{2} + \frac{L^2}{2} - \frac{L^3}{2} + \frac{L}{2} + \frac{L^3}{6} - \frac{L}{6} \\
K &= \frac{L^3 + 3L^2 + 2L}{6} \\
&= \frac{N(N^2 - 1)}{6}
\end{aligned}
\tag{4.50}
$$

A comparison of equations (4.49) and (4.50) indicates that the equation for K is the same, regardless of whether N is odd or even. In both cases, the optimal weights c_i
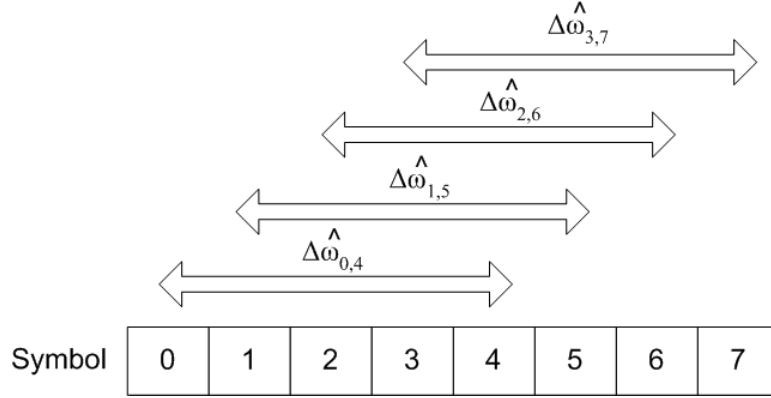
Figure 4.3 The set of independent estimators which are combined in the equal average-length technique.

and the variances of the optimal estimators are:

$$c_i = \frac{(N - 2i - 1)^2}{K} = \frac{6(N - 2i - 1)^2}{N(N^2 - 1)} \tag{4.51}$$

$$\sigma^2_{\text{decrease}} = \frac{1}{K \cdot SNR} = \frac{6}{N(N^2 - 1) \cdot SNR} \tag{4.52}$$

The variance of the optimal decreasing average-length estimator calculated in equation (4.52) matches the CRB of (4.24). Since the CRB-achieving estimator for a given parameter is unique, the above derivation provides an alternative way of viewing the two well-known estimators of Tretter and Kay.

An alternative to the averaging structure of Figure 4.2 is shown in Figure 4.3. These estimators are referred to as an equal average-length set of estimators. While this approach necessarily produces a composite estimator whose variance is higher than that of the decreasing average-length scheme, it has a major advantage: the variance of each individual estimator is equal, removing the need for unequal weighting. Consequently, for the general case of a composite estimator utilizing $N - M$ independent estimators of averaging length M, the composite estimator output may be expressed as:

$$\widehat{\Delta\omega}_{\text{eq-len}} = \frac{1}{N - M} \sum_{i=0}^{N-M-1} \widehat{\Delta\omega}_{i,M+i}, \quad \text{floor}\left(\frac{N+1}{2}\right) \leq M \leq N \tag{4.53}$$

where M is the averaging length of each averaging estimator, as before. The variance

of this estimator is easily shown to be:

$$\sigma^2_{\text{eq}-\text{len}} = \frac{1}{M^2(N-M)\text{SNR}} \tag{4.54}$$

The value of M that minimizes $\sigma^2_{\text{eq}-\text{len}}$ in the interval floor $\left(\frac{N+1}{2}\right) \leq M \leq N$ is $M_{\text{opt}} = \text{round}(2N/3)$. For the case where N is divisible by 3, the variance of the composite equal average-length estimator becomes:

$$\sigma^2_{\text{eq}-\text{len}-\text{best}} = \frac{1}{(\frac{2N}{3})^2(N-\frac{2N}{3})\text{SNR}} = \frac{27}{4N^3\text{SNR}}, \tag{4.55}$$

which is approximately 0.5dB higher than the CRB for $N >> 1$. It could be argued that the simplicity of implementation more than compensates for the small performance penalty of 0.5dB. However, the real value of this composite equal average-length estimator is not its economy, but that it produces unbiased estimates for ISI-laden channels.

The Effect of ISI

One of the major challenges posed by the DOCSIS upstream channel is the large amount of ISI caused by micro-reflections in the cable network. According to the DOCSIS standard, these micro-reflections can be as large as -10dB relative to the carrier, and may arrive up to seven symbol durations later than the main path. Error in the demodulator timing recovery circuit is another (although generally much less severe) possible source of ISI. From the perspective of the upstream frequency estimation algorithm, the ISI generated by these two sources may be modeled as a complex discrete-time FIR filter with complex coefficients h running at the symbol rate, as illustrated in Figure 4.4.

The figure also shows that the downconversion operation in the receiver, which creates the frequency offset, operates upon the output of this channel filter. The input signal to the frequency recovery module may thus be written as:

$$
\begin{aligned}
y_{\text{ISI}}[n] &= (a_n \star h_n)e^{j(\Delta\omega n + \phi_o + \psi[n])} \\
&= e^{j(\Delta\omega n + \phi_o + \psi[n])} \sum_{k=-L_1}^{L_2} h_k a_{n-k}
\end{aligned} \tag{4.56}
$$
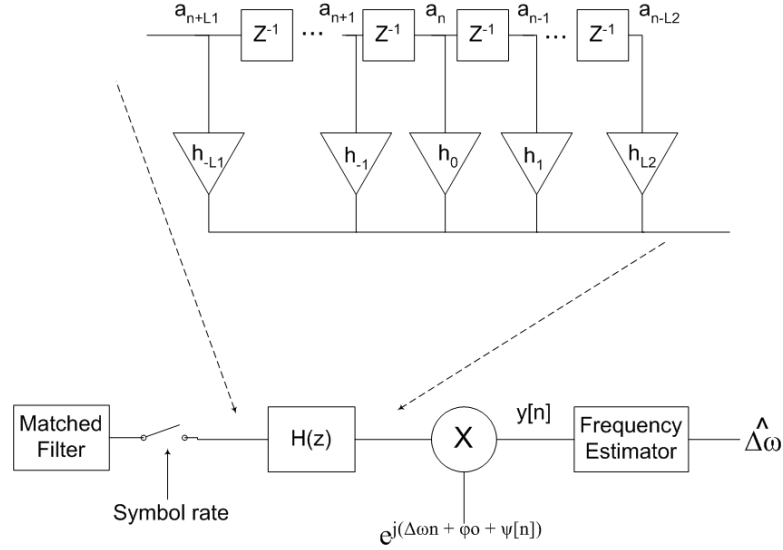
Figure 4.4 Modeling the channel ISI as a symbol-rate linear filter.

where $\star$ represents convolution, h_k are the complex channel filter coefficients, and L_1 and L_2 represent the number of filter taps on each side of the main tap, which is h_0.

ISI present at the input to the frequency offset estimator typically has a significant negative impact upon the estimator's performance. Consider the output of a differential detector of differential width M in response to the input signal of equation (4.56):

$$
\begin{aligned}
y_{\text{dd}}[n] &= y_{\text{ISI}}[n]y_{\text{ISI}}[n-M]^* \\
&= e^{j(\Delta\omega M + \psi[n] - \psi[n-M])}\left(\sum_{k_1=-L_1}^{L_2} h_{k_1}a_{n-k_1}\right)\left(\sum_{k_2=-L_1}^{L_2} h_{k_2}a_{n-k_2-M}\right)^* \\
&= e^{j(\Delta\omega M + \psi[n] - \psi[n-M])}\sum_{k_1=-L_1}^{L_2}\sum_{k_2=-L_1}^{L_2} h_{k_1}h_{k_2}^*a_{n-k_1}a_{n-k_2-M}^* \\
&= B[n]e^{j(\Delta\omega M + \psi[n] - \psi[n-M])}
\end{aligned}
\tag{4.57}
$$

where the unwanted double sum in (4.57) has been defined as:

$$
B[n] \equiv \sum_{k_1=-L_1}^{L_2}\sum_{k_2=-L_1}^{L_2} h_{k_1}h_{k_2}^*a_{n-k_1}a_{n-k_2-M}^*
\tag{4.58}
$$

In general, $B[n]$ in (4.57) is a complex number that scales and rotates the differential detector output. Since $B[n]$ is a function of the symbol values and the echoes in the

61

channel, the frequency offset estimator acquires a channel-and-sequence-specific bias which is unknown at the time of transmission. In order for a frequency estimator based upon the differential detector output of (4.57) to avoid this bias and work correctly, the argument of $B[n]$ must be known.

Fortunately, the argument of $B[n]$ is known if the preamble sequence is periodic with period M. In this case, $a_n = a_{n-M}$, allowing $B[n]$ to be rewritten as:

$$B[n] \equiv \sum_{k_1=-L_1}^{L_2} \sum_{k_2=-L_1}^{L_2} h_{k_1} h_{k_2}^* a_{n-k_1} a_{n-k_2}^* \qquad (4.59)$$

Due to the symmetry of (4.59), $B[n] = B[n]^*$, which means that $B[n]$ is real regardless of the channel ISI coefficients h, and therefore its argument is zero. By selecting a periodic preamble, it is possible to prevent ISI from biasing the frequency estimator.

Implementation Details

As shown in the previous section, it is possible to make any differential-based frequency offset estimator immune to ISI-induced biasing through the selection of an appropriate preamble. However, what constitutes an appropriate preamble differs for various averaging algorithms.

Many of the well-known frequency offset estimators, including the Kay estimator (or equivalently the composite decreasing average-length estimator of Section 4.4.2), the Mengali and Morelli (M&M) estimator [18], and the Luise and Reggiannini (L&R) [17] estimator are constructed out of a number of differential detectors of different lengths. With this type of structure, in order for the overall estimator to be unbiased, each of the component estimators must also be unbiased. This in turn requires the period of the preamble sequence to be a common factor of all of the averaging lengths. If the number of symbols in the preamble is even, this requirement forces the preamble sequence to have a period of one symbol. On the other hand, if the number of symbols in the preamble is odd, the preamble must have a period of either one or two symbols. Either way, the number of possible preambles which produces unbiased estimators is extremely limited.

Being limited to the use of either a constant or alternating preamble is an unwelcome constraint in many applications, as such a preamble necessarily concentrates the transmitted energy at one or two discrete frequencies. Preambles of this type are not suitable for sounding a channel, as good channel sounding sequences distribute the transmitted energy evenly across the channel bandwidth. This means that reliable channel estimation can not be performed in parallel with the frequency estimation. It should also be mentioned that sequences which concentrate the transmitted energy at one or two frequencies magnify the ill effects of noise if the transmitted energy coincides with a dip in the channel magnitude response.

In contrast to these well-known estimators, the equal average-length composite estimator allows for a great deal of choice in terms of preamble selection. Since the estimator is composed of a series of smaller estimators which each average across M symbol durations, it will be unbiased for any preamble with a period of M symbols, regardless of the ISI induced by the channel. If, as is typical, M is chosen to be significantly greater than one, the number of available preambles which meet the ISI criterion is large, giving the system designer much more flexibility.

When constructing the composite equal average-length estimator, a question arises: is it better to implement each of the constituent estimators using (4.37), which averages the arguments of M outputs from a $1-$wide detector, or using (4.38), which utilizes the argument of a single $M-$wide detector? In general, a differential detector experiences ambiguity in its output if the magnitude of the angular difference between its inputs exceeds π radians. If undetected, such a phase ambiguity has a catastrophic effect upon the generated frequency estimate. There are two main sources of angular difference between the input vectors: frequency offset and AWGN. Since the effects are additive and errors of more than π are catastrophic, it is sensible to budget the worst case difference between AWGN and frequency offset induced phase differences. While the optimum partition of the maximum π difference could be done with careful analysis, it is reasonable to allow $\pi/4$ for the AWGN induced error and $3\pi/4$ for the frequency offset induced error. When an estimator is constructed using $1-$wide

differential detector outputs, the above partition implies that the maximum tolerable frequency offset is $\Delta f = \frac{3R_s}{8}$ in Hz. This very large estimation range is the main advantage of the averaging implementation.

In contrast, if the $M-$wide detector implementation of (4.38) is used, in order for the magnitude of the angular difference caused by the frequency offset to be less than $\frac{3\pi}{4}$, the frequency offset must not exceed $\Delta f = \frac{3R_s}{8M}$. The frequency estimation range has been reduced by a factor of M with respect to that of averaging M $1-$wide detectors. However, the $M-$wide implementation is more economical, and is thus preferable, so long as the frequency estimation range is sufficient. For a system where frequency offset is known to be less than Δf, M is constrained by $M \leq \frac{3R_s}{8\Delta f}$. If the optimum value of M is used, then N is limited by $N = \frac{3M_{\text{opt}}}{2} \leq \frac{9R_s}{16\Delta f}$.

There may be situations where N must be larger than $\frac{9R_s}{16\Delta f}$ to achieve the desired $\sigma^2_{\text{eq-len}}$. For these situations, there is an equivalent composite equal average-length estimator that uses a differential width of $N - M_{\text{opt}} = \text{round}(N/3)$, which is half that of $M_{\text{opt}} = \text{round}(2N/3)$. This compact estimator averages M_{opt} outputs of an $N - M_{\text{opt}}$ wide differential detector and is given by:

$$\widehat{\Delta\omega}_{\text{eq-len}} \quad = \quad \frac{1}{M_{\text{opt}}} \sum_{i=0}^{M_{\text{opt}}-1} \widehat{\Delta\omega}_{i,N-M_{\text{opt}}+i} \tag{4.60}$$

This estimator produces estimates identical to those of (4.53). Therefore its variance is given by (4.54) and also by (4.55) if N is divisible by three. With the compact estimator, the sequence length can be as large as $N = \frac{9R_s}{8\Delta f}$ before the frequency estimator's budget for worst case phase difference is exceeded.

The frequency offset of a DOCSIS 3.0 upstream channel is almost certain to be less than 1.5% of the symbol rate. This means that values of M as large as $\frac{3}{8\times0.015} = 25$ can safely be chosen. Therefore, if $\sigma^2_{\text{eq-len}}$ is sufficiently small for $N \leq 37$, $M_{\text{opt}} = \text{round}(2N/3)$ can be used for M. In the event that a smaller variance is required, the variance $\sigma^2_{\text{eq-len}}$ can be further reduced by using $M = N - M_{\text{opt}}$ to allow values of N up to 75 symbols. In either case, it is desirable to make M as large as possible in order to facilitate channel estimation.
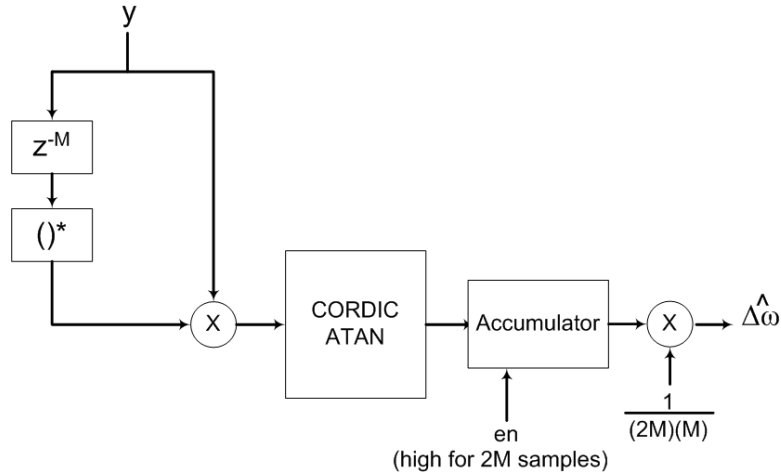
Figure 4.5 Block diagram of proposed frequency offset estimator.

Using the composite equal averaging-length estimator with a periodic preamble produces an ISI-resisting frequency offset estimator which is very well-suited to the DOCSIS upstram channel. The proposed implementation, shown in Figure 4.5, utilizes a preamble of length $3M$ which is made up of three repetitions of an $M-$symbol sequence. Although any $M-$symbol sequence will mitigate the effects of ISI, a sequence which produces a relatively even spectral distribution of energy, such as a Barker sequence [30] is recommended for channel estimation purposes.

Due to the fact that the period of the preamble is equal to the width of the differential detector, no symbol phase compensation is required at the CORDIC output, since $a_n a_{n-M}^*$ has a constant value.

Simulation Results

Two computer simulations have been performed in order to verify the performance of the proposed frequency offset estimator. The first simulation was designed to verify the performance of the estimator in the absence of ISI. In this simulation, a series of packets containing a 33-symbol preamble consisting of three repetitions of an 11-symbol Barker code was input to the frequency estimator depicted in Figure 4.5. AWGN was added to each incoming packet in order to model the input to the fre-
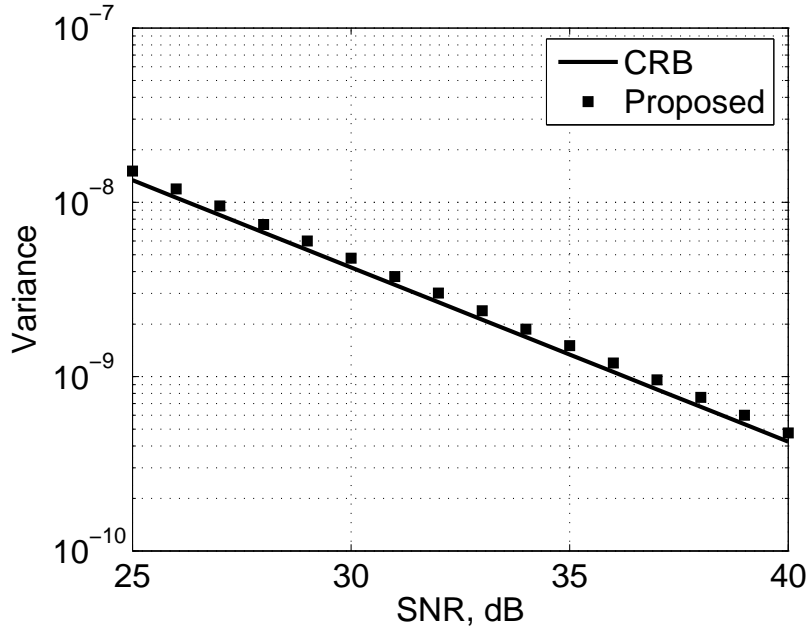
Figure 4.6   Variance of proposed frequency offset estimator.

quency estimator. The level of the noise was set to achieve a range of SNR values typical of DOCSIS upstream packets in real cable networks, but no ISI was injected. For each SNR, 50,000 packets were processed and the variance of the frequency offset estimator was computed from these estimates.

The results of this simulation are summarized in Figure 4.6. It is clear from these results that the proposed estimator has a variance which is approximately 0.5dB worse than the CRB, as expected. The simulation also verified that the proposed estimator is unbiased.

The high-level purpose of the second simulation was to verify the ISI immunity claimed in Section 4.4.2. More concretely, the simulation was designed to highlight the advantage provided by the proposed estimator over the Kay, M&M, and L&R estimators in terms of the variety of preamble sequences over which each is unbiased. As before, this test consisted of passing a large number of packets with appropriate SNRs to the frequency estimators. Each incoming packet was passed through a symbol-rate ISI equivalent filter whose coefficients were chosen in accordance with
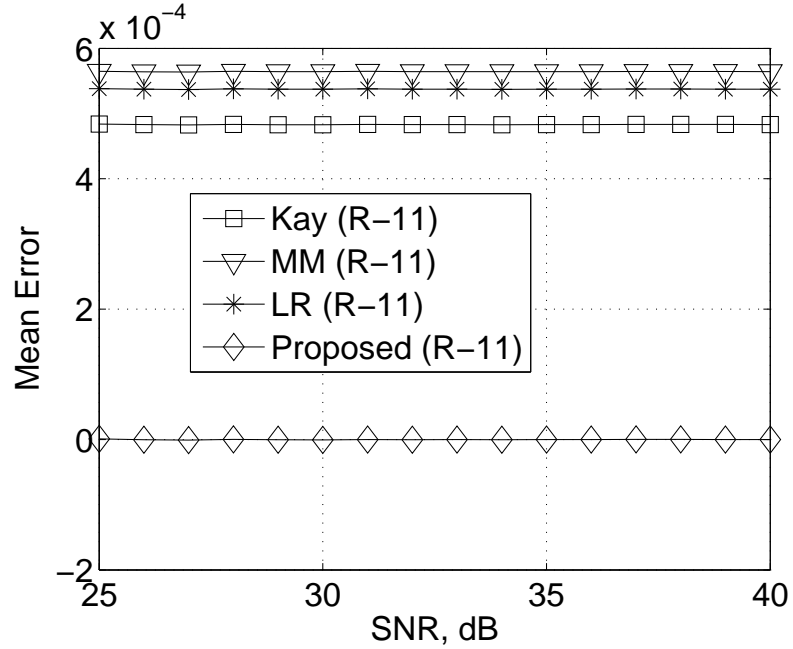
Figure 4.7 Means of proposed estimator and three well-known estimators in first ISI channel.

a worst-case set of upstream micro-reflections. The characteristic parameters of the three simulated micro-reflections are summarized in Table 5.1.

Table 4.1 First channel model for ISI simulation.

Amplitude (dBc)	Delay (sym)	Carrier Phase (rad)
-10	2.5	$\pi/3$
-20	5	π
-30	7	$-\pi/2$

For this test, each of the four estimators were applied to each of the modeled incoming packets, allowing any differences in the performance of the estimators to be tracked. The test was repeated twice: once using a preamble consisting of a single symbol repeated 33 times (labelled R-1 in the results), and once using a preamble consisting of three repetitions of a more desirable 11-symbol Barker sequence (labeled R-11).

The results of this simulation, some of which are shown in Figures 4.7 and 4.8,

67
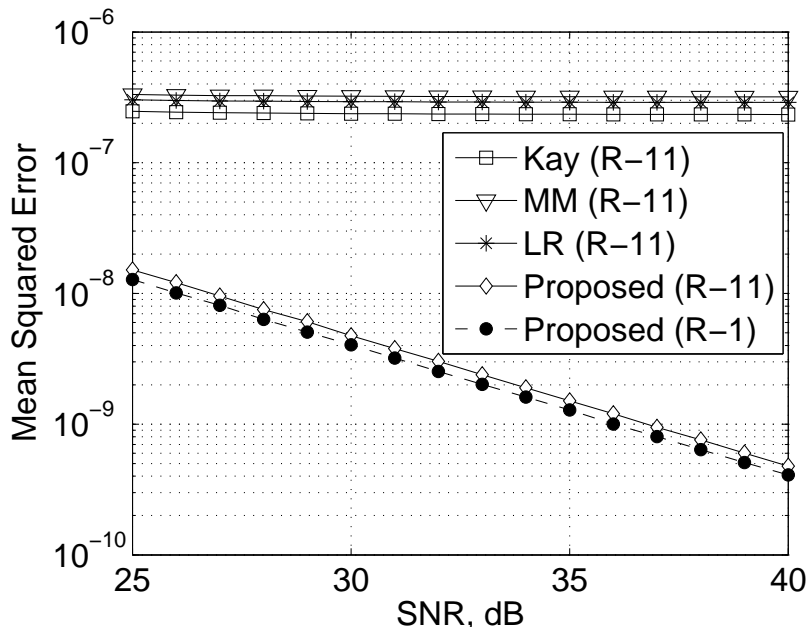
Figure 4.8 Mean squared errors of proposed estimator and three well-known estimators in first ISI channel.

were in agreement with the theory presented in Section 4.4.2. Although not shown in the figures, all of the estimators were immune to ISI when all 33 symbols in the preamble were the same, as predicted. However, Figure 4.7 indicates that only the proposed estimator is unbiased for the 11-symbol Barker sequence. When the well-known estimators were used with the Barker sequence, they acquired a significant bias. It is apparent from Figure 4.8 that this bias term tends to dominate the MSE for higher SNRs. Consequently, the proposed estimator has a decided advantage over the three incumbents in channels with significant ISI.

It is interesting to notice in Figure 4.8 that the MSE of the proposed estimator is slightly worse with the Barker sequence than the constant preamble. This occurred because the channel happened to have a magnitude response containing a peak near the center of the channel bandwidth, which is where the transmitted energy is concentrated for the constant preamble. In contrast, if the channel's magnitude response happened to have a dip near the center of the channel, one would expect the Barker sequence to outperform the constant preamble. To verify this, a second 'worst-case'
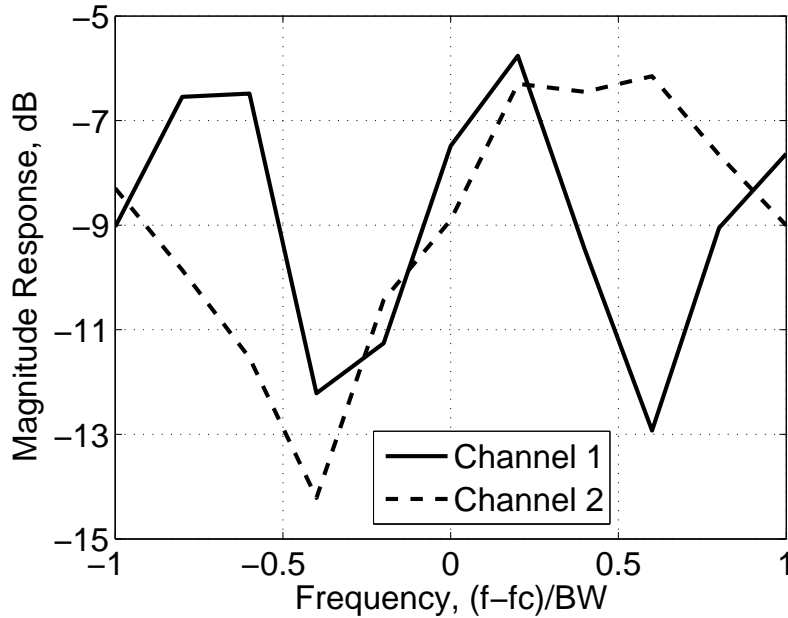
Figure 4.9 Magnitude responses of simulated ISI channels.

channel was generated: The frequency responses of the two simulated channels are

Table 4.2 Second channel model for ISI simulation.

Amplitude (dBc)	Delay (sym)	Carrier Phase (rad)
-10	1.25	$\pi/2$
-20	5	π
-30	7	π

shown in Figure 4.9.

The simulation was repeated using this second channel, yielding the results shown in Figures 4.10 and 4.11. As with the initial channel, the three well-known estimators became significantly biased when a Barker sequence was transmitted, while the proposed estimator did not. It is obvious from Figure 4.11 that the proposed estimator once again has a decided performance advantage over the three well-known estimators. Finally, it may also be seen in Figure 4.11 that the Barker sequence outperforms the constant sequence for this second channel, as expected.
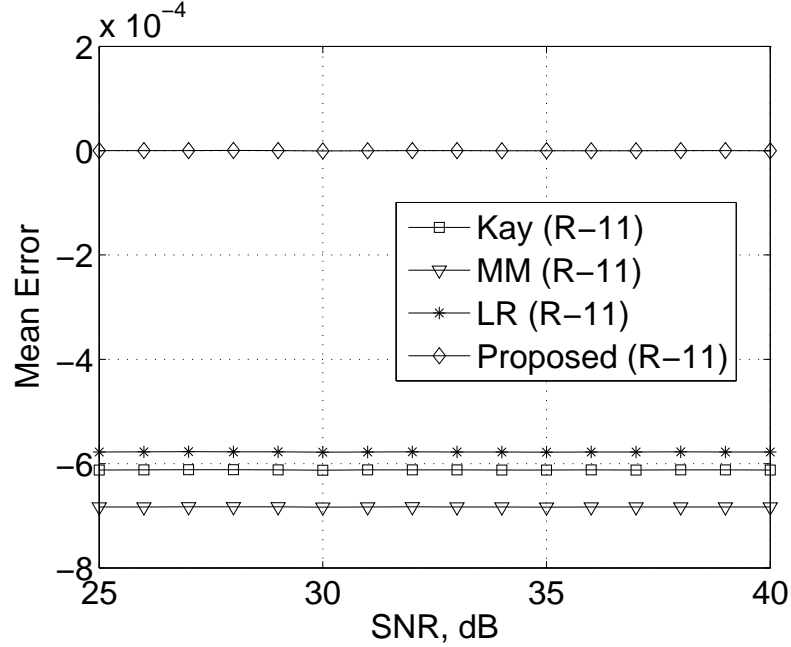
Figure 4.10 Means of proposed estimator and three well-known estimators in second ISI channel.

Frequency Offset Correction

Once the frequency offset has been estimated for a received packet, correcting for this offset is a relatively simple process. In order to do so, it is necessary to multiply the input to the frequency offset estimator, $y_f[n]$, by a complex sinusoid with a frequency equal to the negative of the estimated frequency offset, as shown in equation (4.61):

$$
\begin{aligned}
y_{fc}[n] &= y_f[n] \cdot e^{-j\widehat{\Delta\omega}n} \\
&= (a_n e^{j(\Delta\omega n + \phi_o)} + \eta[n]) \cdot e^{-j\widehat{\Delta\omega}n} \\
&= a_n e^{j(\omega_e n + \phi_o)} + \eta[n]'
\end{aligned}
\tag{4.61}
$$

where the subscript fc in $y_{fc}[n]$ indicates 'frequency corrected', $\omega_e = \Delta\omega - \widehat{\Delta\omega}$ and $\eta'[n] = \eta[n]e^{-j\widehat{\Delta\omega}n}$. Since $\eta'[n]$ is a rotation of a sequence of random variables $\eta[n]$ which have circular symmetry, the statistics of $\eta'[n]$ and $\eta[n]$ are identical. Note that a residual frequency offset term equal to the error in frequency estimate still
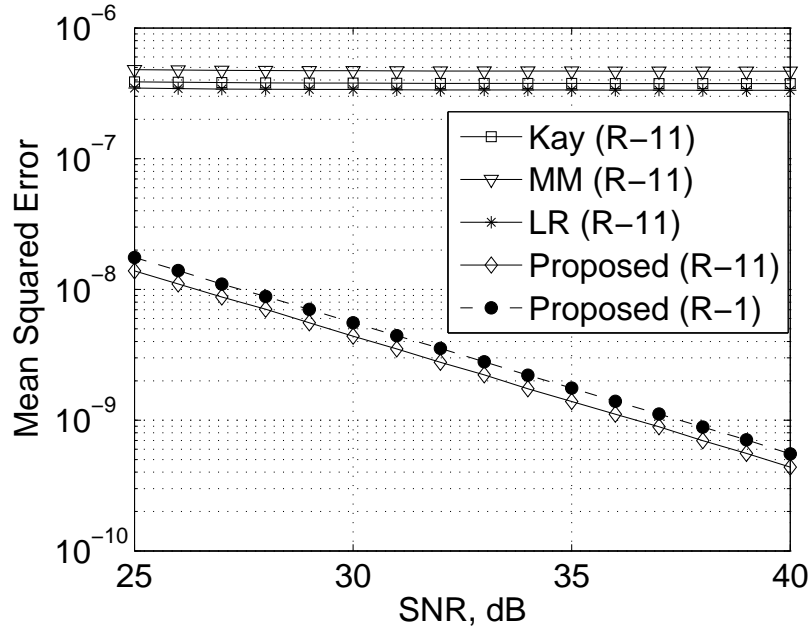
Figure 4.11 Mean squared errors of proposed estimator and three well-known estimators in second ISI channel.

remains in the expression for $y_{fc}[n]$. However, this residual error will typically be much smaller than the initial frequency offset.

The hardware structure used to implement this frequency offset correction is shown in Figure 4.12. As depicted in the figure, a numerically controlled oscillator (NCO) is typically used to generate the complex sinusoid required for derotation.
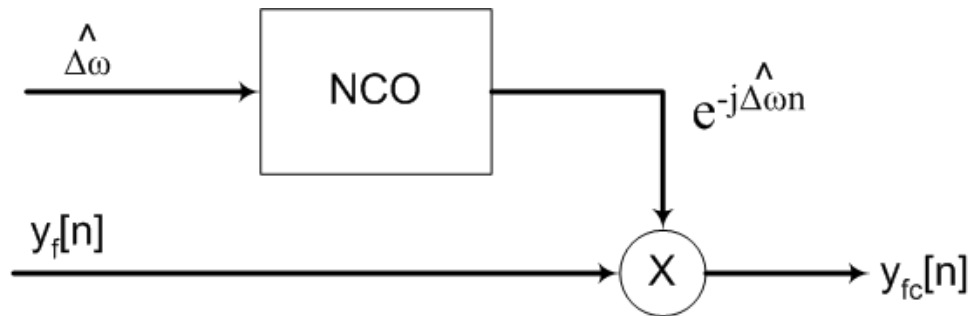
Figure 4.12 Block diagrm of circuit used to correct for frequency offset.

4.5 Phase Estimator

After the frequency offset has been estimated, the phase estimation problem is greatly simplified. The input to the phase estimation circuit is taken to be the output of the frequency correction circuit, $y_{fc}[n]$. Since the residual frequency offset in $y_{fc}[n]$ is very small, it may be neglected, allowing the input to the phase estimation circuit, $y_{pi}[n]$, to be approximated as follows:

$$y_{pi}[n] = a_n e^{j\phi_o} + \eta[n]' \approx y_{fc}[n] \tag{4.62}$$

where the subscript pi in $y_{pi}[n]$ is used as a shorthand for 'phase estimator input'.

The task of the phase estimator is made easier if the phase modulation due to the preamble symbols is removed. It is possible to remove the modulation during the preamble component of the packet, since the transmitted symbols, a_n, are known. Multiplying by a_n^* removes the phase modulation:

$$y_{pu}[n] = a_n^* y_{pi}[n] = e^{j\phi_o} + \eta[n]'' \tag{4.63}$$

where $\eta[n]''$ is a rotated version of the noise, which has the same statistics as $\eta[n]'$. The subscript pu on y_{pu} in equation (4.63) is shorthand for 'phase estimator unmodulated'.

The phase estimation CRB was derived for the case where $\Delta\omega$ and ϕ_o were both unknown parameters in Section 4.2. The Fisher information matrix for that case is given by equation (4.20) on page 47 and its inverse is given by equation (4.21) on page 47. The element in row 2, column 2 of (4.21) provides a lower bound on the variance of the phase estimator when both the frequency offset and phase offset are unknown.

However, in this case, the frequency offset is taken to be 0, so the input signal $y_{pu}[n]$ has only ϕ_o as a parameter. Thus, the CRB for the individual phase estimator may be found by inverting the 1x1 Fisher information matrix involving only the phase. The value of this 1x1 matrix is the 'phase' entry in the Fisher information matrix of (4.20) (which is located in row 2, column 2). Thus, the CRB for the phase estimator

is:

$$\text{var}(\widehat{\phi}_o) \geq 1/\left[I(p)\right]_{22} = \frac{1}{(2N)SNR} \tag{4.64}$$

This lower bound is about a factor of 4 lower than that of equation (4.64), which is the variance of the phase estimator for the case of simultaneous estimation of both frequency and phase offset.

4.5.1 Maximum Likelihood Estimator

As before, the first logical step in searching for an estimator is to apply the maximum likelihood technique. The likelihood and log-likelihood functions of the unmodulated phase estimator input, which is $y_{pu}[n]$, are:

$$f_{y_{pu}}(y_{pu}; \phi_o) = \left(\frac{1}{\pi\sigma^2}\right)^N e^{\frac{-1}{\sigma^2}\sum_{n=0}^{N-1}|y_{pu}[n]-e^{j\phi_o}|^2} \tag{4.65}$$

$$\Lambda_{y_{pu}}(y_{pu}; \phi_o) = N \cdot \ln\left(\frac{1}{\pi\sigma^2}\right) + \frac{-1}{\sigma^2}\sum_{n=0}^{N-1}|y_{pu}[n] - e^{j\phi_o}|^2 \tag{4.66}$$

The ML estimator is found by setting the derivative of the log-likelihood function with respect to ϕ_o equal to zero:

$$\frac{\partial \Lambda_{y_{pu}}(y_{pu}; \phi_o)}{\partial \phi_o} = \frac{-1}{\sigma^2}\sum_{n=0}^{N-1}(-jy_{pu}[n]^*e^{j\phi_o} + jy_{pu}[n]e^{-j\phi_o}) = 0 \tag{4.67}$$

Equation (4.67) implies that:

$$\sum_{n=0}^{N-1} y_{pu}[n]^*e^{j\phi_o} = \sum_{n=0}^{N-1} y_{pu}[n]e^{-j\phi_o} \tag{4.68}$$

which requires:

$$e^{j2\phi_o} = \frac{\sum_{n=0}^{N-1} y_{pu}[n]}{\sum_{n=0}^{N-1} y_{pu}[n]^*} \tag{4.69}$$

Solving equation (4.69) for ϕ_o yields the ML estimator:

$$\widehat{\phi}_{oML} = \angle\left(\sum_{n=0}^{N-1} y_{pu}[n]\right) \tag{4.70}$$

$$\widehat{\phi}_{oML} = \tan^{-1}\left(\frac{\Im(\sum_{n=0}^{N-1} y_{pu}[n])}{\Re(\sum_{n=0}^{N-1} y_{pu}[n])}\right) \tag{4.71}$$

73
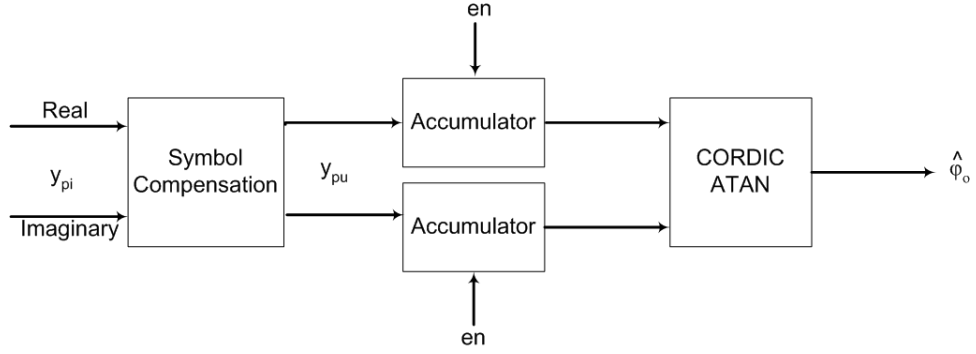
Figure 4.13 Hardware implementation of the maximum likelihood phase offset estimator.

4.5.2 Estimator Selection

Fortunately, this ML estimator is simple and inexpensive to implement from a hardware perspective. As shown in Figure 4.13, the implementation requires two accumulators which sum the real and imaginary components of the input signal and a single CORDIC inverse tangent block.

In general, ML estimators tend to achieve the CRB for high SNRs and large preamble lengths. As discussed previously, the minimum SNR in a DOCSIS upstream channel is specified as 25dB, which certainly qualifies as high. Thus, the ML phase estimator should provide nearly optimal performance in DOCSIS upstream channels. This fact, coupled with the observation that the ML phase estimator has a very simple hardware implementation suggests there is no need to continue the search for a phase estimation algorithm.

The proposed phase estimator uses the final two repetitions of the 11-symbol differentially-encoded Barker code in order to estimate the phase offset. Thus, the variance is:

$$\text{var}(\widehat{\phi}_o) = \frac{1}{44 \cdot SNR} \quad \text{radians}^2 \tag{4.72}$$

74

4.5.3 Estimator Analysis

The derivation above assumed that the error in the frequency offset estimate is equal to 0. In reality, this is not the case. Rather, a small residual frequency error is likely to be present at the input to the phase recovery circuit due to the random influence of AWGN on the frequency recovery circuit. As a result, the input signal to the ML phase estimator has the form

$$y_{puf}[n] = e^{j\phi_o + n\omega_e} + \eta[n]''$$ (4.73)

where the subscript puf in y_{puf} is shorthand for 'phase estimator unmodulated with frequency offset', and ω_e is the residual frequency offset error. The resulting output from the ML estimator is:

$$
\begin{aligned}
\widehat{\phi}_{oML} &= \angle \left(\sum_{n=0}^{N-1} y_{puf}[n] \right) \\
\widehat{\phi}_{oML} &= \angle \left(\sum_{n=0}^{N-1} e^{j\phi_o + n\omega_e} + \eta[n]'' \right) \\
\widehat{\phi}_{oML} &= \phi_o + \angle \left(\sum_{n=0}^{N-1} e^{jn\omega_e} + \eta[n]'' \right)
\end{aligned}
$$ (4.74)

Since ω_e is very small, we may replace $e^{jn\omega_e}$ in equation (4.74) with its first-order Taylor series approximation, which is $1 + jn\omega_e$.

$$
\begin{aligned}
\widehat{\phi}_{oML} &= \phi_o + \angle \left(\sum_{n=0}^{N-1} 1 + jn\omega_e + \eta[n]'' \right) \\
\widehat{\phi}_{oML} &= \phi_o + \angle \left(N + j\frac{N(N-1)\omega_e}{2} + \sum_{n=0}^{N-1} \eta[n]'' \right)
\end{aligned}
$$ (4.75)

The expected value of equation (4.75) is:

$$
\begin{aligned}
E[\widehat{\phi}_{oML}] &= \phi_o + \angle \left(N + j\frac{N(N-1)}{2}\omega_e \right) \\
E[\widehat{\phi}_{oML}] &= \phi_o + \tan^{-1} \left(\frac{N(N-1)}{2N}\omega_e \right)
\end{aligned}
$$ (4.76)

Equation (4.76) may be simplified using the approximation $\tan(x) \approx x$, which is valid for small angles, yielding the result:

$$E[\widehat{\phi}_{oML}] \approx \phi_o + \frac{N-1}{2}\omega_e$$ (4.77)

It is apparent from equation (4.77) that the ML phase estimator is biased when a residual frequency offset is present. The magnitude of this bias is approximately $\frac{N-1}{2}\omega_e$ radians.

It is worthwhile to consider the mean squared error of the phase estimator when this bias is included. Assuming that the frequency estimator and the phase estimator are independent, the overall mean squared error of the system may be written as the sum of the variances as follows:

$$
\begin{aligned}
\text{MSE}_{\phi_o} &= \text{var}(\widehat{\phi}_o) + \left(\frac{N-1}{2}\right)^2 \cdot \text{var}(\omega_e) \\
\text{MSE}_{\phi_o} &= \frac{1}{(2N_p)SNR} + \left(\frac{N_p-1}{2}\right)^2 \cdot \frac{27}{4N_f^3 \text{SNR}}
\end{aligned}
\tag{4.78}
$$

where the number of samples used by the phase and frequency estimators are N_p and N_f respectively. The variances for the phase and frequency estimators, given by equations (4.64) and (4.55) have been substituted into equation (4.78). The proposed estimators have $N_f = 1.5N_p$, which results in $\text{MSE}_{\phi_o} \approx \frac{1}{N_p SNR}$, which is a factor of 2 higher than the case where no residual frequency error is present.

As with frequency offset estimation, any potential ISI in the upstream channel will tend to bias the phase offset estimator. In the frequency estimator, it is possible to avoid this bias by using a wide differential detector and by choosing the preamble carefully. However, in the case of phase estimation, there does not appear to be an easy way to eliminate this bias. The extent of this bias will be discussed in the following section.

4.5.4   Simulation Results

The performance of the proposed phase offset estimation algorithm has been verified through three sets of MATLAB simulations, which are discussed below. In each of the simulations, 10,000 DOCSIS upstream packets with random timing, frequency, and phase offsets were generated and passed to the demodulator under test. As in the case of the frequency offset simulations discussed previously, the preamble used for these packets consisted of three repetitions of an 11-symbol differentially-encoded
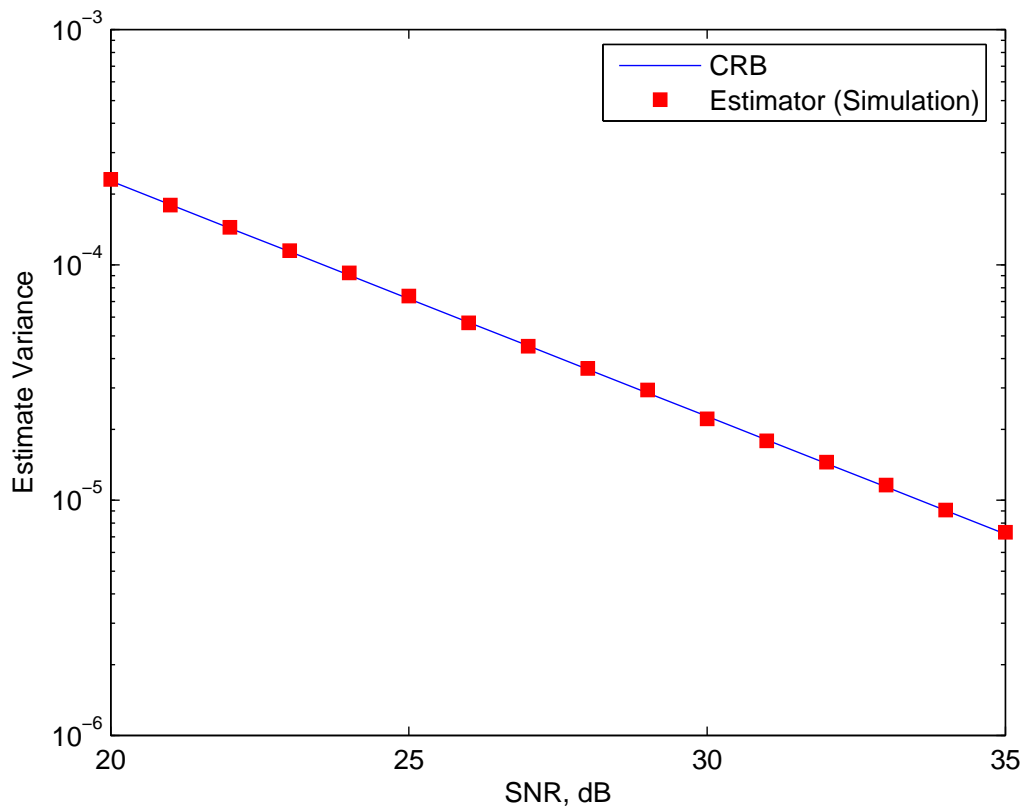
Figure 4.14 Variance of proposed phase estimation algorithm with no residual frequency offset and no channel ISI.

Barker sequence. The phase estimator operated using the final two of these Barker sequences.

The purpose of the initial simulation was to confirm that the proposed phase offset estimator works properly if no residual frequency offset and no channel ISI are present on its input signal. Thus, the output of the timing recovery circuit was passed directly to the frequency correction block, bypassing the frequency estimator. The correct frequency offset was passed to the frequency correction block, ensuring that no residual frequency offset was passed to the phase estimator. The resulting performance of the phase estimator is shown in Figure 4.14, along with the CRB for phase estimators. It is clear from this figure that the phase estimator essentially achieves the bound under these nearly-ideal conditions.
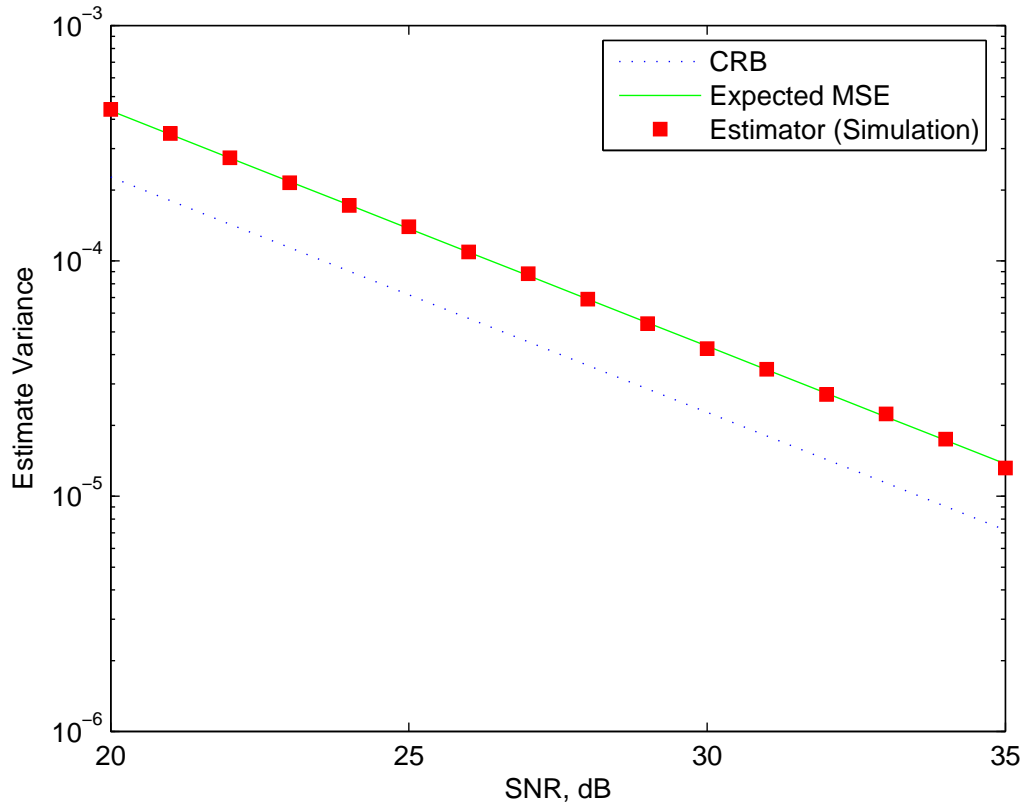
Figure 4.15 Variance of proposed phase estimation algorithm with typical residual frequency offset and no channel ISI.

A second simulation was performed in which the phase offset estimator operated using the output from the proposed frequency offset estimator. The purpose of this simulation was to investigate the effect of residual frequency error on the phase estimator. For this simulation, the demodulator performed timing, frequency, and phase compensation just as it would in a real DOCSIS system, although the channel was taken to be perfect so there was no ISI. The results of this simulation, presented in Figure 4.15, validate the residual frequency error theory presented in Section 4.5.3. As expected, the results indicate that the small amount of residual frequency error at the output of the frequency correction circuit causes the MSE of the proposed phase estimator to increase by a factor of approximately 2.

The final simulation attempted to quantify the effect of typical DOCSIS upstream

channel ISI on the proposed phase offset estimator. In this simulation, the received packet was modeled as noise-free, which should theoretically allow the phase offset estimator to work perfectly. However, a channel with three random echoes with the maximum amplitudes allowed by the DOCSIS standard was incorporated into the model that generated the received packet. The expectation was that each set of echoes would impart a channel-specific bias onto the phase estimator. Since no noise was present, any variation in the generated phase estimates may be attributed to this biasing effect of the channel ISI. The simulation used 10,000 sets of random echoes to generate 10,000 phase estimates, the observed variance of which was .012 radians^2. This variability in the phase estimates indicates that the phase estimator can be biased by ISI, as expected. The bias may or may not be a concern, depending on the equalization algorithm which operates upon the phase estimator's output.

4.5.5 Phase Offset Correction

In order to compensate for a phase offset, the straightforward approach is to multiply the complex input signal by a complex number whose angle is equal to the negative of the phase offset:

$$y_{pc}[n] = y_{pi}[n]e^{-j\widehat{\phi_o}} \tag{4.79}$$

$$y_{pc}[n] = a_n e^{j\phi_o} e^{-j\widehat{\phi_o}} + \eta[n]'e^{-j\widehat{\phi_o}} \tag{4.80}$$

$$y_{pc}[n] = a_n e^{j(\phi_o - \widehat{\phi_o})} + \eta[n]''' \tag{4.81}$$

where the subscript pc is shorthand for 'phase corrected', and $\eta[n]''' = \eta[n]'e^{-j\widehat{\phi_o}}$. This operation requires one complex multiplication per input sample.

In order to implement equation (4.79) in hardware, a look-up-table (LUT) is typically used to map a given $\widehat{\phi}_o$ to the corresponding complex number $e^{-j\widehat{\phi_o}}$, as shown in Figure 4.16.

In a DOCSIS system, it is not possible to send a phase adjustment to the transmitter in response to a ranging packet. Consequently, the receiver needs only to correct for the phase offset, rather than acually computing the value of $\widehat{\phi}_o$. The cor-
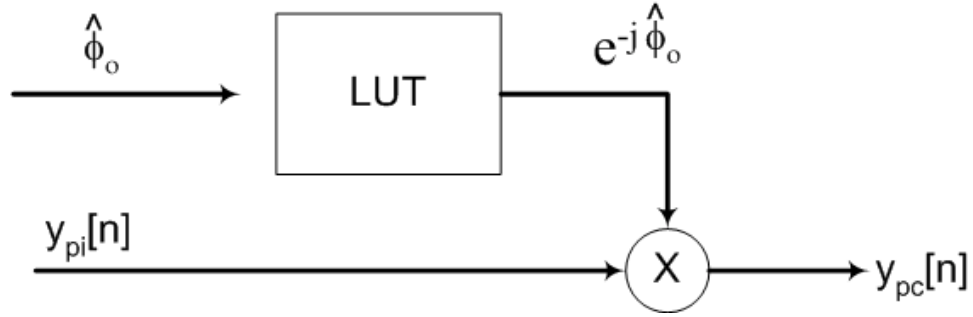
Figure 4.16 Block diagrm of circuit used to correct for phase offset.

rection is performed by multiplying $y_{pi}[n]$ with $e^{-j\widehat{\phi_o}}$, as indicated by equation (4.79). The complex constant $e^{-j\widehat{\phi_o}}$ can be obtained directly using equation (4.69), with the result:

$$e^{-j\widehat{\phi_o}} = \frac{1}{N} \sum_{n=0}^{N-1} y_{pu}[n]^*$$ (4.82)

Note that the output of the summation is scaled by a factor of $\frac{1}{N}$ to ensure the magnitude of the resulting complex number is unity. In practice, this implementation of the phase correction is preferable, as it computes the required correction vector directly. Computing $e^{-j\widehat{\phi_o}}$ with (4.82) eliminates the need for the CORDIC inverse tangent block shown in Figure 4.13 as well as the LUT shown in Figure 4.16.

5. Equalization

5.1 Introduction

As shown in Figure 3.7, the final block in the proposed upstream demodulator is the equalizer, which operates upon the output of the frequency and phase correction circuits. The purpose of the equalizer is to remove any remaining distortion from the received signal so that it can be accurately mapped to the original sequence of transmitted symbols.

The problem of ISI corrupting a received signal and causing degradation to the overall system performance is certainly not unique to the DOCSIS upstream channel. Accordingly, equalization techniques which are capable of mitigating the effects of ISI have been well-studied in the open literature. In general these techniques may be broken down into two main categories: static equalizers and adaptive equalizers. Both types of equalizers essentially perform a filtering operation upon the incoming signal in order to remove ISI. The difference is that the coefficients of an adaptive equalizer can vary over time in order to track changes to the channel. In contrast, the coefficients of a static equalizer are fixed.

For upstream DOCSIS channels, the impulse response of the channel differs for each CM and is not known initially, so the filter coefficients for the equalizer must be computed based upon observations of the incoming signal. Additionally, it is possible for the channel impulse response to change over time, either due to oscillator drift or changes to the actual physical topology of the cable network. For these reasons, it is preferable to use an adaptive equalizer in the upstream receiver, rather than a static

equalizer.

DOCSIS specifies that each cable modem should pre-equalize its upstream transmissions using a 24-tap linear equalizer. It is the responsibility of the CMTS to determine the required pre-equalizer tap values during the modem initialization process and to send these values to the cable modems via a downstream channel. The CMTS demodulator determines the pre-equalizer coefficients for each upstream channel through the use of an adaptive equalizer.

As mentioned in the introduction, when a cable modem first attempts to connect to the network, an initialization process takes place. This initialization process requires the cable modem to transmit a packet with a known preamble, the length and content of which is specified by the CMTS. This preamble is used in the CMTS for several functions: to train the adaptive equalizer, recover symbol timing, and recover the carrier. Since training the equalizer is the most difficult and computationally intensive of these functions, the total required preamble length is largely determined by the convergence time of the equalizer.

The time required for an adaptive equalizer to converge depends largely upon the algorithm used to adapt the coefficients. The two main classes of algorithms used for this task are least mean squares (LMS) algorithms and recursive least squares (RLS) algorithms. RLS-based algorithms tend to converge more quickly than LMS algorithms, but suffer from a major downside: they are much more complex to implement. In general, for each update, RLS-based algorithms require a number of multiplications proportional to N^2, where N is the number of coefficients in the equalizer, whereas the number of multiplications required for an LMS-based algorithm is proportional to N. In the case of a DOCSIS upstream receiver, $N = 24$, so the difference between these two algorithms in terms of implementation complexity is dramatic.

A considerable amount of research, such as [31], [32], and [33] has been focused on so-called 'fast-RLS' techniques, which attempt to decrease the computational complexity of RLS equalizers. Although this work has been very successful, the resulting

algorithms are still 3-5x more expensive to implement than the basic LMS. Furthermore, fast-RLS equalizers tend to be prone to finite precision effects, leading to instability [21]. Additional circuitry is frequently required in order to combat this problem, further increasing the hardware cost. Overall, while the use of an RLS equalizer may be practical in an ASIC-based demodulator, an FPGA-based implementation is likely limited to the use of the LMS algorithm.

The objective of the research discussed in this chapter is to get around this limitation by increasing the convergence speed of an LMS-based equalizer. The approach to achieving this goal is to coarsely estimate an ISI equivalent for the channel using a special short 'excitation word' placed at the beginning of the training sequence. The ISI equivalent of the channel is then crudely inverted to initialize ('seed') the adaptive equalizer. Seeding the equalizer shortens the length of training sequence needed, which reduces the overhead in the packets and increases the efficiency of the upstream channel.

5.1.1   Previous Work

The operation of adaptive equalizers is well-known [19], [21], and much work has been done to analyze their performance. However, little work has been published with the specific goal of optimizing adaptive equalizers for up-stream DOCSIS channels. Wolf and Gatherer [34] investigated low complexity equalizers in cable modems for downstream channels. They determined that the most effective low complexity equalizer was a 12 complex-tap equalizer that used a least mean square (LMS) algorithm to update the taps. Some of the rationale had its roots in work done previously by Gatherer [35], which deals with the effect of micro-reflections on fractionally-spaced decision feedback equalizers. More recently, Kim et al. [36] suggested an LMS-updated 24-tap linear equalizer be used if the intent was to send the tap weights to a pre-equalizer. Dluna et al. [37] proposed a sign-LMS decision feedback equalizer with 24 feedback taps and 8 feed-forward taps for use in a single-chip cable set-top box.

The convergence behavior of the LMS and sign-LMS algorithms is discussed in [19].

While these algorithms are desirable from an implementation perspective due to their low complexity, their slow convergence, which demands a relatively long training sequence, is known to be a disadvantage.

Sellars et al. [38] looked at decreasing the convergence time for the equalization of an indoor radio channel. They proposed seeding the equalizer with tap weights determined from a power ratio approximation scheme to initialize decision feedback equalizer tap values. Ysebaert et. al [39] found that by combining the LMS and RLS algorithms, the convergence time of a discrete multitone modulation receiver's equalizer was reduced. Yet another way to decrease convergence time was proposed by Lee et al [40]. Their approach was based on changing the statistics of the equalizer input.

Wang and Kraemer [41] looked at initializing a decision feedback equalizer for the purpose of reducing the convergence time. They estimated the channel with a cyclic correlation method and then initialized the equalizer with an inverse of the estimated channel.

The structure of the preamble can affect the convergence behavior of an equalizer. No literature on the relationship between preamble structure and convergence time was found. However, training sequence structures have been proposed. Kim et al. [36] proposed a preamble pattern for upstream cable modems and then developed synchronization and channel equalization schemes that utilized the proposed preamble pattern. Their proposed preamble consists of a concatenation of oversampled constant-amplitude, zero-autocorrelation (CAZAC) sequences of length 32. Wang and Speidel [28] created a preamble specifically for packet acquisition, which included packet detection, symbol timing estimation, carrier frequency offset estimation and carrier phase estimation, but did not include equalization.

One published work which appears to be fairly closely related to the current problem is that presented by harris and Dick (henceforth h&D) in [13]. In the cited paper, the authors proposed a technique for determining the initial coefficients of an adaptive
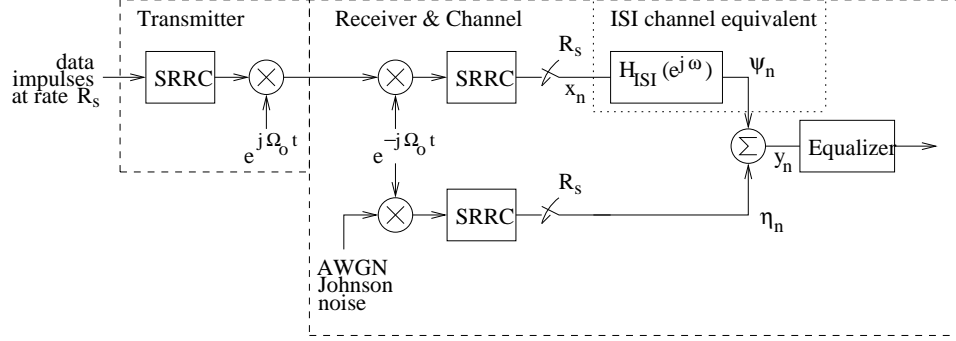
Figure 5.1 Model of the end-to-end system.

equalizer. The technique consists of transmitting a pair of 32-chip complementary code spreading sequences to estimate the channel impulse response, then computing the equalizer's coefficients using the well-known normal equations discussed in [19].

5.1.2 Problem Formulation

For purposes of analysis, the system will be modeled as shown in Figure 5.1. In the model, the upstream channel has been removed from its rightful location and placed (in a different form) inside the receiver. The channel is labeled $H_{ISI}(e^{j\omega})$, which is a discrete time finite impulse response filter that runs at the symbol rate. It is placed after the square root raised cosine (SRRC) filter. The channel filter, which is referred to as the ISI equivalent filter, models the ISI caused by the upstream channel.

Since the Johnson noise at the front end of the receiver does not go through the upstream channel, it is modeled as a separate path in the receiver and then added to the output of the channel equivalent filter. The noise samples are denoted by η_n.

DOCSIS specifies the maximum echo strength seen in an upstream channel as a function of the echo delay. The echo strength can be as high as -10dBc for delays up to 0.5 μs, -20dBc for delays between 0.5 and 1 μs and -31.5dBc for delays greater than 1 μs.

The ISI equivalent filter is shown as a transversal filter in Figure 5.2. The filter is driven at the symbol rate, i.e., z^{-1} is a delay of one symbol interval. The theoretical
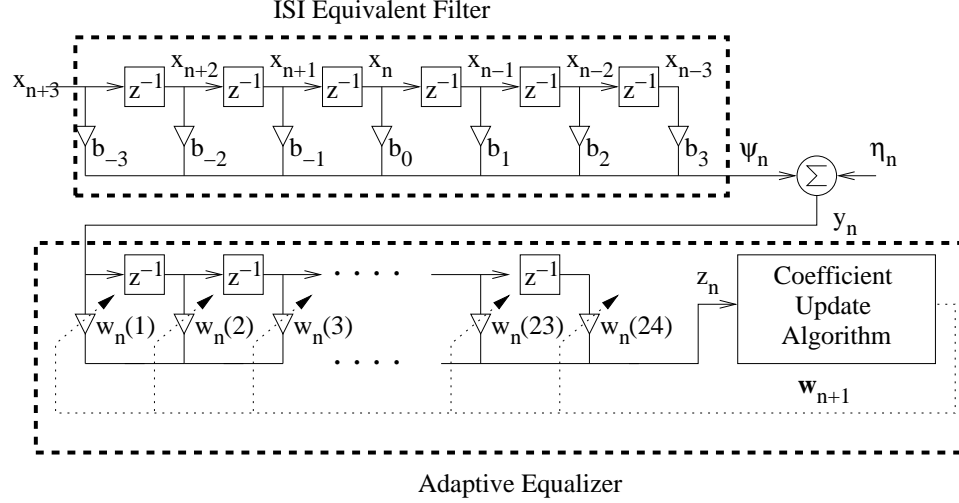
Figure 5.2 ISI model and adaptive equalizer.

length of this filter is the sum of the lengths of the impulse responses of the channel, the pulse shaping filter, and matched filter, all measured in symbol intervals. The coefficients for the filter are given by $h_{channel}(t) \star h_{pulse\_shaping}(t) \star h_{matched}(t)|_{t=t_o+nT}$ where $t_o + nT$ marks the times at which the output of the SRRC filter is sampled to get the decision variables. This is a causal filter, but is shown as a non-causal filter in Figure 5.2 to simplify the notation. The input to the ISI equivalent filter is referred to as a sequence of pristine decision variables x_n, which are the decision variables in the absence of channel distortion and Johnson noise. The outputs of the ISI equivalent filter, denoted by ψ_n, are the pristine decision variables corrupted by channel distortion. The subscript n on all variables indicates time in symbols with respect to t_o.

The ISI equivalent filter is an FIR filter of length $L_1 + L_2 + 1$ with coefficients

$$b_{-L_1}, b_{-L_1+1},\ \dots\ , b_{-1}, b_0, b_1,\ \dots\ , b_{L_2},$$

where b_0 corresponds to the direct, unreflected path from CM to CMTS. b_0 is the largest of the coefficients and is referred to as the main tap or main path. L_1 and L_2 represent the number of pre-main path coefficients and post-main path coefficients respectively. In the event the channel has no echoes, then all coefficients except b_0 are zero and $b_0 = 1$. The output of the ISI equivalent filter is then $\psi_n = x_n$.

As shown in Figure 5.2, the input to the equalizer is a noise-corrupted version of the ISI equivalent filter's output. This signal, which is denoted y_n, is modeled as follows:

$$y_n = \sum_{k=-L_1}^{L2} x_{n-k} b_k + \eta_n \tag{5.1}$$

The overall structure of the feedforward equalizer is also shown in Figure 5.2. As shown in the figure, an adaptive algorithm is used to update the tap weights of the 24-tap linear equalizer. The error in the decision variable for the nth symbol is given by

$$e_n \quad = \quad x_n - z_n, \tag{5.2}$$

where x_n is the transmitted symbol and z_n is the corresponding equalizer output. As previously discussed, for an FPGA-based implementation, the equalizer's taps will be updated iteratively using the LMS algorithm:

$$\mathbf{w}_{n+1} \quad = \quad \mathbf{w}_n + \Delta \mathbf{y}_n e_n^*, \tag{5.3}$$

where Δ is the step size, $\mathbf{w}_n = [w_n(1), w_n(2), \ldots, w_n(24)]^T$ is a vector of tap weights, and $\mathbf{y}_n = [y_{n-7}, y_{n-6}, \ldots, y_{n+16}]^T$ is a vector of 24 consecutive inputs to the equalizer. The output of the equalizer is $z_n = \mathbf{w}_n^T \mathbf{y}_n$ for the nth symbol.

In the absence of channel information, LMS equalizers are typically initialized to have one of the taps unity and the others zero. By updating the coefficients iteratively according to equation (5.3), the equalizer eventually settles on a set of coefficients $\mathbf{w^o}$ which are optimal for the upstream channel. However, if the optimal coefficients for an upstream channel are significantly different from the initialization values $\mathbf{w_o}$, the convergence process may require many iterations.

Figure 5.3 illustrates the idea behind the proposed method for decreasing the convergence time of the upstream equalizer at a very abstract level. The fuzzy cloud in Figure 5.3 represents the 48-dimensional vector space (24 complex dimensions) in which the equalizer coefficient vector $\mathbf{w}$ lies. As illustrated in the figure, the proposed technique will attempt to initialize the equalizer with a set of coefficients which is
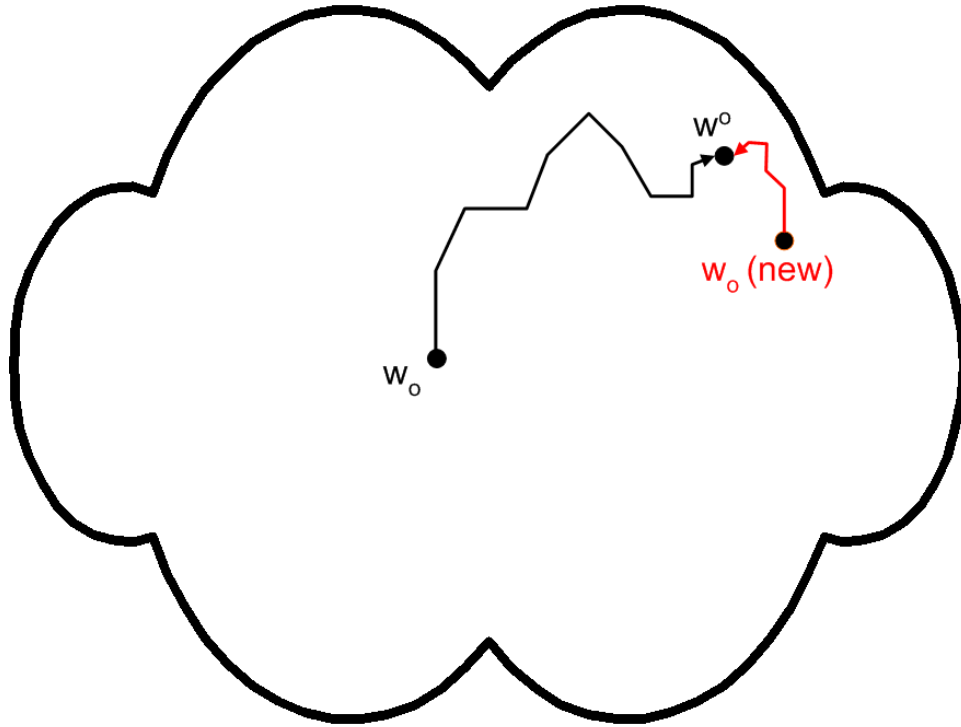
Figure 5.3 An abstract view of the idea behind the proposed equalizer seeding technique.

closer to the global minimim solution than the default starting point. Intuitively, one would expect that starting the equalizer from a position in the vector space which is closer to the optimal solution should speed up the convergence process..

At a high level, the proposed technique may be broken up into two main steps:

1. Estimate the coefficients of the ISI equivalent filter.

2. Determine an initial set of equalizer coefficients which partially compensates for the ISI caused by the filter coefficients estimated in step 1.

These two steps are considered in detail in Sections 5.2 and 5.3.

5.2   Estimation of the ISI Equivalent Filter Coefficients

The following sections will address the task of estimating the coefficients of the ISI equivalent filter. First, the 'intuitive' technique presented in [42] will be discussed in Section 5.2.1. Next, analysis is performed in order to determine an appropriate length for the ISI equivalent filter in Section 5.2.2. Linear channel estimation theory is introduced in Section 5.2.3. Section 5.2.4 then uses this linear estimation theory to propose a number of low-complexity estimators for the ISI equivalent filter. Finally, Section 5.2.5 briefly discusses the effect of phase offset on the proposed estimators.

5.2.1   Intuitive Method

In order to estimate the coefficients of the ISI equivalent filter, it is necessary to observe its output in response to a known input stimulus. The ISI equivalent filter coefficients can then be determined through algebraic manipulation of the observed output sequence. To facilitate this process, a carefully chosen excitation sequence of length M is embedded in the preamble.

In reality, the excitation word is filtered using the CM's pulse shaping filter prior to transmission. After being distorted by the channel, the signal enters the Nyquist filter in the receiver. The ISI equivalent filter hides these details, allowing the system to be conceptualized much more simply. Going forward, the (unfiltered) symbols of the excitation sequence will be considered to directly enter the ISI equivalent filter, the output of which is connected to the adaptive equalizer.

Both the performance and the complexity of the ISI estimator are affected by the choice of the excitation word. Given that the specific frequency response of the channel is unknown, it makes intuitive sense to select an excitation word sequence which distributes its transmitted energy relatively evenly across the channel bandwidth. One such discrete-time signal is the unit impulse (Kronecker delta) function,

89

i.e.:

$$\delta_n = \begin{cases} 1, & n = 0 \\ 0, & n \neq 0. \end{cases} \qquad (5.4)$$

The DOCSIS standard does not allow CMs to transmit symbols with zero energy, which precludes the selection of a Kronecker delta function as the excitation sequence. However, it is possible to select an excitation sequence which constitutes a Kronecker delta function with a DC offset. In order to do so, the M symbols in the excitation word must be such that their constellation points (i.e., the pristine decision variables x_n) are $\pm A e^{j\theta}$, where A and θ are constants. Such symbols can be generated from any square QAM constellation, including binary phase shift keying (BPSK). Without loss of generality and for reasons of notational convenience, A will be set to 1 and θ set to zero in the sequel. With these values, the M pristine decision variables take on values of ± 1.

To further simplify the notation, assume for the time being that the numbers of coefficients on each side of the main tap of the ISI equivalent filter are equal, ie. $L_1 = L_2$. This implies that the number of coefficients in the filter, which is $L = L_1 + L_2 + 1$, must be odd. These restrictions will be removed in Section 5.2.3 when the general case is considered.

If M is even, the sequence of interest generates the sequence $x_{-M/2}, \ldots, x_{M/2-1}$. Alternatively, for odd values of M, the sequence is $x_{-(M-1)/2}, \ldots, x_{(M-1)/2}$. In either case, all x_n are -1 except x_0, which is 1. In order to ensure that no symbols from before or after the excitation word can influence the estimator, the length of the excitation word must satisfy $M \geq 2L$, where L is odd and is the length of the ISI equivalent filter. For such an excitation sequence the output of the ISI equivalent filter is

$$\psi_n = \sum_{k=-(L-1)/2}^{(L-1)/2} x_{n-k} b_k; \quad \text{for } \frac{-(L+1)}{2} \leq n \leq \frac{(L-1)}{2} \qquad (5.5)$$

For $n = -(L+1)/2$, the summation over k in (5.5) does not include x_0, which means all values of x_{n-k} are -1. This has $\psi_{-(L+1)/2} = -\sum_{k=-(L-1)/2}^{(L-1)/2} b_k$. This allows

equation (5.5) to be expressed as

$$\psi_n = \begin{cases} -\sum_{k=-(L-1)/2}^{(L-1)/2} b_k; & \text{for } n = \frac{-(L+1)}{2} \\ 2b_n - \sum_{k=-(L-1)/2}^{(L-1)/2} b_k; & \text{for } |n| \leq \frac{(L-1)}{2}, \end{cases} \quad (5.6)$$

and thus

$$\psi_n = 2b_n + \psi_{-(L+1)/2}; \text{ for } |n| \leq \frac{(L-1)}{2}. \quad (5.7)$$

Rearranging (5.7) provides an equation for the coefficients b_n:

$$b_n = \frac{\psi_n - \psi_{-(L+1)/2}}{2}; \text{ for } |n| \leq \frac{(L-1)}{2}. \quad (5.8)$$

Figure 5.1 shows that ψ_n can be estimated with y_n. This provides the estimator:

$$\hat{b}_n = \frac{y_n - y_{-(L+1)/2}}{2} \text{ for } |n| \leq \frac{(L-1)}{2} \quad (5.9)$$

The quality of estimator $\hat{b}_n$ is determined by its mean and variance. The mean is found by taking the expectation of equation (5.9). It is evident from Figure 5.1 that $y_n = \psi_n + \eta_n$ and that ψ_n is the convolution of x_n and b_n, where η_n results from white noise filtered by a SRRC filter and then sampled at the symbol rate. Since x_n is known, ψ_n is a known function of the parameters to be estimated and therefore not random. The expectation of y_n is therefore $E[y_n] = \psi_n + E[\eta_n]$. Since the Johnson noise is zero mean, $E[y_n] = \psi_n$. Taking the expectation of equation (5.9) yields $E[\hat{b}_n] = (\psi_n - \psi_{-(L+1)/2})/2$, which from equation (5.8) is b_n. This means $\hat{b}_n$ is an unbiased estimator.

The variance of $\hat{b}_n$ is obtained by subtracting $E[\hat{b}_n] = (\psi_n - \psi_{-(L+1)/2})/2$ from the respective sides of equation (5.9), then multiplying each side by its respective conjugate and finally taking the expectation of both sides. Replacing $y_n - \psi_n$ with η_n and $y_{-(L+1)/2} - \psi_{-(L+1)/2}$ with $\eta_{-(L+1)/2}$ makes the right hand side a function of η_n and $\eta_{-(L+1)/2}$. η_n is a sequence of independent zero mean Gaussian random variables with variance equal to the average power of x_n divided by SNR (or by E_s/N_0). Using independence $E[\eta_n \eta^*_{-(L+1)/2}] = 0$ for $-(L-1)/2 \leq n \leq (L-1)/2$, which allows two

91

terms to be removed. Since for this analysis $x_n = \pm 1$, the variance of $\hat{b}_n$ given by equation (5.9) becomes:

$$\sigma_b^2 = \frac{1}{2SNR} \quad \text{for all } \hat{b}_n, \tag{5.10}$$

A better estimator for $\hat{b}_n$ can be obtained using the relation

$$
\begin{aligned}
\sum_{n=-(L-1)/2}^{(L-1)/2} \psi_n &= \sum_{n=-(L-1)/2}^{(L-1)/2} \left(2b_n - \sum_{k=-(L-1)/2}^{(L-1)/2} b_k \right) \\
&= (2-L) \sum_{k=-(L-1)/2}^{(L-1)/2} b_k \\
&= (L-2)\psi_{-(L+1)/2}
\end{aligned}
$$

to get $\psi_{-(L+1)/2} = (L-2)^{-1} \sum_{n=-(L-1)/2}^{(L-1)/2} \psi_n$ and then substituting this into (5.8). The estimator is obtained by replacing ψ_n with y_n, which is

$$\hat{b}_n = \frac{y_n}{2} - \frac{\sum_{k=-(L-1)/2}^{(L-1)/2} y_k}{2(L-2)} \quad \text{for } |n| \le \frac{(L-1)}{2} \tag{5.11}$$

The variance calculation for the estimator given by equation (5.11) is a bit tedious but quite straightforward since the decision variables are independent with known means and variances. First, find the mean of (5.11) (keeping in mind that the noise is zero-mean) as follows:

$$
\begin{aligned}
E[\hat{b}_n] &= \frac{1}{2}E[\psi_n + \eta_n] - \frac{E\left[\sum_{k=-(L-1)/2}^{(L-1)/2}(\psi_k + \eta_k)\right]}{2(L-2)} \\
&= \frac{1}{2}\psi_n - \frac{1}{2(L-2)}\left(\sum_{k=-(L-1)/2}^{(L-1)/2} E[\psi_k] + \sum_{k=-(L-1)/2}^{(L-1)/2} E[\eta_k] \right) \\
&= \frac{1}{2}\psi_n - \frac{1}{2(L-2)} \sum_{k=-(L-1)/2}^{(L-1)/2} \psi_k \\
&= \frac{1}{2}\psi_n - \frac{1}{2}\psi_{-(L+1)/2} = b_n
\end{aligned}
$$

Next, find the variance of the estimator, which will be denoted $\sigma_{b\_better}^2$. To simplify the notation, make the following substitution:

$$\gamma = \sum_{k=-(L-1)/2}^{(L-1)/2} \frac{\eta_k}{L-2}.$$

92

Then

$$
\begin{aligned}
\sigma^2_{b\_better} &= E\left[(\hat{b}_n - b_n)(\hat{b}_n - b_n)^*\right] \\
&= E\left[\left(\frac{\eta_n}{2} - \frac{\gamma}{2}\right)\left(\frac{\eta_n}{2} - \frac{\gamma}{2}\right)^*\right] \\
&= \frac{1}{4}\left(E\left[\eta_n\eta_n^*\right] - E\left[\eta_n\gamma^*\right] - E\left[\eta_n^*\gamma\right] + E\left[\gamma\gamma^*\right]\right)
\end{aligned}
$$

The expectation of the product of noise terms is:

$$
E[\eta_i\eta_j^*] = \begin{cases} 0, & \text{if } i \neq j \\ \frac{1}{SNR}, & \text{if } i = j \end{cases}
$$

The expectation of the product $\eta_n\gamma^*$ is:

$$
E[\eta_n\gamma^*] = E\left[\sum_{k=-(L-1)/2}^{(L-1)/2} \frac{\eta_n\eta_k^*}{L-2}\right] = \begin{cases} \frac{1}{SNR(L-2)}, & \text{if } -\frac{L-1}{2} \leq n \leq \frac{L-1}{2} \\ 0, & \text{otherwise} \end{cases}
$$

Therefore

$$
\begin{aligned}
\sigma^2_{b\_better} &= \frac{1}{4}\left(\frac{1}{SNR} - \frac{2}{SNR(L-2)} + \frac{L}{SNR(L-2)^2}\right) \\
&= \frac{1}{4}\left(\frac{L^2 - 5L + 8}{SNR(L-2)^2}\right)
\end{aligned}
\tag{5.12}
$$

.

Notice that the variance of this estimator does not depend on the channel parameters. For $L \gg 1$, $\sigma^2_{b\_better} \approx 0.25/SNR$, which is half of σ_b^2 in (5.10).

5.2.2 Length of ISI Equivalent Filter

When estimating the ISI in the upstream channel, is important that the length and shape of the filter used to model the channel ISI are carefully chosen. If the channel is modeled with a filter that has too few pre-main or post-main taps to properly represent the ISI, it will not be possible to accurately seed the LMS equalizer. Conversely, if the ISI equivalent filter is longer than required to represent the ISI, a large number of calculations will be performed which contribute little to the overall performance of the system.

In this research, the shortest reasonable length for the ISI equivalent of a DOCSIS upstream channel is determined using the average energy of its coefficients. The average energy of a coefficient is its magnitude squared averaged probabilistically over all the possible channels. It was decided, somewhat arbitrarily, that a reasonable filter would be long enough to span 90% or more of the energy that lies outside the main path coefficient, which is b_0.

The average energy of each coefficient was found using a MATLAB simulation that modeled Figure 5.1. BPSK data was transmitted with an excitation word of length $M = 100$. A three-echo DOCSIS upstream channel was modeled, with the echoes being worst case in magnitude. The echo strengths, delays and arrival phases used in the model are shown in Table 5.1. The average energies of the coefficients, plotted in Figure 5.4 were calculated from 10^6 trials each with randomly chosen channel echo parameters.

Table 5.1   Channel model for simulation to determine length of ISI equivalent filter.

Relative Amplitude (dBc)	Echo Delay (sym)	Echo Phase (rad)
-10	Uniform $(0 \rightarrow 2.5)$	Uniform $(0 \rightarrow 2\pi)$
-20	Uniform $(0 \rightarrow 5)$	Uniform $(0 \rightarrow 2\pi)$
-30	Uniform $(0 \rightarrow 7.5)$	Uniform $(0 \rightarrow 2\pi)$

The total energy in the ISI equivalent filter is distributed as follows: 92.4% in b_0, 7.2% in coefficients b_1, b_2 and b_3 and 0.47% in the other coefficients. Of the average energy that is outside of b_0, 94% is contained in coefficients b_1, b_2 and b_3. This suggests a reasonable ISI equivalent filter would be of length 4, with coefficients b_0, b_1, b_2 and b_3.

The question to be answered next is "When seeding an equalizer, is it better to estimate a coefficient or set it to zero?". When deciding whether to estimate a coefficient or not, one should keep in mind the overall goal of minimizing the mean squared error in the vector of ISI equivalent filter coefficients, i.e. $\sum_i E(\hat{b}_i - b_i)^2$. Since the overall mean squared error is the linear summation of the mean squared
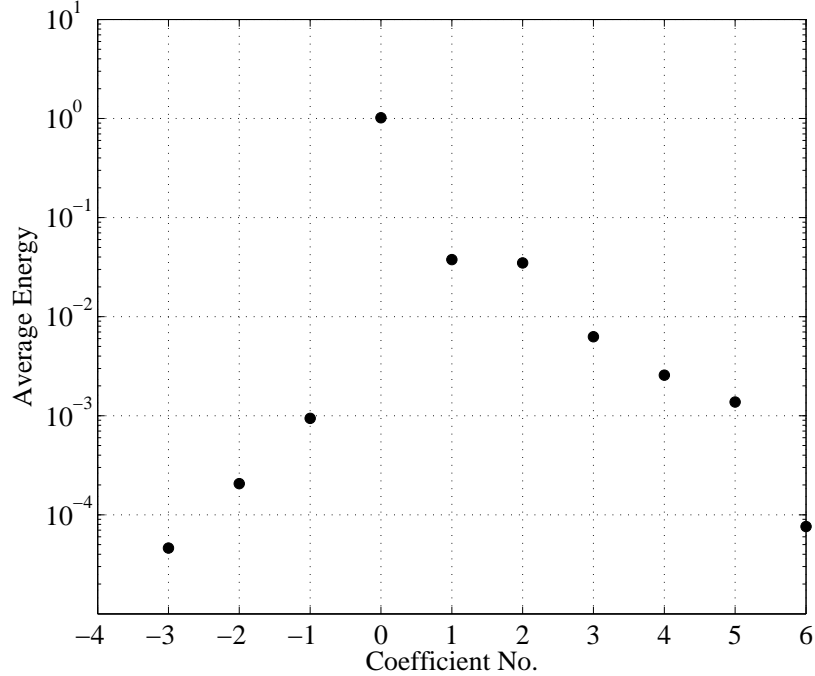
Figure 5.4   Energy distribution in coefficients of ISI equivalent filter.

errors of the individual coefficients, each coefficient can be examined individually.

If a particular coefficient is not estimated and instead set to zero, its contribution to the overall mean square error will be equal to the average energy in that coefficient. If an unbiased estimator is used, then the contribution to the overall mean square error is the variance of the estimator. Therefore, a logical decision rule is to estimate the coefficient only if the variance of the estimator is less than average energy of the coefficient.

DOCSIS states the minimum SNR for upstream channels is 25 dB, i.e., $SNR_{\min} = 316$. With this SNR the simple estimator of equation (5.9) has variance $\sigma_b^2 \approx 1.6 \times 10^{-3}$ and the more elaborate estimator of equation (5.11) has variance of about $\sigma_{b\_\text{better}}^2 \approx 0.8 \times 10^{-3}$. The average energy of b_1, b_2 and b_3 is 38×10^{-3}, 35×10^{-3} and 6.3×10^{-3}, respectively. These energies are well above the variances of both estimators of b_n, which means estimating b_n with either of the estimators is better than setting the coefficients to zero. The average energy of b_{-1} is 0.94×10^{-3}, which is slightly greater than the variance of the more elaborate estimator for b_n.

The argument used in the prequel suggests there will be a modest improvement if b_{-1} is estimated. It is of interest to explore the benefit of estimating b_{-1} for two reasons:

1. to see the improvement provided by an estimator that is marginally better than setting the coefficient to zero, and

2. to demonstrate a method of estimating a pre main-path equalizer tap.

For these two reasons, the ISI equivalent estimators discussed in the remainder of this section will estimate either coefficients b_{-1}, b_0, b_1, b_2, and b_3 or just coefficients b_0, b_1, b_2, and b_3.

5.2.3 Linear MVU Theory for ISI Equivalent Filter

In order to judge the performance of any proposed ISI coefficient estimation technique, it is necessary to have some objective standard against which to compare its variance. Fortunately, such a standard is readily available, as the theory of channel estimation has been reasonably well-studied and high-performance estimators have been described in the open literature [43], [44].

Setting L1 and L2 equal to 1 and 3 respectively as suggested in Section 5.2.2, the input to the equalizer represented by (5.1) may be written in matrix form as

$$
\mathbf{Y} = \mathbf{X} \cdot \mathbf{B} + \mathbf{N}
$$

$$
\begin{bmatrix} y_{n-1} \\ y_n \\ y_{n+1} \\ y_{n+2} \\ y_{n+3} \end{bmatrix} = \begin{bmatrix} x_n & x_{n-1} & x_{n-2} & x_{n-3} & x_{n-4} \\ x_{n+1} & x_n & x_{n-1} & x_{n-2} & x_{n-3} \\ x_{n+2} & x_{n+1} & x_n & x_{n-1} & x_{n-2} \\ x_{n+3} & x_{n+2} & x_{n+1} & x_n & x_{n-1} \\ x_{n+4} & x_{n+3} & x_{n+2} & x_{n+1} & x_n \end{bmatrix} \cdot \begin{bmatrix} b_{n-1} \\ b_n \\ b_{n+1} \\ b_{n+2} \\ b_{n+3} \end{bmatrix} + \begin{bmatrix} \eta_{n-1} \\ \eta_n \\ \eta_{n+1} \\ \eta_{n+2} \\ \eta_{n+3} \end{bmatrix} . \quad (5.13)
$$

In the discussion to follow, the terms 'excitation sequence' and 'excitation word' will be used to refer to the set of values contained in the first column of the matrix $\mathbf{X}$, which will be referred to as the 'excitation matrix'. The values in the first column

of the excitation matrix correspond to the symbols which enter the ISI equivalent filter while the vector $\mathbf{Y}$ is observed. For the example above, the excitation sequence consists of the symbols $x_n...x_{n+4}$ and the observed filter outputs are $y_{n-1}...y_{n+3}$. This discrepancy is due to the fact that the main tap of the ISI equivalent filter is the second tap in the filter. Due to the inherent memory in the FIR filter used to model the channel ISI, some symbols which were transmitted prior to the start of the excitation sequence will affect the observation vector $\mathbf{Y}$. However, these symbols will not be considered part of the excitation word.

Assuming that the excitation sequence is known, it is possible to estimate the ISI equivalent filter coefficients $\mathbf{B}$ based upon observations of the channel output samples $\mathbf{Y}$. The only caveat is that the length of the observation vector $\mathbf{Y}$ must be greater than the length of the coefficient vector $\mathbf{B}$. As more observations are taken, the length of the noise vector $\mathbf{N}$ and number of rows in the excitation matrix $\mathbf{X}$ shown in equation (5.13) increases. Note that the matrices shown in equation (5.13) above are meant to serve as an example only. They are not meant to indicate the number of observations required to provide a good estimate of the channel.

In general, estimation problems which can be expressed in the form of (5.13) are referred to as contrained linear estimation problems. Constrained linear estimation problems are studied at length in [21], and the minimum variance unbiased (MVU) estimator is known to be:

$$\hat{\mathbf{B}} = (\mathbf{X}^* R_N^{-1} \mathbf{X})^{-1} \mathbf{X}^* R_N^{-1} \mathbf{Y}, \tag{5.14}$$

where R_N is the noise covariance matrix, ie. $R_N = E[\mathbf{N}\mathbf{N}^*]$ and $\mathbf{X}^*$ represents the Hermitian transpose of matrix $\mathbf{X}$. In the present application, the noise is modeled as white, which means that $R_N = \frac{1}{SNR}\mathbf{I}$. This allows the expression for the channel estimator to be simplified to:

$$\begin{aligned} \hat{\mathbf{B}} &= (\mathbf{X}^*\mathbf{X})^{-1}\mathbf{X}^*\mathbf{Y} \\ &= \mathbf{KY} \end{aligned} \tag{5.15}$$

where $\mathbf{K} = (\mathbf{X}^*\mathbf{X})^{-1}\mathbf{X}^*$ is the estimator matrix, which is used to convert the incoming

samples to coefficient estimates. The variance of the estimator described by (5.15) is known to be [21]:

$$\mathbf{V}_{\hat{\mathbf{B}}} = \text{Var}(\hat{\mathbf{B}}) = \frac{1}{SNR}(\mathbf{X}^*\mathbf{X})^{-1} \qquad (5.16)$$

The matrix $\mathbf{V}_{\hat{\mathbf{B}}}$, given by equation (5.16) is a square matrix whose diagonal entries represent the variance of the estimates of each of the individual filter coefficients. In order to investigate the merits of various estimators, it is convenient to have a single variance metric to compare, rather than an entire matrix. In this document, the metric chosen is the average of the variances of the individual tap estimators. For the remainder of the document, the term 'average variance' will be used to refer to the result of $\frac{\text{Tr}(\mathbf{V}_{\hat{\mathbf{B}}})}{L}$, which is the average of the variances of the L individual tap estimators.

5.2.4 Estimator Selection

The variance and the implementation complexity of the estimator given by (5.15) depend upon the contents of the matrix $\mathbf{X}$, which in turn depends upon the transmitted excitation sequence. Clearly, the selection of an appropriate excitation sequence is a very important task. If a poor excitation word is chosen, even an MVU estimator for that excitation word may not yield acceptable performance. This section investigates the tradeoffs involved in the excitation sequence selection process.

Ideally, the excitation sequence and estimator used to compute the channel ISI coefficients will fulfill the following conditions:

1. The average variance of the MVU estimator for the chosen excitation sequence should be equal to or at least close to the lowest possible average variance for any excitation sequence of the chosen length.

2. The average variance of the chosen estimators should achieve or at least be close to the performance predicted by the MVU theory presented in Section 5.2.3.

3. The estimators should be computationally inexpensive to implement.

4. The excitation sequence should be well-suited to other synchronization tasks, so that it can be used by multiple circuits in parallel.

Perfect Excitation Sequences

It has been shown in [45] that the best possible excitation sequences of length M for channel estimation satisfy the condition $\mathbf{X}^*\mathbf{X} = M \cdot \mathbf{I_M}$. This implies that the lowest possible variance for an excitation sequence of length M is $\frac{1}{M \cdot SNR}\mathbf{I_M}$. Sequences where $\mathbf{X}^*\mathbf{X} = M \cdot \mathbf{I_M}$ are frequently referred to in the literature as perfect sequences.

Perfect sequences are desirable not only for their optimal performance, but also because they support computationally inexpensive channel estimators. This may be seen by considering the optimal estimator for a perfect sequence:

$$
\begin{aligned}
\hat{\mathbf{B}}_{\mathbf{pM}} &= (\mathbf{X_{pM}}^*\mathbf{X_{pM}})^{-1}\mathbf{X_{pM}}^*\mathbf{Y} \\
&= \frac{1}{M}\mathbf{X_{pM}}^*\mathbf{Y}
\end{aligned}
\tag{5.17}
$$

where the subscript pM is used to indicate a perfect excitation sequence of length M. Equation (5.17) indicates that the optimal estimator for a perfect excitation sequence correlates the received excitation sequence with the transmitted excitation sequence. In practice, this computation may be performed through the use of a matched filter.

Unfortunately, perfect excitation sequences do not exist for all channel lengths. An automated search for perfect excitation sequences of length 4-12 was performed using MATLAB. While no perfect excitation sequences were found for a channel of length 5, a perfect excitation sequence of length 4 was identified for a 4-tap channel. The corresponding excitation matrix is:

$$
\mathbf{X_{p4}} = \begin{bmatrix} -1 & 1 & -1 & -1 \\ -1 & -1 & 1 & -1 \\ -1 & -1 & -1 & 1 \\ 1 & -1 & -1 & -1 \end{bmatrix}
\tag{5.18}
$$

If the goal is to estimate only 4 channel coefficients, the excitation sequence defined in (B.1) is an obvious choice. Details specific to the implementation and performance of

the estimator for this perfect excitation word of length 4 are discussed in Appendix B However, if the goal is to estimate 5 channel coefficients, the situation becomes more complicated.

Complementary Code-Based Excitation Sequences

A technique which is commonly used for channel estimation involves the transmission of a pair of complementary codes (CCs). CCs, originally proposed by Golay in [46], have the time-domain property that the sum of their aperiodic autocorrelation functions is a scaled Kronecker delta function. Mathematically, this property may be expressed as follows:

$$\sum_{k=-\infty}^{\infty} a_n \cdot a_{n-k} + \sum_{k=-\infty}^{\infty} b_n \cdot b_{n-k} = L\delta(k) \qquad (5.19)$$

where $a_n = b_n = 0$ for $n < 0$ and $n \geq L$.

The above property is very convenient for channel estimation, as the receiver need only implement a pair of correlators or matched filters in order to obtain the channel's impulse response. Furthermore, as discussed in [44], the performance of CC-based estimators approaches that of the best possible excitation sequences. Additionally, the recursive structure of the CCs proposed by Golay permits the construction of particularly efficient correlators which require log(L) instead of L operations per output sample, as discussed in [47].

For these reasons, the use of CCs for channel estimation has generated significant interest in recent years, and a number of papers have been published on the topic. Most relevant to the current discussion, [13], h&D proposed the use of CCs for fast channel estimation in a burst QAM modem. However, the proper recovery of the channel impulse response using a CC-based technique requires 'quiet periods' during which no signals are transmitted both before and after the codes are sent. No techniques for avoiding this requirement were found in the literature. Since the DOCSIS standard does not permit the transmission of zero-energy symbols, a 'quiet period' cannot be embedded in the excitation sequence. This eliminates the possibility of

100

using of CCs for DOCSIS upstream channel estimation.

Impulse-Like Excitation Sequences

Having ruled out perfect sequences and CCs for estimation of 5 coefficients of the ISI equivalent filter, one excitation sequence which merits further investigation is the impulse-like (IL) sequence discussed in Section 5.2.1. The IL sequence is particularly promising because, as was shown in equation (5.11), it is possible to inexpensively implement the ISI coefficient estimators for this sequence. However, it is not immediately clear whether or not (5.11) represents the MVU estimator for the IL sequence. The IL sequence may be analyzed using the MVU theory presented in Section 5.2.3 by first noticing that the matrix $\mathbf{X}$ for this sequence may be expressed as:

$$
\begin{aligned}
\mathbf{X_{IL}} &=
\begin{bmatrix}
x_n & x_{n-1} & x_{n-2} & x_{n-3} & x_{n-4} \\
x_{n+1} & x_n & x_{n-1} & x_{n-2} & x_{n-3} \\
x_{n+2} & x_{n+1} & x_n & x_{n-1} & x_{n-2} \\
x_{n+3} & x_{n+2} & x_{n+1} & x_n & x_{n-1} \\
x_{n+4} & x_{n+3} & x_{n+2} & x_{n+1} & x_n
\end{bmatrix}
=
\begin{bmatrix}
1 & -1 & -1 & -1 & -1 \\
-1 & 1 & -1 & -1 & -1 \\
-1 & -1 & 1 & -1 & -1 \\
-1 & -1 & -1 & 1 & -1 \\
-1 & -1 & -1 & -1 & 1
\end{bmatrix} \\
&= \lfloor -\mathbf{1} \rfloor_5 + 2\mathbf{I}_5 \qquad\qquad (5.20)
\end{aligned}
$$

where the notation $\lfloor \mathbf{N} \rfloor_M$ is used to represent an MxM matrix with each entry equal to N and $\mathbf{I}_M$ is used to represent an MxM identity matrix. Generalizing from the case of estimating 5 coefficients from an IL excitation sequence of length 5 to the case of estimating L coefficients from an IL excitation sequence of length L, the variance of the MVU estimator may be written as:

$$
\begin{aligned}
\mathbf{V}_{\hat{\mathbf{B}}_{\mathbf{IL}}} &= \frac{1}{SNR}(\mathbf{X_{IL}}^*\mathbf{X_{IL}})^{-1} \\
&= \frac{1}{SNR}((\lfloor -\mathbf{1} \rfloor_L + 2\mathbf{I}_L)^*(\lfloor -\mathbf{1} \rfloor_L + 2\mathbf{I}_L))^{-1} \\
&= \frac{1}{SNR}(\lfloor \mathbf{L} \rfloor_L - \lfloor \mathbf{2} \rfloor_L - \lfloor \mathbf{2} \rfloor_L + 4\mathbf{I}_L)^{-1} \\
&= \frac{1}{SNR}(\lfloor \mathbf{L} - \mathbf{4} \rfloor_L + 4\mathbf{I}_L)^{-1} \qquad\qquad (5.21)
\end{aligned}
$$

Using the formula for the inverse of the sum of two matrices presented in [48], the variance expression may be simplified as follows:

$$\mathbf{V}_{\hat{\mathbf{B}}_{\mathbf{IL}}} \;=\; \frac{1}{4SNR}\left(\mathbf{I_L} - \left\lfloor \frac{\mathbf{L-4}}{\mathbf{(L-2)^2}} \right\rfloor_L\right) \tag{5.22}$$

provided that $L \neq 2$.

The values on the main diagonal of $\mathbf{V}_{\hat{\mathbf{B}}_{\mathbf{IL}}}$ represent the variances of the estimators of the individual coefficients. It is clear from (5.22) that these variances are all identical, and are equal to:

$$\sigma^2_{\hat{b}_{IL}} \;=\; \frac{1}{4SNR}\left(\frac{L^2 - 5L + 8}{(L-2)^2}\right) \tag{5.23}$$

The average variance for this technique is simply the expression of (5.22), since the variance of each estimator is identical. A comparison of equations (5.12) and (5.23) shows that the variance of the estimation scheme presented in Section 5.2.1 is equal to that of the MVU estimator for the IL sequence, indicating that (5.11) represents the MVU estimator for the IL sequence.

For the present application, the goal is to estimate 5 ISI coefficients. In the case of the IL sequence, this corresponds to an excitation sequence of length 5 and an excitation matrix $\mathbf{X}$ which is 5x5. In general, 5 coefficients can be estimated using an excitation sequence of any length M which is greater than or equal to 5, corresponding to a Mx5 excitation matrix.

However, as will be shown in the sequel, a particularly efficient hardware implementation is possible with the IL sequence if the excitation word length M is chosen to be a multiple of the number of coefficients to be estimated. If this condition is met, a composite sequence consisting of $M/5$ repetitions of the IL sequence may be transmitted, yielding an excitation matrix which has the following structure (example shown for M=10):

$$\mathbf{X_{IL-comp}} = \begin{bmatrix} \mathbf{X_{IL}} \\ \mathbf{X_{IL}} \end{bmatrix} \tag{5.24}$$

The MVU estimator matrix for this structure is:

$$
\begin{aligned}
\mathbf{K_{IL-comp}} &= (\mathbf{X_{IL-comp}}^*\mathbf{X_{IL-comp}})^{-1}\mathbf{X_{IL-comp}}^* \\
&= \left(\begin{bmatrix} \mathbf{X_{IL}}^* & \mathbf{X_{IL}}^* \end{bmatrix} \begin{bmatrix} \mathbf{X_{IL}} \\ \mathbf{X_{IL}} \end{bmatrix} \right)^{-1} \begin{bmatrix} \mathbf{X_{IL}}^* & \mathbf{X_{IL}}^* \end{bmatrix} \\
&= \frac{1}{2}(\mathbf{X_{IL}}^*\mathbf{X_{IL}})^{-1} \begin{bmatrix} \mathbf{X_{IL}}^* & \mathbf{X_{IL}}^* \end{bmatrix} \\
&= \frac{1}{2} \begin{bmatrix} \mathbf{K_{IL}} & \mathbf{K_{IL}} \end{bmatrix}
\end{aligned}
\tag{5.25}
$$

and the variance of the MVU estimator for this sequence is:

$$
\begin{aligned}
\mathbf{V\hat{B}_{IL-comp}} &= \frac{1}{SNR}(\mathbf{X_{IL-comp}}^*\mathbf{X_{IL-comp}})^{-1} \\
&= \frac{1}{SNR} \left(\begin{bmatrix} \mathbf{X_{IL}}^* & \mathbf{X_{IL}}^* \end{bmatrix} \begin{bmatrix} \mathbf{X_{IL}} \\ \mathbf{X_{IL}} \end{bmatrix} \right)^{-1} \\
&= \frac{1}{2SNR}(\mathbf{X_{IL}}^*\mathbf{X_{IL}})^{-1} \\
&= \frac{1}{2}\mathbf{V\hat{B}_{IL}}
\end{aligned}
\tag{5.26}
$$

It is clear from equations (5.26) and (5.25) that the MVU estimator of the composite IL sequence merely averages the results of $\frac{M}{5}$ repetitions of the simple IL excitation sequence, reducing the variance of each coefficient estimator by a factor of $\frac{M}{5}$. This is a welcome result, indicating that the FPGA implementation complexity of implementing the composite estimator will be essentially the same as that of the original simple estimator.

However, the fact that the proposed estimator is the MVU estimator for the IL sequence and its composites is not sufficient to conclude that the estimator's performance is acceptable. It is technically possible that the IL sequence and its composites are suboptimal sequences for ISI estimation and that other sequences with significantly better-performing MVU estimators exist. In order to be sure that the IL sequence is suitable, it is necessary to compare its performance to that of other sequences.

In order to make an informed decision when selecting an excitation sequence,
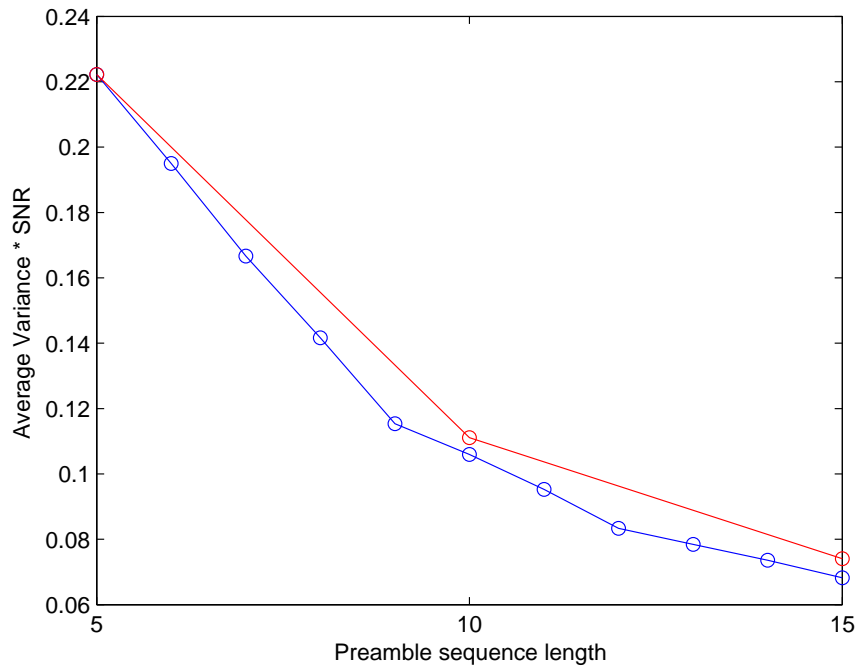
Figure 5.5   Average variance of MVU estimator for best possible excitation sequences of various lengths.

it is prudent to investigate the relationship between excitation sequence length and minimum achievable variance. To this end, a MATLAB simulation was performed, wherein a variety of excitation sequence lengths were considered. For each excitation sequence length M, an analysis was performed upon all 2^M possible sequences which can be constructed from a symbol alphabet of $\{-1, 1\}$. The average variance of the MVU estimator for each sequence was computed.

The results of this investigation are presented in Figure 5.5, which plots the average variance of the MVU estimator for the best possible excitation sequence of each length. For sequence lengths which are multiples of 5, the total variance of the MVU estimator for the IL sequence and its composites was also plotted in Figure 5.5. It is apparent from the figure that the achievable average variance for the IL sequence and its composites is reasonably close to that of the best possible sequence of the same length. In fact, for $M = 5$, the IL sequence actually achieves the lowest possible

variance for any sequence. The degradation in the average variance of the composite IL sequences with respect to the best possible sequences when $M = 10$ or $M = 15$ is -0.21dB and -0.36dB respectively.

After the independent completion of the simulation discussed above, it was discovered that Crozier, Falconer, and Mahmoud described a similar computer search to find the best excitation sequences for channel estimation in [43]. However, the work presented here differs from theirs in two main ways. First, the current work is concerned with finding a sequence which can be used not only for channel estimation, but also for other synchronization functions. As will be discussed in the sequel, this fact places restrictions upon the autocorrelation properties of the excitation sequence. Second, [43] does directly discuss the computational complexity of the estimators for the chosen sequences, which is of paramount importance in the present work.

There is one downside to the IL sequence: it has poor autocorrelation properties. This limitation is highlighted in Figure 5.6, which plots the autocorrelation function($R_x[k] = \sum x[n]x^*[n - k]$) of an 11-symbol IL sequence. For purposes of comparison, the autocorrelation function of an 11-symbol Barker sequence is also plotted in Figure 5.6. Barker sequences are well-known to have autocorrelation functions which are very low outside of the main lobe. For this reason, they are used extensively for synchronization in wireless systems [49], [50].

Since many timing recovery schemes operate by looking for peaks in the autocorrelation function of the transmitted preamble sequence [51], it is desirable to use a sequence which has the sharpest possible peak in the main lobe. This is achieved by choosing a sequence that maximizes the difference between the peak of the main lobe and the values at the neighbouring sample points. It is clear from Figure 5.6 that the peak of the Barker sequence's main lobe is much sharper than that of the IL sequence, which suggests that the IL sequence is not particularly useful for timing recovery. This fact severely limits the ability of the IL sequence to be used for multiple synchronization tasks simultaneously.
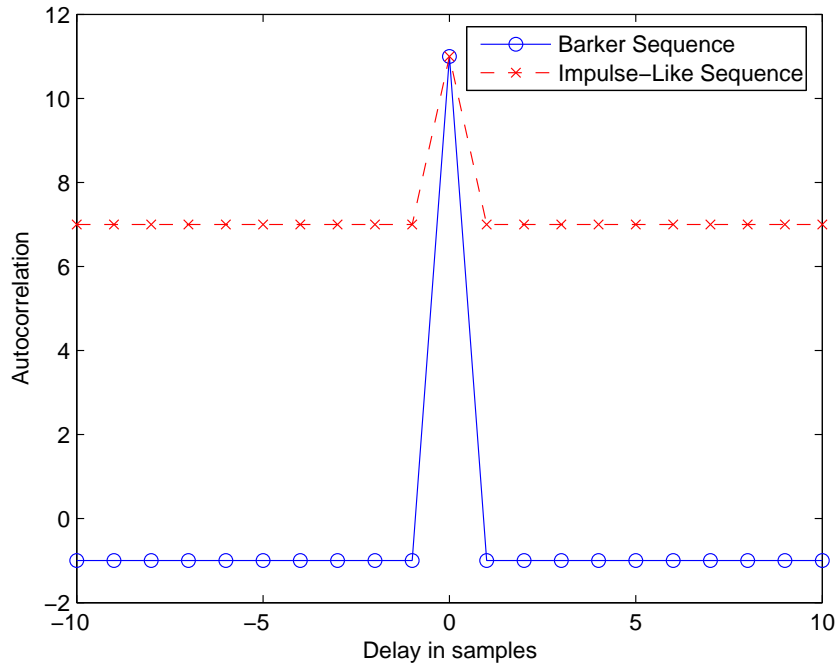
Figure 5.6   Autocorrelation function of Barker sequence and Impluse-Like sequence.

It should be noted that the proposed perfect excitation sequence for estimating a 4-coefficient ISI equivalent filter is made up of a portion of an 11-symbol Barker sequence, which means that it is well-suited to working in parallel with timing recovery or frequency recovery circuits.

Barker-Based Excitation Sequences

Based upon the preceding discussion, a logical candidate for the excitation sequence and also for the unique synchronization word is a Barker sequence or some portion thereof. Using MATLAB, the variances of the MVU estimators for excitation words consisting of various portions of an 11-symbol Barker sequence was evaluated. This investigation yielded two promising candidates:

Partial-Barker-Based 5-symbol excitation word:

When 5 symbols of an 11-symbol Barker sequence are used as the excitation word

for ISI estimation, the performance achievable by an MVU estimator depends greatly upon which set of 5 symbols are chosen. Suppose that the unique synchronization word contains an 11-symbol Barker code:

$$\begin{bmatrix} 1 & 1 & 1 & -1 & -1 & \mathbf{-1} & \mathbf{1} & \mathbf{-1} & \mathbf{-1} & \mathbf{1} & -1 \end{bmatrix} \tag{5.27}$$

If the symbols that are typeset in **bold** in the above expression are used as the excitation word for ISI estimation, the matrix $\mathbf{X}$ takes on the following form:

$$\mathbf{X_{BB5}} = \begin{bmatrix} -1 & -1 & -1 & 1 & 1 \\ 1 & -1 & -1 & -1 & 1 \\ -1 & 1 & -1 & -1 & -1 \\ -1 & -1 & 1 & -1 & -1 \\ 1 & -1 & -1 & 1 & -1 \end{bmatrix} \tag{5.28}$$

Note that the second through fourth symbols of the Barker sequence, i.e., the sequence $\begin{bmatrix} -1 & -1 & 1 & 1 \end{bmatrix}$ arrive prior to the first symbol of the excitation word. Consequently, these four symbols populate the final four elements in the top row of $\mathbf{X_{BB5}}$.

The excitation sequence represented by $\mathbf{X_{BB5}}$ will be referred to as the Barker-Based 5-symbol excitation word (BB5). When the MVU estimator for the BB5 sequence is used, the average variance in the ISI coefficient estimates is $0.2222/SNR$, which is the lowest possible average variance for any excitation sequence of length 5.

At first glance, it appears as though the MVU estimator for the BB5 sequence will be more computationally expensive to implement than the IL sequence, due to the relative lack of symmetry in its excitation matrix $\mathbf{X_{BB5}}$. However, it turns out that this estimator can be implemented in an inexpensive fashion if a few optimizations are performed. The complete implementation details of the MVU estimator for the BB5 sequence are presented in Appendix B.

Barker-Based 11-symbol excitation word:

If an entire 11-symbol barker sequence is used as the excitation word for ISI

estimation, the excitation matrix becomes:

$$\mathbf{X_{BB11}} = \begin{bmatrix} 1 & -1 & 1 & -1 & -1 \\ 1 & 1 & -1 & 1 & -1 \\ 1 & 1 & 1 & -1 & 1 \\ -1 & 1 & 1 & 1 & -1 \\ -1 & -1 & 1 & 1 & 1 \\ -1 & -1 & -1 & 1 & 1 \\ 1 & -1 & -1 & -1 & 1 \\ -1 & 1 & -1 & -1 & -1 \\ -1 & -1 & 1 & -1 & -1 \\ 1 & -1 & -1 & 1 & -1 \\ -1 & 1 & -1 & -1 & 1 \end{bmatrix} \tag{5.29}$$

Note that the representation above assumes that the four symbols preceding the excitation word in the preamble are the last four symbols of an 11-symbol Barker sequence. In practice, this is not a significant limitation, as the timing and frequency recovery circuits will likely require multiple copies of the Barker sequence to be transmitted consecutively. The excitation word represented by (5.29) will be referred to as the Barker-Based 11-symbol sequence (BB11).

The MVU estimator for the BB11 sequence achieves the lowest possible average variance for any 11-symbol sequence, which is $0.0952/SNR$. Furthermore, if multiple Barker sequences are transmitted for the benefit of the timing or frequency recovery circuits (as is likely to be the case), it is possible to further reduce the average variance of the ISI coefficient estimators without adding computational complexity by simply averaging multiple estimates generated using the BB11 scheme, similar to the composite method discussed previously for the IL sequence.

More details regarding the variance of this estimator and its implementation may be found in Appendix B.

Summary of ISI estimation options:

In this section, four excitation words which can be effectively used for the estimation of the ISI equivalent coefficients of a DOCSIS upstream channel have been presented. Each of these excitation words is optimal in the sense that it yields an MVU estimator which has the lowest achievable average variance for any sequence of the same length. As shown in Table 5.2 below, the implementation of these estimators requires only a modest number of computations. Note that the 'multiplications' and 'additions' entries in the table correspond to multiplications and additions of real numbers.

Table 5.2   Performance and complexity of MVU estimators of ISI equivalent coefficients.

Sequence	Length (symbols)	Implementation Complexity		Average Variance
		Multiplications	Additions	
P4	4	0	24	0.250 / SNR
IL	5	2	18	0.2222/SNR
BB5	5	2	18	0.2222/SNR
BB11	11	10	72	0.0952/SNR

It is apparent from Table 5.2 that the Impulse-Like and 5-symbol Barker-Based sequences are equivalent in terms of ISI estimator performance and also complexity. As a result, the BB5 sequence is probably preferred in most cases, due to its favorable autocorrelation properties. Unsurprisingly, the BB11 sequence provides an average variance which is lower than that obtained using either the IL or BB5 sequences. The downside to this sequence is that its MVU estimator is approximately four times as expensive to implement than those of the proposed 5-symbol estimators.

Deciding between the BB5 and BB11 sequences then becomes a matter of trading off the conflicting goals of implementation complexity and estimator performance. In order to make an intelligent decision, it is necessary to determine how much each of the sequences speeds up the convergence of the adaptive equalizer. To aid in this decision making process, a number of simulations were performed, the details of which may be found in Section 5.4.

5.2.5 Effect of Phase Rotation on ISI Estimation

In order to simplify the notation, the alphabet for the excitation sequence up to this point has consisted of two symbols: $+1$ and -1. However, the symbols in a DOCSIS upstream preamble must be selected from the following QPSK alphabet: $e^{j\pi/4}$, $e^{j3\pi/4}$, $e^{-j3\pi/4}$, and $e^{-j\pi/4}$. This discrepancy may be resolved by building the excitation sequence from a pair of antipodal symbols present in the QPSK alphabet. Without loss of generality, it will be assumed in the sequel that the mappings $+1 \rightarrow e^{j\pi/4}$ $-1 \rightarrow e^{-j3\pi/4}$ are used. It is noted that this mapping corresponds to a counterclockwise rotation of $\pi/4$ radians.

Updating the excitation sequence matrix to reflect this mapping has $\mathbf{X_R} = e^{j\pi/4}\mathbf{X}$, where $\mathbf{X_R}$ is the rotated version of the excitation matrix. The variance of the MVU estimator for this excitation matrix is:

$$\begin{aligned} \mathbf{V}_{\hat{\mathbf{B}}_\mathbf{R}} &= \text{Var}(\hat{\mathbf{B}}_\mathbf{R}) = \frac{1}{SNR}(\mathbf{X_R}^*\mathbf{X_R})^{-1} \\ &= \frac{1}{SNR}(e^{-j\pi/4}\mathbf{X}^* e^{j\pi/4}\mathbf{X})^{-1} = \frac{1}{SNR}(\mathbf{X}^*\mathbf{X})^{-1} \end{aligned} \tag{5.30}$$

which is equal to the variance of the MVU estimator for the nonrotated case, which is given by (5.16). The corresponding MVU estimator is given by:

$$\begin{aligned} \hat{\mathbf{B}}_\mathbf{R} &= (\mathbf{X_R}^*\mathbf{X_R})^{-1}\mathbf{X_R}^*\mathbf{Y} \\ &= (\mathbf{X}^*\mathbf{X})^{-1}e^{-j\pi/4}\mathbf{X}^*\mathbf{Y} \\ &= \mathbf{K_R}\mathbf{Y} = e^{-j\pi/4}\mathbf{K}\mathbf{Y} \end{aligned} \tag{5.31}$$

where $\mathbf{K}$ is the original MVU estimation matrix, given by (5.15). Equation (5.31) indicates that the estimation matrix for the rotated case, which is $\mathbf{K_R}$, is merely a rotated version of the estimation matrix for the nonrotated case.

For reasons of computational complexity, it is preferable to implement $\mathbf{K}$ in hardware, rather than $\mathbf{K_R}$. This is due to the fact that each element in $\mathbf{K}$ is purely real, whereas each element in $\mathbf{K_R}$ contains both real and imaginary components. If the receiver estimates the channel using $\mathbf{K}$ instead of $\mathbf{K_R}$, the channel estimate will contain

an unwanted rotation of $+\pi/4$ radians. However, this rotation is not problematic, as it may be easily counteracted by derotating the resulting channel estimate, given that the magnitude and sign of the rotation are known a priori.

A similar phenomenon occurs if an unexpected phase offset is present at the input to the channel estimator. In this case, a rotated version of the observation vector $\mathbf{Y}$ is presented to the channel estimator: $\mathbf{Y_R} = e^{j\phi_o}\mathbf{Y}$. When the receiver estimates the channel by multiplying $\mathbf{K}$ with $\mathbf{Y_R}$, the resulting channel estimate is itself rotated by ϕ_o radians.

The preceding argument implies that the channel estimator also performs phase offset estimation. When the channel's impulse response is crudely inverted in order to initialize the adaptive equalizer, the equalizer's coefficients will have a built-in rotation which compensates for any phase offset. This means that a standalone phase offset estimator, such as that described in Section 4.5 is pointless if one of the proposed channel estimation schemes is utilized.

5.3 Initialization of Equalizer Coefficients

Regardless of which excitation word is used in the estimation of the channel ISI, the next step in the proposed technique for increasing the convergence rate of the upstream equalizer is to utilize the estimated ISI coefficients to initialize the adaptive equalizer.

5.3.1 Overview of Common Equalization Techniques

In practice, there are two main criteria which are commonly used to optimize the coefficients of a linear equalizer:

Mean Squared Error Criterion:

The mean squared error (MSE) criterion evaluates the performance of an equalizer by considering the average power in the error in the equalizer's output signal. In the context of a DOCSIS upstream channel, this error is defined as the difference between

the equalizer's output and the originally transmitted value for a given signal:

$$MSE = E[(x_n - z_n) \cdot (x_n - z_n)^*] \tag{5.32}$$

An equalizer whose coefficients are chosen in order to minimize the MSE in its output is known as a minimum MSE equalizer. Both the LMS and RLS adaptive algorithms are designed to eventually converge to the minimum MSE set of equalizer coefficients.

Peak Distortion Criterion:

As an alternative to the MSE criterion, it is possible to evaluate the performance of an equalizer based upon the peak distortion caused by ISI at its output. The ISI at the output of the equalizer may be modeled using a single equivalent filter operating at the symbol rate, the coefficients of which will be denoted as q. The coefficients of this overall equivalent filter may be computed as the cascade of the channel ISI equivalent filter and the equalizer's linear filter, i.e. $q = b \star w$.

The ISI present in a given output symbol from the equalizer depends upon the sequence of symbols which enter the overall equivalent filter. In the worst case, all of the symbols will align with the filter coefficients in such a way that the ISI terms will add constructively. In this case, the value of the ISI is:

$$PD = \sum_n |q_n| \tag{5.33}$$

where PD denotes peak distortion. An equalizer which attempts to minimize the peak distortion in its output is known as a zero-forcing (ZF) equalizer.

The main difference between minimum MSE equalizers and ZF equalizers relates to how they deal with AWGN. A ZF equalizer does not consider noise when selecting coefficients. Rather, it merely attempts to remove all of the ISI added by the channel. In contrast, a minimum MSE equalizer takes into account both ISI and AWGN in order to select a set of coefficients which provides the lowest total MSE. In many cases, particularly when the SNR is low, it is not optimal to remove all of the channel ISI, as doing so would require a set of equalizer coefficients which enhance the power in the AWGN. In such a case, a minimum MSE equalizer will balance the competing

goals of ISI cancellation and minimization of noise enhancement. For this reason, minimum MSE equalizers tend to provide lower BERs when used in a receiver than do ZF equalizers.

In [13], after estimating the channel impulse response, h&D proposed directly computing the minimum MSE equalizer coefficients which compensate the channel using the so-called normal equations. By proceeding in this manner, it is possible to determine the equalizer coefficients to a very high degree of accuracy, which eliminates the need for an additional training sequence for the adaptive equalizer. As a result, this technique is desirable from a channel throughput perspective, since it eliminates much of the overhead associated with training the equalizer. The downside of this approach is its computational complexity. Solving the normal equations involves the multiplication and inversion of autocorrelation matrices which are unknown a priori [25].

To mitigate this computational complexity, a new approach is proposed which trades performance for computational efficiency. In this approach, the equalizer's coefficients are seeded with the approximate inverse of the channel, which may be computed using a relatively small number of operations. Because the proposed technique generates only a rough approximation of the ideal coefficients, an additional training sequence is required for the equalizer to further adapt before entering traffic mode.

As briefly touched upon in Section 5.2.2, two variations of the proposed technique will be explored. The first method, discussed in Section 5.3.2 compensates for only the post main-path ISI, i.e., b_0, b_1, b_2 and b_3, while the second uses both pre main-path and post main-path information, i.e., b_{-1}, b_0, b_1, b_2 and b_3.

5.3.2 Post-Main-Path Initialization Technique

When developing the proposed techniques, it is useful to represent the ISI equivalent filter as two filters in parallel, as shown in Figure 5.7. These two parallel filters are referred to as the pre-main-path and the post main-path filters, although the
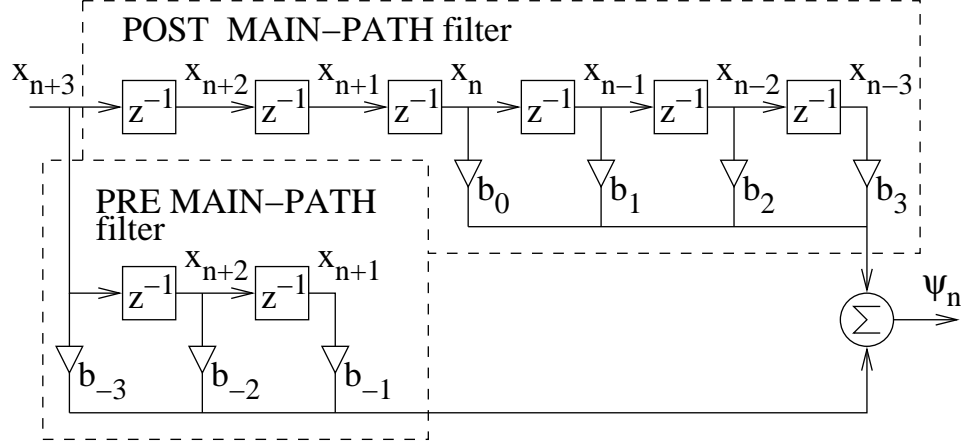
Figure 5.7   Parallel representation of the ISI equivalent filter.

post main-path filter also contains the main path. The main path is represented by coefficient b_0, which is the largest in magnitude. The coefficients of the ISI equivalent filter map to the coefficients in the parallel structure without changing value. The coefficients b_n, for $n < 0$ are set to zero in the post main-path filter and the coefficients b_n, for $n \geq 0$ are set to zero in the pre-main-path filter.

When attempting to seed the coefficients of an adaptive equalizer, the ZF approach may be preferable to the minimum MSE approach for reasons of computational complexity. Assuming the channel is minimum phase, the coefficients of a ZF equalizer which equalizes a given channel may be found relatively inexpensively. Since the goal of a ZF equalizer is to remove ISI without regard for noise enhancement effects, a ZF equalizer which is operating perfectly will remove all of the ISI present in its input signal, such that:

$$
\begin{aligned}
Q(z) &= B(z)W(z) = 1 \\
W(z) &= \frac{1}{B(z)}
\end{aligned}
\tag{5.34}
$$

where $Q(z)$, $B(z)$, and $W(z)$ are the Z-transforms of q, b, and w, respectively [24]. It is clear from (5.34) that the optimal set of ZF equalizer coefficients is generated by inverting the ISI equivalent filter b. Based upon the techniques discussed in Section 5.2, an estimate of the ISI equivalent filter coefficients is readily available. By inverting this filter, it is possible to generate an estimate of the ZF equalizer coefficients which

compensate for the ISI in the upstream channel.

Whenever a filter is inverted, stability becomes an important consideration. In order for the inverse of a filter to be stable, the original filter must be minimum phase, which ensures that all of its zeros are inside the unit circle [52]. If this is true, the inverted version of the filter will have all of its poles inside the unit circle and will thus be stable. On the other hand, if a nonminimum phase filer is inverted, one or more poles in the inverted filter will be outside of the unit circle, resulting in an unstable filter.

Using the inverted post-main path ISI filter to seed the equalizer is sensible only if the post-main path ISI filter is a minimum phase system. As the validity of the proposed technique depends on the post-main path ISI filter being a minimum phase system, the performance analysis is now interrupted to prove this is the case.

Proof that Post-Main-Path Filter is Minimum Phase

This proof is for the case of an upstream DOCSIS 3.0 channel, pulse-shaping filter, and matched filter.

It has been shown in [53] and [54] that a sufficient condition for a causal digital filter with complex impulse response h_k to be minimum phase is:

$$|h_0| > \sum_{k=1}^{\infty} |h_k| \tag{5.35}$$

The ISI equivalent filter has an impulse response which is generated by convolving the channel impulse response with that of the transmitter pulse shaping filter and the receiver matched filter. In a DOCSIS upstream channel, the pulse shaping filter and the corresponding matched filter combine to generate a raised-cosine impulse response with a rolloff factor of 0.25. In the analog domain, the ISI equivalent filter may be written as follows:

$$b(t) = c(t) \star h_{rc}(t) \tag{5.36}$$

where $c(t)$ denotes the complex low-pass equivalent channel impulse response, $h_{rc}(t)$

denotes a raised cosine impulse response, and $b(t)$ denotes the ISI equivalent filter impulse respone. As discussed in the DOCSIS standard, the worst-case channel contains three micro-reflections in addition to the main-path signal. In the complex low-pass equivalent model of the channel, each micro-reflection causes a delayed, rotated, and attenuated version of the transmitted signal to reach the receiver. Thus, the ISI equivalent response may be rewritten as:

$$
\begin{aligned}
b(t) &= \left(\delta(t) + \sum_{i=1}^{3} G_i e^{-j\phi_i} \delta(t - \tau_i) \right) \star h_{rc}(t) \\
&= h_{rc}(t) + \sum_{i=1}^{3} G_i e^{-j\phi_i} h_{rc}(t - \tau_i)
\end{aligned}
\tag{5.37}
$$

where G_i, ϕ_i, and τ_i are the attenuation, phase rotation, and delay of the i-th micro-reflection. Assuming that the receiver has recovered timing, the observed ISI equivalent response is a sampled version of the analog response $b(t)$, with the samples taken at $t = nT$:

$$
b_n = b(nT) = h_{rc}(nT) + \sum_{i=1}^{3} G_i e^{-j\phi_i} h_{rc}(nT - \tau_i)
\tag{5.38}
$$

Since the raised cosine filter meets the Nyquist criterion for zero ISI, the $h_{rc}(nT)$ term in (5.38) is zero for all samples except $n = 0$, for which it has a value of 1. Thus, for $n \geq 1$, b_n and $|b_n|$ may be expressed as:

$$
b_n = \sum_{i=1}^{3} G_i e^{-j\phi_i} h_{rc}(nT - \tau_i) \qquad n \geq 1
\tag{5.39}
$$

$$
|b_n| \leq \sum_{i=1}^{3} \left| G_i e^{-j\phi_i} \right| |h_{rc}(nT - \tau_i)| \qquad n \geq 1
\tag{5.40}
$$
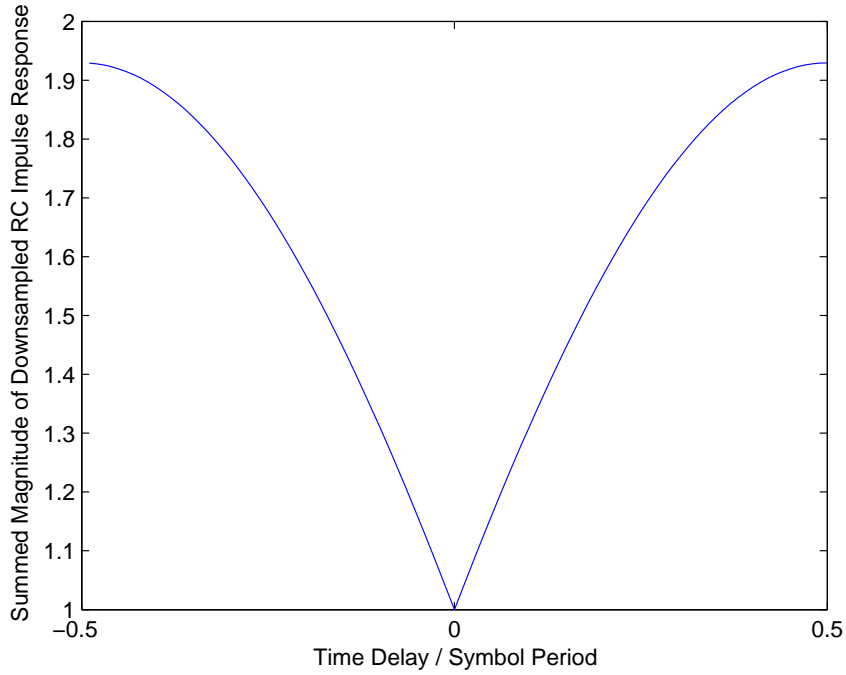
Figure 5.8   Summed Magnitude of downsampled raised cosine impulse response.

Summing the absolute values of the filter coefficients for $n \geq 1$:

$$\sum_{n=1}^{\infty} |b_n| \leq \sum_{n=1}^{\infty} \sum_{i=1}^{3} |G_i| \, |h_{rc}(nT - \tau_i)|$$

$$\sum_{n=1}^{\infty} |b_n| \leq \sum_{i=1}^{3} |G_i| \sum_{n=1}^{\infty} |h_{rc}(nT - \tau_i)| \tag{5.41}$$

$$\sum_{n=1}^{\infty} |b_n| \leq \sum_{i=1}^{3} |G_i| \sum_{n=1}^{\infty} |h_{rc}(nT - \tau_i)| + \sum_{i=1}^{3} |G_i| \sum_{n=-\infty}^{-1} |h_{rc}(nT - \tau_i)| \tag{5.42}$$

$$\sum_{n=1}^{\infty} |b_n| \leq \sum_{i=1}^{3} |G_i| \sum_{n=-\infty}^{\infty} |h_{rc}(nT - \tau_i)| - \sum_{i=1}^{3} |G_i| \, |h_{rc}(-\tau_i)| \tag{5.43}$$

$$\sum_{n=1}^{\infty} |b_n| \leq \sum_{i=1}^{3} |G_i| \sum_{n=-\infty}^{\infty} |h_{rc}(nT - \tau_i)| - W_s \tag{5.44}$$

where W_s has been defined as the weighted sum $\sum_{i=1}^{3} |G_i| \, |h_{rc}(-\tau_i)|$. Using MATLAB, the value of

$$\sum_{n=-\infty}^{\infty} |h_{rc}(nT - \tau_i)| \tag{5.45}$$

was computed and plotted for τ_i between -0.5 and +0.5 symbols. The plot, which is

117

shown in Figure 5.8, indicates that this sum does not exceed 2. Since the amplitudes of the three worst case micro-reflections cannot exceed -10, -20, and -30dBc respectively, equation (5.44) may be written as:

$$\sum_{n=1}^{\infty} |b_n| \leq 2(.3162 + .1 + .0316) - W_s = .8957 - W_s \tag{5.46}$$

From (5.38), the absolute value of b_0 is:

$$|b_0| = \left| 1 + \sum_{i=1}^{3} G_i e^{-j\phi_i} h_{rc}(-\tau_i) \right|$$

$$|b_0| \geq 1 - \sum_{i=1}^{3} |G_i| |h_{rc}(-\tau_i)| \tag{5.47}$$

$$|b_0| \geq 1 - W_s \tag{5.48}$$

Using (5.48) and (5.46):

$$|b_0| \geq 1 - W_s > .8957 - W_s \geq \sum_{n=1}^{\infty} |b_n| \tag{5.49}$$

$$|b_0| > \sum_{n=1}^{\infty} |b_n| \tag{5.50}$$

Therefore, the post-main-path portion of the ISI equivalent filter is a minimum phase filter.

END OF PROOF

Coefficient Computation

Since the post-main-path filter is a minimum phase system, it can be safely inverted. As a result, the ZF equalizer for the post-main-path portion of the ISI equivalent filter may be computed as follows:

$$W_{\text{post\_equ}}(z) = \frac{1}{b_0 + b_1 z^{-1} + b_2 z^{-2} \cdots}. \tag{5.51}$$

The impulse response for this filter can be found though polynomial division, yielding the following set of coefficients: $w_0 = 1/b_0$, $w_1 = -b_1/b_0^2$, $w_2 = -b_2/b_0^2 + b_1^2/b_0^3$, $w_3 = -b_3/b_0^2 + 2b_1 b_2/b_0^3 - b_1^3/b_0^4$, etc.

The coefficients for the ZF equalizer can be estimated using ISI equivalent filter estimates $\hat{b}_n$ to provide:

$$\hat{w}_0 = 1/\hat{b}_0 \tag{5.52}$$

$$\hat{w}_1 = -\hat{b}_1/\hat{b}_0^2 \tag{5.53}$$

$$\hat{w}_2 = -\hat{b}_2/\hat{b}_0^2 + \hat{b}_1^2/\hat{b}_0^3 \tag{5.54}$$

$$\hat{w}_3 = -\hat{b}_3/\hat{b}_0^2 + 2\hat{b}_1\hat{b}_2/\hat{b}_0^3 - \hat{b}_1^3/\hat{b}_0^4. \tag{5.55}$$

etc...

The variances of coefficients $\hat{w}_n$ can be found roughly by making two simplifying approximations, for which the theoretical validity is demonstrated in Appendices C and D. The first approximation involves the reciprocal of a complex random variable. If complex random variable ζ has variance σ_ζ^2 then $1/\zeta$ has approximate variance $\sigma_{1/\zeta}^2 \approx \sigma_\zeta^2/|\mathrm{E}[\zeta]|^4$. The error in this approximation is small, provided that $\sigma_\zeta^2 << |\mathrm{E}[\zeta]|^2$. The second approximation is for the variance of a random variable raised to a power. The approximate variance of ζ^m is $\sigma_{\zeta^m}^2 = m^2|\mathrm{E}[\zeta]|^{2(m-1)}\sigma_\zeta^2$. This approximation is valid if $(\frac{m-1}{2})^2\sigma_\zeta^2 << |\mathrm{E}[\zeta]|^2$.

Using these two approximations and assuming $\hat{b}_n$ are independent identically distributed random variables yields the following "rough" approximations for the variances of the equalizer taps when estimated by (5.52) to (5.55):

$$\sigma_{w_0}^2 \approx \frac{\sigma_b^2}{|b_0|^4} \tag{5.56}$$

$$\sigma_{w_1}^2 \approx \left(1 + 4\left|\frac{b_1}{b_0}\right|^2\right)\frac{\sigma_b^2}{|b_0|^4} \tag{5.57}$$

$$\sigma_{w_2}^2 \approx \left(1 + 4\left|\frac{b_2}{b_0}\right|^2 + 9\left|\frac{b_1}{b_0}\right|^4\right)\frac{\sigma_b^2}{|b_0|^4} \tag{5.58}$$

$$\sigma_{w_3}^2 \approx \left(1 + 4\frac{|b_1|^2 + |b_2|^2 + |b_3|^2}{|b_0|^2} + 9\left|\frac{b_1}{b_0}\right|^4 + 36\left|\frac{b_1 b_2}{b_0^2}\right|^2 + 16\left|\frac{b_1}{b_0}\right|^6\right)\frac{\sigma_b^2}{|b_0|^4}, \tag{5.59}$$

where σ_b^2 is the variance of the i.i.d. $\hat{b}_n$ and depends on the estimator used to determine the ISI equivalent coefficients.

Since $|b_0|$ is much greater than the magnitudes of the other coefficients, any terms with either b_1 or b_2 or b_3 in the numerator will be much less than 1 and can be removed without introducing much error. This implies $\sigma^2_{w_0} \approx \sigma^2_{w_1} \approx \sigma^2_{w_2} \approx \sigma^2_{w_3} \approx \sigma^2_b / |b_0|^4$.

To get a general appreciation for the quality of this equalizer tap estimator, at least for a DOCSIS upstream channel, the approximations above are evaluated with the RMS values for b_0, b_1, b_2 and b_3 given in Figure 5.4 on page 95. The variance used for all $\hat{b}_n$ is that of the IL estimator described by equation (5.11) on page 92, which is $\sigma^2_b \simeq 0.25 / SNR$. With $SNR = 25dB = 10^{2.5}$, the results obtained by (5.56) to (5.59) are:

$\sigma^2_{w_0} \approx 0.79 \times 10^{-3}$, $\sigma^2_{w_1} \approx 0.90 \times 10^{-3}$, $\sigma^2_{w_2} \approx 0.91 \times 10^{-3}$, $\sigma^2_{w_3} \approx 1.1 \times 10^{-3}$. As expected, the variances are nearly the same.

It is now argued that the quality of $\hat{w}_n$ is sufficient if $\sigma^2_{w_n}$ is less than the average energy of tap n. The argument is essentially the same as that used in verifying the quality of $\hat{b}_n$. Tap n should be seeded with either 0 or $\hat{w}_n$, whichever produces the least estimation error. If tap n is seeded with 0, then the variance of estimation error is the average energy of tap n. Therefore, $\hat{w}_n$ should only be used if $\sigma^2_{w_n}$ is smaller than the average energy of tap n.

The mean squared values of the magnitudes of the equalizer coefficients were found through simulation. The simulation consisted of modeling Figure 5.1 on page 85 using a three-echo DOCSIS channel with echo strengths, delays and arrival phases given in Table 5.1 on page 94. The AWGN was set to 0, i.e. $SNR = \infty$ and the step size set to 1/64, i.e., $\Delta = 1/64$. The simulation length was sufficient for the adaptive equalizer to reach steady state in all trials. The magnitudes of the steady state tap weights so obtained were squared and averaged over 5000 trials with results as shown in Figure 5.9. Figure 5.9 shows that the average energies for taps 0, ..., 3 are 1.015, 29×10^{-3}, 35×10^{-3}, and 9.1×10^{-3} respectively, which are larger than the respective $\sigma^2_{w_n}$ by factors of 1265.8, 32.2, 38.5, and 8.3 respectively.

The circuit that estimates equalizer taps 0 to 3 from the ISI equivalent filter
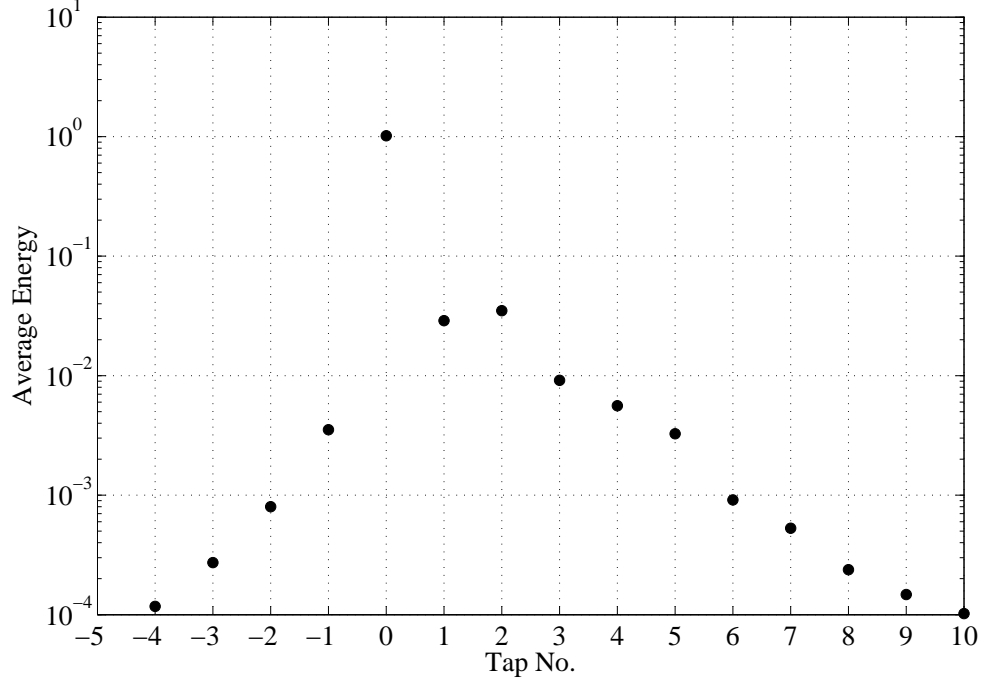
Figure 5.9   Energy distribution in the equalizer taps.

coefficients 0 to 3 is shown in Figure 5.10.

It should be mentioned that there may at first glance appear to be an inconsistency in the proposed equalization technique. This inconsistency arises from the fact that a ZF equalizer is used to generate an initial guess at the optimal set of coefficients for an LMS adaptive equalizer. Since the ZF and LMS algorithms strive to optimize different cost functions, they will inherently have differing sets of optimal equalizer coefficients. Consequently, it may seem counterproductive to seed an LMS equalizer with a set of coefficients generated using the ZF technique. However, as the signal-to-noise ratio is increased, the two techniques are known to converge to identical solutions, as discussed in [24]. Since DOCSIS upstream channels have high SNRS, the error introduced as a result of this algorithmic difference is small.
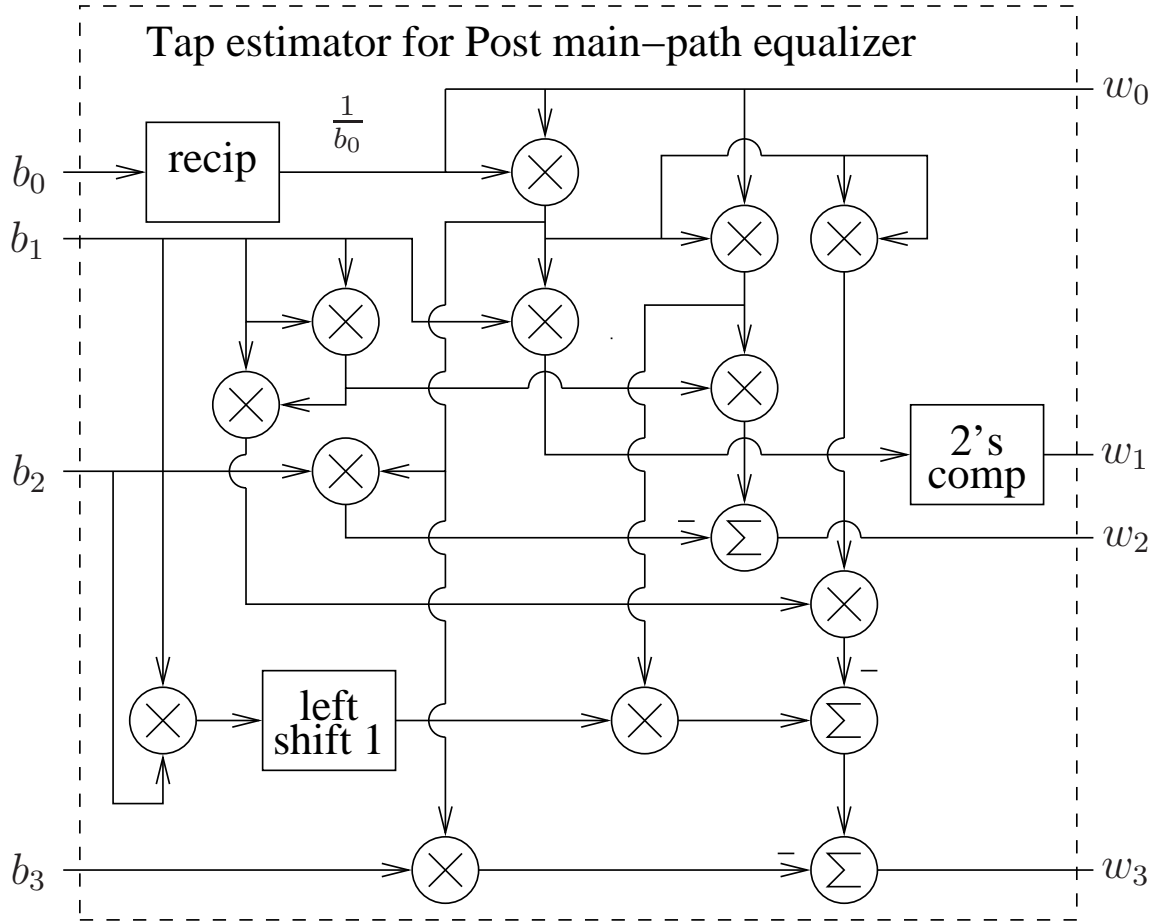
Figure 5.10 Circuit for generating estimates of 4 of the most influential coefficients of the equalizer.

5.3.3 Incorporating Pre-Main-Path Information for Initialization

The average energy of the pre-main-path coefficients is smaller than that of the post main-path coefficients, but possibly large enough to be worth estimating and using to seed a pre-main-path tap of the equalizer. The average normalized energies of b_{-2} and b_{-1} found by simulation are 0.94×10^{-3} and 3.5×10^{-3}, respectively. Since 3.5×10^{-3} is larger than the estimator variances computed in the previous section for the post-main-path taps, seeding w_{-1} should somewhat improve the performance of the equalizer. The same cannot be said for w_{-2}.
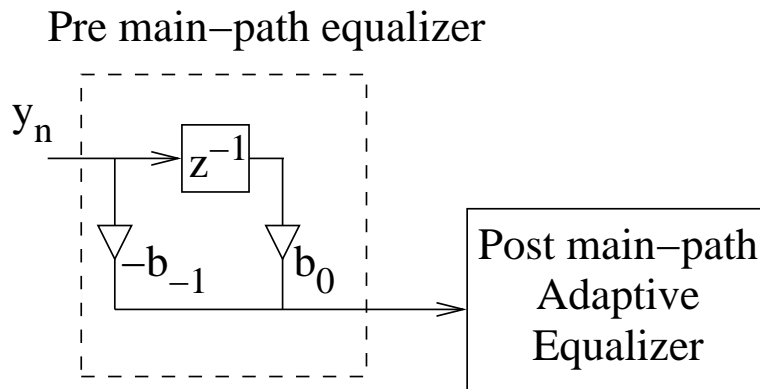
Figure 5.11 Structure of cascaded equalizers used to incorporate pre main-path information.

Unlike the post-main-path taps, w_{-1} cannot be estimated with long division. In fact, any attempt to use a ZF approach and directly invert the channel will be ineffective, due to the fact that the response of a filter with coefficients b_{-1}, b_0, b_1, b_2, and b_3 is no longer minimum phase. When a nonminumum phase system is inverted, the result is an unstable system.

To get around this problem, the approach taken is to construct an equalizer from two filters in cascade, as shown in Figure 5.11. The first of these filters is a simple length-two filter with fixed coefficients $s_{-1} = -b_{-1}$ and $s_0 = b_0$. The second is the post main-path equalizer for the simple length two filter in cascade with the ISI equivalent. When the simple filter s is placed in cascade with the ISI equivalent filter b, the adaptive equalizer effectively sees a new ISI equivalent filter which has an impulse response of $c = s \star b$. The simple two-tap filter is designed to cancel the ISI created by the first pre-main-path coefficient b_{-1} of the original ISI equivalent filter, which results in $c_{-1} = 0$. Intuitively, one would expect that an adaptive post main-path equalizer should be more effective if the first pre-main-path coefficient of the filter it is equalizing is zero.

The coefficients for the composite filter that is the cascade of the ISI equivalent filter (coefficients b_n) and the simple length-two filter (coefficients $s_{-1} = -b_{-1}$ and

$s_0 = b_0)$ are given by:

$$c_n = s_{-1}b_{n+1} + s_0 b_n$$
$$c_n = -b_{-1}b_{n+1} + b_0 b_n \qquad (5.60)$$

Clearly $c_{-1} = 0$, as desired.

After compensating for the ISI from the first pre-main-path coefficient through the use of the simple two-tap filter, the remaining ISI in the pre-main-path portion of c is small enough to be neglected. Consequently, the task which remains is to seed the adaptive equalizer based upon the post-main-path portion of the new ISI equivalent filter c. Given that this is essentially the same task faced in Section 5.3.2, the zero-forcing channel inversion solution proposed in said section applies equally well here.

The taps for the post main-path equalizer that compensates for the ISI remaining in c can be found by substituting c_0 to c_3 for b_0 to b_3 into (5.52) to (5.55). The cascade of the simple filter with the new post main-path filter creates a 5-tap sequence, which is used to seed the LMS equalizer. A circuit which calculates the weights for the 5-tap equalizer from the coefficients of the ISI equivalent filter is shown in Figure 5.12.

5.3.4 Computational Complexity

In order to properly evaluate the suitability of the proposed equalizer seeding algorithms, it is important to consider their computational complexity. Note that this analysis excludes the computational complexity of the estimation of the ISI equivalent filter coefficients, which was discussed in Section 5.2.4 and Appendix B.

As shown in Figure 5.10, the implementation of the post-main-path inversion technique discussed in Section 5.3.2 requires one reciprocal calculation, 48 real multiplications, and 27 real additions. The inclusion of one pre-main-path coefficient when seeding the adaptive equalizer requires 64 real multiplications and 39 real additions on top of the requirements of the post-main-path technique. Of course, these computations need to be performed only once per packet. After the excitation sequence is
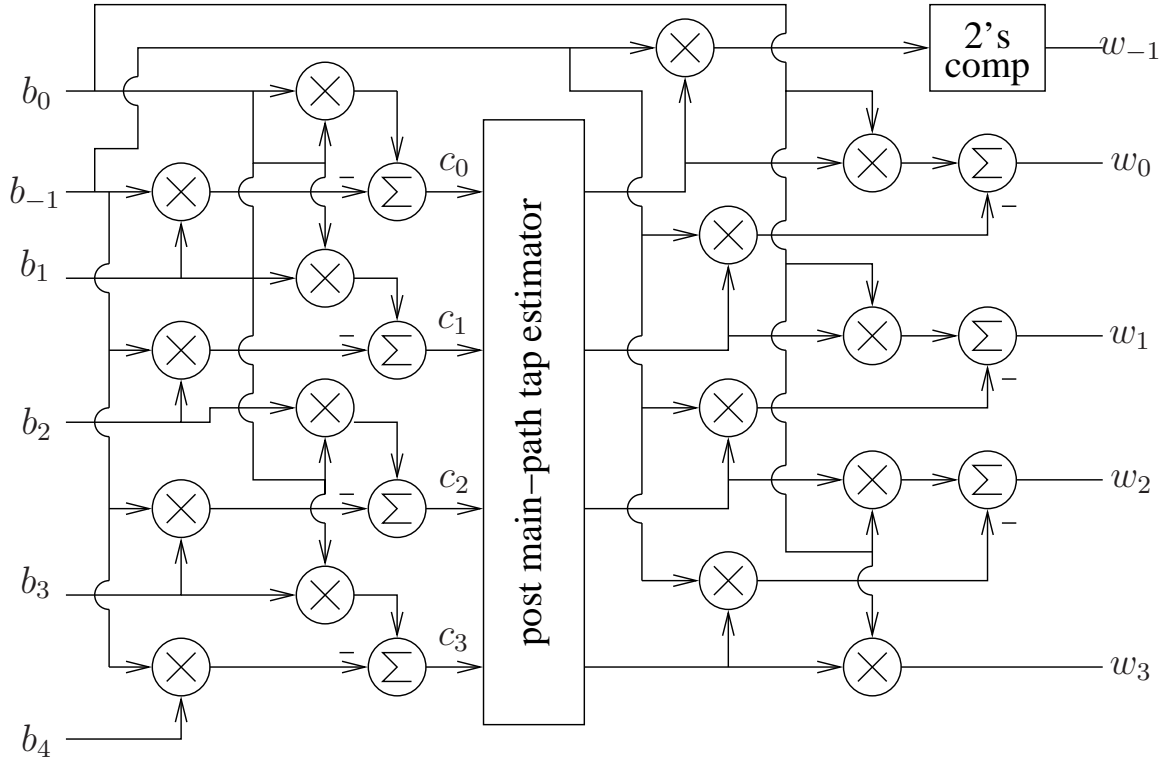
Figure 5.12 Circuit for equalizer utilizing pre main-path information.

complete and the equalizer has been seeded, the hardware resources used to seed the equalizer could potentially be utilized for some other purpose.

Table 5.3   Computational complexity of equalization algorithms.

Algorithm	Multiplications	Additions	Divisions
Post-main (one-time cost)	48	27	1
Pre-main + Post-main (one-time cost)	112	66	1
LMS (per update)	192	192	0
RLS (per update)	2689	2591	1

Table 5.3 summarizes the computational complexity of the proposed techniques. For the sake of comparison, the computational complexities of standard 24-tap LMS and RLS adaptive equalizers are also included in Table 5.3. Note that the computational complexity of the LMS and RLS algorithms was obtained from [21]. It is clear from the table that the computational costs of the proposed algorithms are relatively minor when compared to the complete adaptive equalizers.

5.4   Simulation Results

A series of MATLAB simulations was executed in order to evaluate the effectiveness of the proposed algorithms. The main goal of these simulations was to determine the decrease in the convergence time achieved by seeding the adaptive equalizer using the techniques discussed above.

A secondary goal was to determine the relative value of the ISI coefficient estimators that were considered in Section 5.2.4. To this end, the simulations were broken down into two categories: tests using the Impulse-Like sequence for ISI estimation, and tests using a Barker-Based sequence for ISI estimation. Sections 5.4.1 and 5.4.2 discuss these simulations in detail.

5.4.1   Impulse-Like ISI Estimator

In order to evaluate the effectiveness of the proposed algorithms, a collection of simulations were performed using a three-echo channel model which is based on the upstream portion of the DOCSIS standard. As before, the amplitudes, delays, and phases of these echoes were selected as in Table 5.1.

Additionally, uniformly distributed sample time errors and carrier phase offsets were incorporated into the input signal. As described in the DOCSIS up-stream channel model, AWGN was added to the system such that $E_s/N_0 = 25$ dB. Five thousand packets were generated, each experiencing a separate realization of the considered channel model. Each packet consisted of two sections: a variable-length preamble and a fixed-length one thousand symbol payload. The preamble portion of a DOCSIS upstream packet typically consists of a concatenation of two sequences: one used for timing, frequency, and phase estimation, and the other used to train the equalizer. In the following simulations, this typical preamble was augmented by a third sequence: the 5 symbol Impulse-Like excitation word for equalizer tap estimation, which was inserted immediately prior to the equalizer training sequence.

The signals described above were passed to an upstream DOCSIS demodulator.

126

This demodulator performed burst detection, timing recovery, carrier phase compensation, and channel equalization on each of the packets. For each packet, four different styles of equalization were performed:

1. *No Information:* A basic LMS equalizer for which all equalizer taps except the main tap start at zero.

2. *Post-Main:* The LMS equalizer is seeded with the four tap values given by equations (5.52) to (5.55) on page 119, which use only post-main-path ISI information. The coefficients for the ISI equivalent were estimated using equation (5.11) on page 92.

3. *Pre-and-Post-Main:* The LMS equalizer is seeded with five tap values found using the system shown in Figure 5.12 on page 125. The equalizer tap estimator uses coefficients from both the pre and post-main-path portions of the ISI filter. Once again, these coefficients are determined using equation (5.11) on page 92.

4. *RLS:* An unseeded equalizer which uses the RLS tap update algorithm is applied to the incoming symbols.

The performance of the proposed schemes is measured by the Modulation Error Ratio (MER). The adaptive equalizer was configured to adapt only during the preamble portion of the packet. The equalizer taps were then held constant for the duration of the payload, over which the MER of the final decision variable was computed for each packet. A high-level overview of the simulation setup is provided in Figure 5.13

One of the major factors influencing the convergence speed of an LMS-based adaptive equalizer is the tap update step size, Δ. Clearly, choosing a larger step size will allow the equalizer to converge more quickly. However, larger step sizes also lead to larger steady-state errors after convergence. In order to more precisely determine the relationship between step size and MER, a simulation was performed using the channel model and DOCSIS demodulator previously described. Since DOCSIS CMs

127
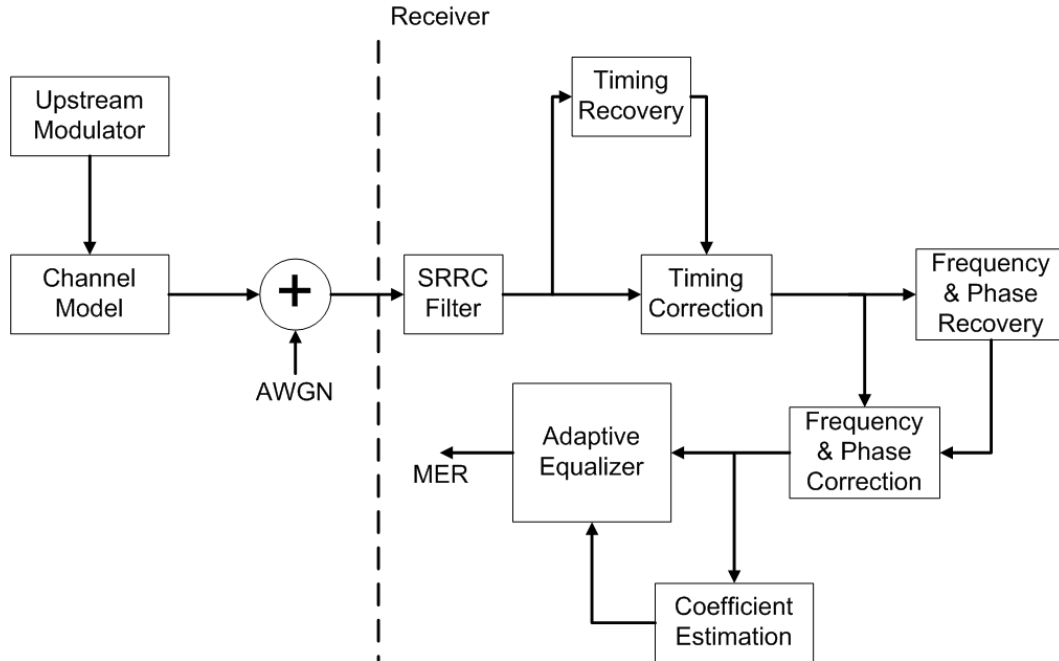
Figure 5.13 High-level overview of simulation for MER measurement.

allocate a fixed amount of memory to store preamble sequences, the equalizer training sequence is practically limited to approximately 160 symbols. Accordingly, an unseeded equalizer was used in conjunction with a fixed-length 160 symbol training sequence for this simulation. A choice of Δ which is a power of two is ideal for implementation, since the required multiplication may then be performed as a simple shift operation. For this reason, the simulation considered only step sizes which are powers of two. The results, which are plotted in Figure 5.14 indicate that the power of two which provides the most reasonable tradeoff between steady-state MER and convergence time is $\Delta = 1/64$ for an LMS equalizer with a 160-symbol training sequence.

Extensive simulations were performed to examine the convergence properties of the system using this so-called optimal step size. In these simulations, the equalizers were first initialized using the techniques discussed above, after which they were trained using a variable-length pseudorandom training sequence. For a variety of training sequence lengths, the probability of a payload's MER exceeding thresholds
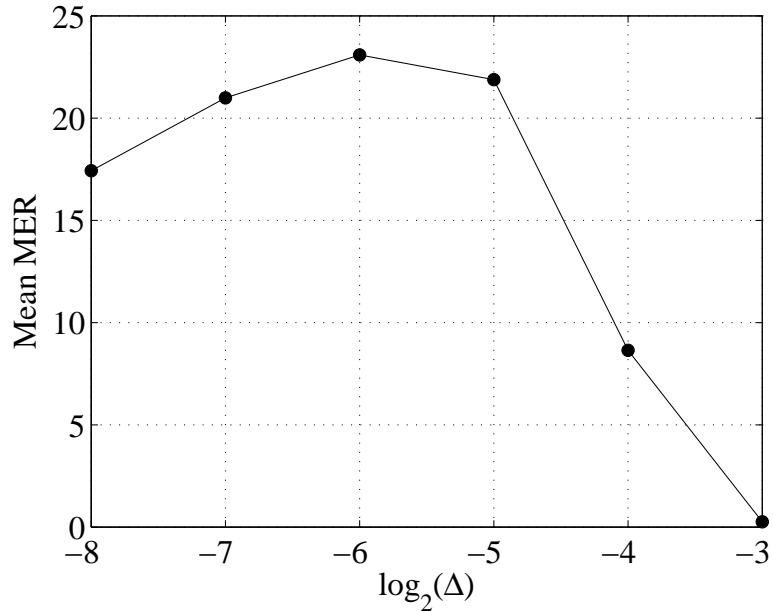
Figure 5.14 Tradeoff between step size and MER after 160 updates using the LMS
algorithm.

of 19dB and 22dB was determined using 5000 trials. In practice, system designers
would likely program the MAC to operate using MER thresholds that correspond to
target bit error rates. Accordingly, the thresholds in question were chosen for two
reasons: because they approximately correspond to bit error rates of 10^{-2} and 10^{-3}
for a 64-QAM system, and because they provide a good illustration of the advantages
of the proposed techniques.

Figures 5.15 and 5.16 plot the results of these simulations. It is clear from these
results that the proposed equalizer seeding techniques significantly improve the prob-
ability of obtaining high MERs during the payload phase of the packets. Although
the selections of target MERs and probabilities are implementation issues which need
to be sorted out by system designers, it appears likely that the proposed algorithms
can be used to reduce the length of the preamble by 50 to 60 symbols. It should be
pointed out that the excitation word used to estimate the channel ISI may be buffered
and then passed through the equalizer after the tap estimates have been obtained.
By proceeding in this manner, the system is able to utilize the excitation word as the
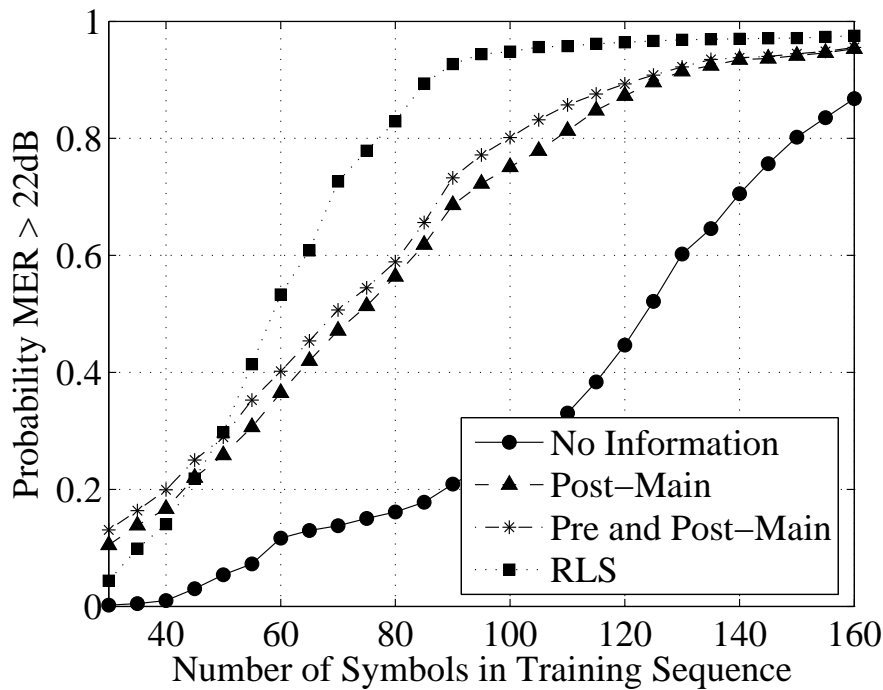
Figure 5.15 Equalizer convergence rates using IL sequence for ISI estimation, $\Delta = 1/64$, threshold = 22dB.

first symbols of the equalizer's training sequence. This allows the training sequence to be shortened, reducing the overall length of the preamble.

The same set of simulations was repeated using the simpler channel ISI estimator described by equation (5.9) on page 91 in place of the estimator given by equation (5.11). As expected, the estimator of equation (5.11) clearly outperformed the simpler estimator. The curves for the simpler estimator looked very similar to those in Figures 5.15 and 5.16, except that they were shifted approximately ten symbols to the right.

As expected, the results presented in Figures 5.15-5.16 indicate that a performance gain is possible by using the RLS algorithm to update the equalizer's coefficients. However, it is also apparent from Table 5.3 on page 125 that this additional performance at the cost of a roughly tenfold increase in computational complexity. Thus, it appears as though the proposed equalizer seeding techniques provide a sensible
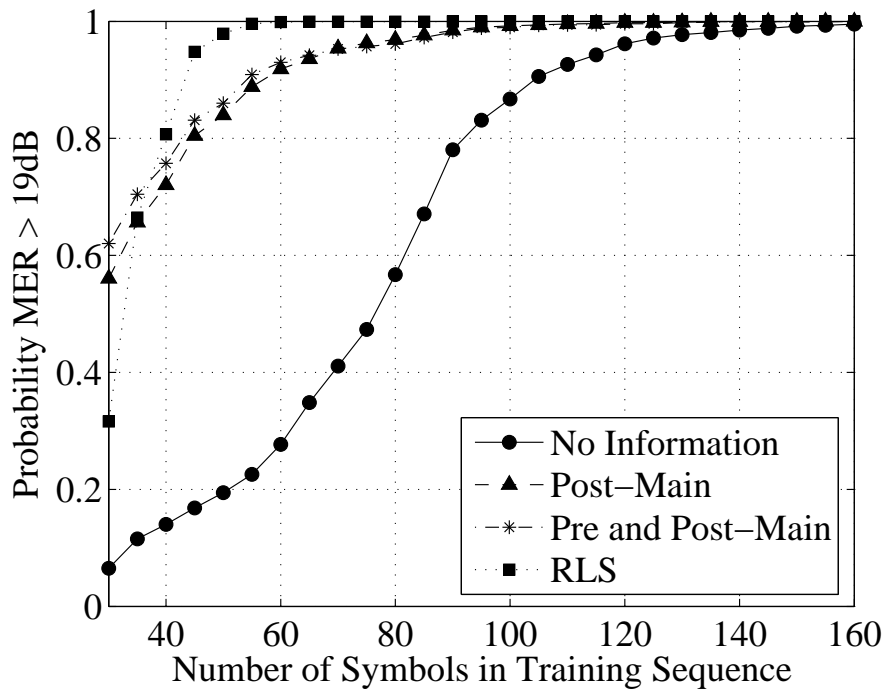
Figure 5.16 Equalizer convergence rates using IL sequence for ISI estimation, $\Delta = 1/64$, threshold $= 19$dB.

balance between the conflicting goals of fast convergence and low complexity when combined with an LMS equalizer.

5.4.2 Barker-Based ISI Estimators

As outlined in Section 5.2.4, an excitation word which is based upon a Barker sequence may be preferred over the Impulse-Like sequence for reasons related to the autocorrelation properties of the sequences. In order to determine the performance of the proposed equalizer seeding techniques when the Barker-Based excitation words are used for channel estimation, a series of MATLAB simulations were performed.

These simulations were identical to those discussed in Section 5.4.1, except that the excitation word used for ISI estimation was changed from the IL sequence to the BB5 and BB11 sequences. The simulations were repeated three times, each with a different excitation sequence and ISI estimator. The three combinations used were:

Figure 5.17 Comparison of equalizer convergence rates using IL, BB11, and BB11x3 for ISI estimation, $\Delta = 1/64$, threshold = 22dB.

1. A BB5 excitation sequence with the estimator detailed in Section B.3

2. A BB11 excitation sequence with the estimator detailed in Section B.4

3. A BB11x3 excitation sequence, which is obtained by repeating BB11 three times to make the sequence 33 symbols long. The estimator was average of three individual BB11 estimates, which were obtained from the estimator detailed in Section B.4.

The convergence properties of the equalizers which were seeded using the above sequences are presented in Figures 5.17 and 5.18, along with the results for the IL sequence. Note that in these figures, the abbreviations 'PM' and 'PPM' stand for 'Post-Main' and 'Pre-and-Post-Main', respectively.

The performance of the BB5 sequence was indistinguishable from that of the IL sequence, previously presented in Figures 5.15 and 5.16. This was expected, given
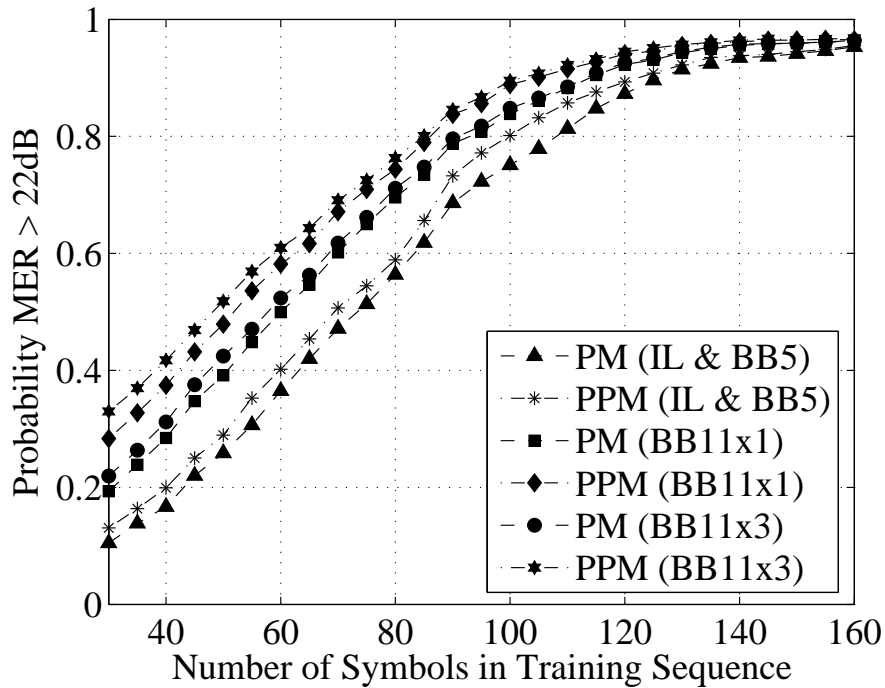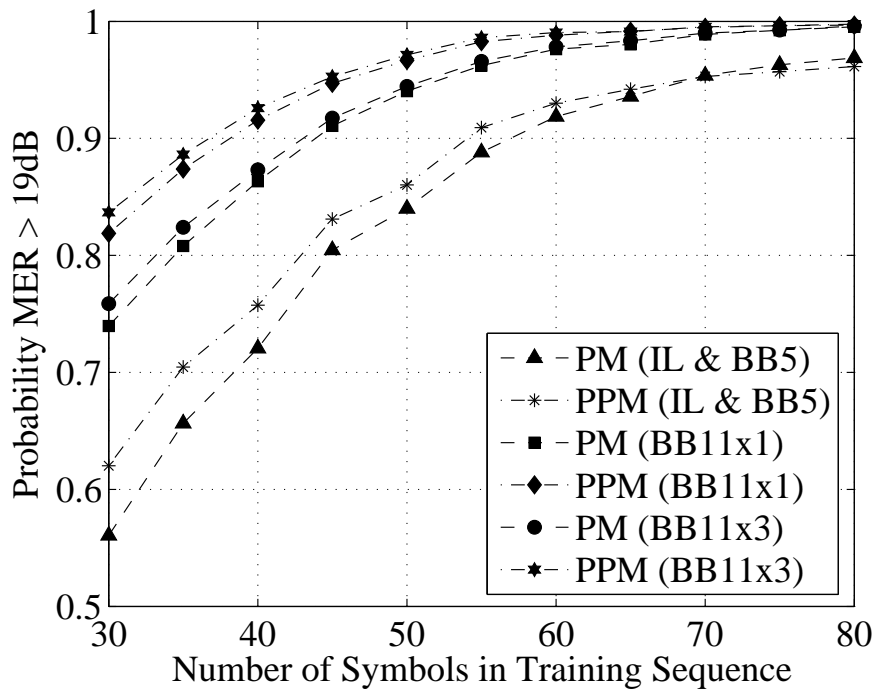
Figure 5.18 Comparison of equalizer convergence rates using IL, BB11, and BB11x3 for ISI estimation, $\Delta = 1/64$, threshold $= 22$dB.

that the theoretical average variances of the ISI estimators for these sequences are identical. To aid in readability, the curves which represent the IL and BB5 results have been combined in Figures 5.17 and 5.18.

As expected, the simulations indicated that the performance of the unseeded LMS and RLS equalizers are insensitive to the excitation word used for ISI estimation. Since the current goal is to compare the performance of various excitation sequences, the curves corresponding to the uninitialized equalizers were omitted from Figures 5.17 and 5.18, greatly improving their readability.

Unsurprisingly, the ISI estimation techniques with lower average variances allowed the LMS equalizer to converge more quickly. The simulation results indicate that the difference in convergence time between the BB11 and BB11x3 excitation sequences is very small for both the PM and PPM seeding techniques. Both of these sequences appear to have an advantage of around 10 to 15 symbols over the IL and BB5 se-

quences, which themselves are about 50 to 60 symbols faster than an unseeded LMS equalizer. In all cases, the PPM initialization technique converges faster than the PM technique, typically requiring approximately 5 fewer equalizer training symbols.

The cost-performance tradeoff for the proposed equalizer seeding techniques is summarized in Table 5.4. Note that the displayed costs correspond to real multiplications and additions. For each of the techniques, the approximate convergence speed increase in symbols with respect to an unseeded LMS equalizer is highlighted. It is apparent from Table 5.4 that the more complex techniques perform better, as expected. However, the costs of these more expensive approaches may outweigh the incremental improvements they provide over the simpler techniques. In terms of a cost-versus-benefit ratio, the most cost-effective techniques appear to be the BB5 excitation sequence with PM seeding and the IL excitation sequence with PM seeding.

Table 5.4   Computational complexity of equalization seeding techniques.

Excitation Word	Seeding	Multiplications	Additions	Excitation Word Length	Convergence Time Decrease
IL	PM	29	66	5	≈ 50
IL	PPM	68	130	5	≈ 55
BB5	PM	29	66	5	≈ 50
BB5	PPM	68	130	5	≈ 55
BB11	PM	37	120	11	≈ 65
BB11	PPM	76	184	11	≈ 70
BB11x3	PM	62	264	33	≈ 67
BB11x3	PPM	101	328	33	≈ 72

6. Contributions and Conclusions

The design of a DOCSIS upstream demodulator is a challenging problem due to the constraints imposed by the standard and the impairments in upstream cable channels. A high-performance demodulator must be able to estimate and correct for timing error, frequency error, phase error, and micro-reflections caused by the channel and do so on the fly. This implies the demodulator must contain a number of relatively complex circuits. It is especially challenging to implement these circuits in an FPGA, which has relatively few computational resources when compared with an ASIC.

This research has addressed issues related to the implementation of DOCSIS upstream synchronization and equalization circuits. The goal was to obtain algorithms that lead to economical implementations, yet perform at near-optimal levels. Although a large number of near-optimal algorithms are presented in the open literature, many of these are not appropriate for this application. A general contribution of this research is an analysis of the suitability of many prominent algorithms for frequency recovery and channel estimation in an FPGA-based DOCSIS upstream demodulator.

The specific research contributions in the areas of frequency synchronization and channel equalization are summarized separately in Sections 6.1 and 6.2.

6.1 Frequency Recovery Contributions

The main contribution in the area of frequency recovery is a novel economical frequency offset estimator for burst PSK signals, which has been derived from first principles. It is a suboptimal estimator that has economic and bandwidth efficiency

135

advantages over the optimum estimators described in the literature. Despite requiring minimal computation, theory predicts and simulation results verify that this estimator is unbiased and experiences a degradation of only 0.5dB with respect to the CRB. It has been shown that this estimator may be made immune to the effects of micro-reflections through the selection of a periodic preamble. Furthermore, the proposed estimator can be structured to allow unbiased operation for preambles of arbitrary periods. It is this flexibility that makes the estimator bandwidth efficient, as a system designer may select a preamble with segments that can be used in multiple synchronization tasks that are performed in parallel.

There are a number of well-known high-performance frequency recovery algorithms for burst channels, many of which are sufficiently inexpensive for use in an FPGA. However, the performance of these estimators in ISI-laden channels does not appear to have been studied in the open literature. This research has contributed an analysis of the impact of micro-reflections upon burst frequency estimators. The results of this analysis are a second main contribution of the research. It has been demonstrated that micro-reflections generally bias differential detector-based frequency estimators. A rule to predict whether a differential detector-based frequency offset estimator will be unbiased has been presented. Furthermore, it has been shown that a differential detector of width M will be an unbiased estimator if the segment of the preamble over which it operates is periodic with period M.

This research has demonstrated that a number of well-known frequency offset estimators such as those proposed by Kay, Mengali and Morelli, and Luise and Reggiannini require a segment of the preamble have a period of either one or two symbols in order to guarantee unbiased operation in ISI channels. This limitation makes the periodic segment of the preamble of little value for other parameter estimation circuits. Since these are well-known estimators which are likely used in a number of real-world applications, this revelation is very likely a significant contribution.

This research also provided two contributions related to maximum likelihood phase recovery. While these contributions have merit, they are of perhaps of lesser impor-

136

tance than the preceding contributions. First, a method for predicting the mean squared error of the maximum likelihood phase estimator for a PSK signal in the presence of a residual frequency offset has been presented. Second, a method for directly generating the complex constant required for correcting a phase offset has been demonstrated. The latter eliminates the need for an inverse tangent calculation and a look-up table, thereby reducing the computational cost of phase correction.

6.2   Equalization Contributions

To compensate for time-dependent micro-reflections in the upstream channel, DOCSIS upstream receivers must contain an adaptive equalizer. In an FPGA-based demodulator, this equalizer must rely upon the LMS algorithm, as the use of the RLS technique is impractical due to its high computational cost. However, the LMS algorithm is much slower to converge than the RLS, which necessitates longer training sequences, thereby reducing the amount of useful data which can be passed through the channel.

The main research contribution in this area is a novel technique for increasing the efficiency of the DOCSIS upstream channel by decreasing the convergence time of an adaptive equalizer. The technique models the user-specific upstream channel with an ISI equivalent filter. The coefficients of the ISI equivalent filter are estimated with a segment of the preamble referred to as the channel excitation sequence. Finally, the technique coarsely inverts the channel in order to estimate the four or five most important coefficients of the adaptive equalizer and seed the equalizer with these estimates. Simulation results show that the segment of the preamble used for training the equalizer can be reduced in length by up to 70 symbols if the equalizer is seeded using the proposed technique. In all cases, the computational costs of this technique are modest compared with those of the adaptive equalizer.

The selection of an excitation sequence for estimating the impulse response of a channel can have a significant impact on both the performance and complexity of the channel estimator. This research included an in-depth search for excitation

sequences which provide optimal or near-optimal performance, low channel estimation complexity, and are suitable for simultaneous use in other synchronization functions, such as timing recovery or frequency recovery. As a result of this search, four desirable sequences have been identified, representing a significant research contribution.

A second significant contribution of this research is a proof that the causal portion of the complex baseband ISI equivalent filter for a DOCSIS upstream channel is a minimum phase system. This result is critical to the method used to seed the equalizer, as it guarantees that the post-main path of the ISI equivalent filter will be stable if it is inverted.

When a pre-main-path coefficient is included in the complex baseband ISI equivalent model of the upstream channel, the overall equivalent filter is no longer minimum phase. As a result, any attempt to directly invert the filter's impulse response would result in instability. It has been proposed that a simple two-tap FIR filter be used to compensate for the pre-main-path ISI. The resulting impulse response of the cascade of the ISI equivalent filter and the simple filter is minimum phase, and can thus be safely inverted. This technique represents another significant contribution of this research.

A contribution of some importance is the observation that a phase offset estimator is of little value and therefore unnecessary if the equalizer is seeded. An equalizer will correct for phase offset, so in that respect, a phase offset estimator is always redundant. However, if the equalizer is not seeded, a phase estimator will decrease the equalizer's convergence time. If the equalizer is seeded with the inverse of the channel then that seeding will correct for the phase offset. This observation suggests that a standalone phase estimator is unnecessary in a system that utilizes a linear MVU channel estimator for the purpose of seeding the equalizer.

Two further contributions of lesser importance involve approximations of the statistical properties of nonlinear functions of a random variable. Specifically, taking the reciprocal of a random variable and raising a random variable to an arbitrary

power have been investigated, and approximations for the means and variances of the resulting random variables have been produced. These approximations can be used to simplify the performance analysis of communications systems.

6.3   Conclusions

In this research, a number of frequency recovery, phase recovery, and channel equalization algorithms have been investigated and considered for use in an FPGA-based DOCSIS upstream demodulator. The thesis is now concluded with a brief set of recommendations for DOCSIS upstream synchronization.

For frequency offset estimation, the equal averaging length estimator depicted in Figure 4.5 is recommended. The differential width M should be chosen to be 11, such that the frequency estimator operates using a segment of 33 symbols from the preamble. The preamble segment used for synchronization should include 4 repetitions of an 11-symbol Barker sequence, with the final 3 repetitions being used for frequency offset estimation. This will ensure the frequency offset estimator is unbiased in the presence of micro-reflections.

For channel equalization, a 24-tap adaptive equalizer should be used. The equalizer should be configured to adapt using the LMS algorithm with a step size of $\Delta = 1/64$. Using each of the 4 repetitions of the 11-symbol Barker sequence, four post-main path coefficients of the channel ISI equivalent filter should be estimated using either the P4 excitation sequence detailed in Section B.1 or the BB5 excitation sequence detailed in Section B.3. The channel estimates from each repetition of the Barker sequence should be averaged. The averaged channel estimate should be inverted using the post-main path technique discussed in Section 5.3.2 to yield 4 coefficients which may be used to seed the adaptive equalizer. It is anticipated that this seeding will allow the length of the equalizer training sequence to be reduced by approximately 65 symbols.

Since equalizer seeding is recommended, there is no need for a standalone phase

estimator.

Although timing recovery has not been directly covered in this research, it is anticipated that timing could be estimated by locating the peak of the output of a filter matched to the 11-symbol Barker sequence. The final timing estimate could potentially be the average of the estimates obtained for each of the four incoming Barker sequences.

A. Maximum Likelihood Frequency and Phase Offset Estimation

It is possible to obtain closed form expressions for the maximum likelihood (ML) frequency and phase offset estimators if we assume that the SNR of the input signal is high. From Section 4.3, the ML estimators must satisfy equations (4.27) and (4.28), which are restated here for reference:

$$
\begin{aligned}
0 = \frac{\partial \Lambda(y)}{\partial \Delta \omega} &= \frac{-1}{\sigma^2} \sum_{n=0}^{N-1} \left(y[n] e^{-j(\widehat{\Delta\omega}n + \widehat{\phi_o})}(jn) - y[n]^* e^{j(\widehat{\Delta\omega}n + \widehat{\phi_o})}(jn) \right) \\
0 &= \sum_{n=0}^{N-1} \left(-n y[n] e^{-j(\widehat{\Delta\omega}n + \widehat{\phi_o})} + n y[n]^* e^{j(\widehat{\Delta\omega}n + \widehat{\phi_o})} \right) \quad\quad (A.1)
\end{aligned}
$$

$$
\begin{aligned}
0 = \frac{\partial \Lambda(y)}{\partial \phi_0} &= \frac{-1}{\sigma^2} \sum_{n=0}^{N-1} \left(j y[n] e^{-j(\widehat{\Delta\omega}n + \widehat{\phi_o})} - j y[n]^* e^{j(\widehat{\Delta\omega}n + \widehat{\phi_o})} \right) \\
0 &= \sum_{n=0}^{N-1} \left(-y[n] e^{-j(\widehat{\Delta\omega}n + \widehat{\phi_o})} + y[n]^* e^{j(\widehat{\Delta\omega}n + \widehat{\phi_o})} \right) \quad\quad (A.2)
\end{aligned}
$$

The first step in the derivation is to decompose the input signal $y[n]$, into magnitude and phase terms:

$$
y[n] = |y[n]| e^{j \angle y[n]} \quad\quad (A.3)
$$

Substituting this expression into equations (A.1) and (A.2), we have:

$$
0 = \sum_{n=0}^{N-1} \left(-n |y[n]| e^{-j(\widehat{\Delta\omega}n + \widehat{\phi_o} - \angle y[n])} + n |y[n]| e^{j(\widehat{\Delta\omega}n + \widehat{\phi_o} - \angle y[n])} \right) \quad\quad (A.4)
$$

$$
0 = \sum_{n=0}^{N-1} \left(-|y[n]| e^{-j(\widehat{\Delta\omega}n + \widehat{\phi_o} - \angle y[n])} + |y[n]| e^{j(\widehat{\Delta\omega}n + \widehat{\phi_o} - \angle y[n])} \right) \quad\quad (A.5)
$$

If the SNR of the input signal is high, the argument of the exponential terms

in (A.4) and (A.5) will be close to zero. Thus, the expontial terms may be approximated using a first-order Maclaurin series as follows:

$$e^{-j(\widehat{\Delta\omega}n+\widehat{\phi_o}-\angle y[n])} \approx 1 - j(\widehat{\Delta\omega}n + \hat{\phi}_o - \angle y[n]) \tag{A.6}$$

$$e^{j(\widehat{\Delta\omega}n+\widehat{\phi_o}-\angle y[n])} \approx 1 + j(\widehat{\Delta\omega}n + \hat{\phi}_o - \angle y[n]) \tag{A.7}$$

Substituting these approximations into equation (A.4), we have:

$$0 = \sum_{n=0}^{N-1} \left(n|y[n]|2j(\widehat{\Delta\omega}n + \hat{\phi}_o - \angle y[n])) \right)$$

$$\sum_{n=0}^{N-1} n|y[n]| = \hat{\Delta\omega} \sum_{n=0}^{N-1} n^2|y[n]| + \hat{\phi}_o \sum_{n=0}^{N-1} n|y[n]| \tag{A.8}$$

Similarly, substituting the Maclaurin series approximations into equation (A.5) yields:

$$0 = \sum_{n=0}^{N-1} \left(|y[n]|2j(\widehat{\Delta\omega}n + \hat{\phi}_o - \angle y[n])) \right)$$

$$\sum_{n=0}^{N-1} |y[n]| = \hat{\Delta\omega} \sum_{n=0}^{N-1} n|y[n]| + \hat{\phi}_o \sum_{n=0}^{N-1} |y[n]| \tag{A.9}$$

Equations (A.8) and (A.9) may be written in matrix form as follows:

$$\begin{bmatrix} \sum_{n=0}^{N-1} n^2|y[n]| & \sum_{n=0}^{N-1} n|y[n]| \\ \\ \sum_{n=0}^{N-1} n|y[n]| & \sum_{n=0}^{N-1} |y[n]| \end{bmatrix} \begin{bmatrix} \hat{\Delta\omega} \\ \\ \hat{\phi}_o \end{bmatrix} = \begin{bmatrix} \sum_{n=0}^{N-1} n|y[n]|\angle y[n] \\ \\ \sum_{n=0}^{N-1} |y[n]|\angle y[n] \end{bmatrix} \tag{A.10}$$

$$A \begin{bmatrix} \hat{\Delta\omega} \\ \\ \hat{\phi}_o \end{bmatrix} = B \tag{A.11}$$

Clearly, in order to solve for the estimators, we must right multiply the inverse of matrix A by matrix B. The inverse of matrix A is found to be:

$$A^{-1} = \frac{\begin{bmatrix} \sum_{n=0}^{N-1} |y[n]| & -\sum_{n=0}^{N-1} n|y[n]| \\ \\ -\sum_{n=0}^{N-1} n|y[n]| & \sum_{n=0}^{N-1} n^2|y[n]| \end{bmatrix}}{\sum_{n=0}^{N-1} n^2|y[n]| \sum_{n=0}^{N-1} n|y[n]| - \left(\sum_{n=0}^{N-1} n|y[n]|\right)^2} \tag{A.12}$$

142

Finally, the ML estimators may be found using the matrix A^{-1}:

$$\begin{bmatrix} \hat{\Delta\omega} \\ \\ \hat{\phi}_o \end{bmatrix} = A^{-1}B$$

$$\begin{bmatrix} \hat{\Delta\omega} \\ \\ \hat{\phi}_o \end{bmatrix} = \frac{\begin{bmatrix} \sum_{n=0}^{N-1} |y[n]| \sum_{n=0}^{N-1} n|y[n]|\angle y[n] - \sum_{n=0}^{N-1} n|y[n]| \sum_{n=0}^{N-1} |y[n]|\angle y[n] \\ \\ -\sum_{n=0}^{N-1} n|y[n]| \sum_{n=0}^{N-1} n|y[n]|\angle y[n] + \sum_{n=0}^{N-1} n^2|y[n]| \sum_{n=0}^{N-1} |y[n]|\angle y[n] \end{bmatrix}}{\sum_{n=0}^{N-1} n^2|y[n]| \sum_{n=0}^{N-1} n|y[n]| - \left(\sum_{n=0}^{N-1} n|y[n]| \right)^2}$$

As can clearly be seen above, the estimators described by these equations involve a large number of calculations, making them unsuitable for a practical FPGA-based hardware implemenatation.

B. Detailed Discussion of ISI Estimation Schemes

In Section 5.2, the estimation of the coefficients of an upstream ISI equivalent filter was discussed. To recap, an argument based upon the average energy in the filter taps was used to conclude that it is sufficient to estimate either four or five coefficients, comprising one main tap, one optional pre-main tap, and three post-main taps. It was shown that the selection of an excitation word for ISI estimation can have a significant impact upon both the performance and the complexity of the ISI estimator. Section 5.2.4 investigated the properties of desirable excitation words for ISI estimation, leading to the selection of one suitable sequence for the case of a channel of length 4, and three suitable sequences for the case of a channel of length 5:

- 4-symbol perfect excitation sequence (for 4-tap channel)

- 5-symbol Impulse-Like (IL) excitation sequence (for 5-tap channel)

- 5-symbol Barker-Based (BB) excitation sequence (for 5-tap channel)

- 11-symbol Barker-Based (BB) excitation sequence (for 5-tap channel)

This appendix will consider the performance and implementation complexity of each of these sequences in detail.

B.1 4-Symbol Perfect Sequence

A 4-symbol perfect excitation word which is ideal for estimating the coefficients of a channel of length 4 has been identified. The excitation word in question consists of

the values $\begin{bmatrix} -1 & -1 & -1 & 1 \end{bmatrix}$. In order for this excitation word to generate a perfect excitation matrix, the registers in the ISI equivalent filter must initially contain with the values $\begin{bmatrix} 1 & -1 & 1 \end{bmatrix}$. Fortunately, the proposed excitation word and these 3 companion precursor symbols form a 7 symbol subset of an 11-symbol Barker sequence. Thus, if an 11-symbol Barker sequence is used for synchronization purposes, it is possible to capture a sequence of 4 outputs from the ISI equivalent filter having the following excitation matrix:

$$\mathbf{X_{p4}} = \begin{bmatrix} -1 & 1 & -1 & -1 \\ -1 & -1 & 1 & -1 \\ -1 & -1 & -1 & 1 \\ 1 & -1 & -1 & -1 \end{bmatrix} \tag{B.1}$$

Since the excitation matrix is perfect, the variance matrix for its MVU channel estimator is $\frac{1}{4 \cdot SNR} \mathbf{I_4}$. The estimator which achieves this variance is:

$$\hat{\mathbf{B}}_{\mathbf{p4}} = \frac{1}{4} \mathbf{X_{p4}}^* \mathbf{Y} \tag{B.2}$$

As noted in Section 5.2.4, the MVU estimator for a perfect excitation word may be implemented as a simple matched filter. The structure of the matched filter may be seen in Figure B.1 While the excitation sequence propagates through the matched filter, the filter's output is an estimate of the channel impulse response.

The matched filter implementation of Figure B.1 performs three complex additions for each output. Thus, the estimation of four channel coefficients requires 12 complex additions, or 24 real additions. The scaling by 1/4 indicated in the figure can be implemented as a bit shift, so the matched filter implementation does not require any multiplications.

B.2   5-Symbol Impulse-Like Sequence

When the IL sequence is transmitted, the sequence of values entering the ISI equivalent filter is $\begin{bmatrix} 1 & -1 & -1 & -1 & -1 \end{bmatrix}$. Assuming that all of the registers in the
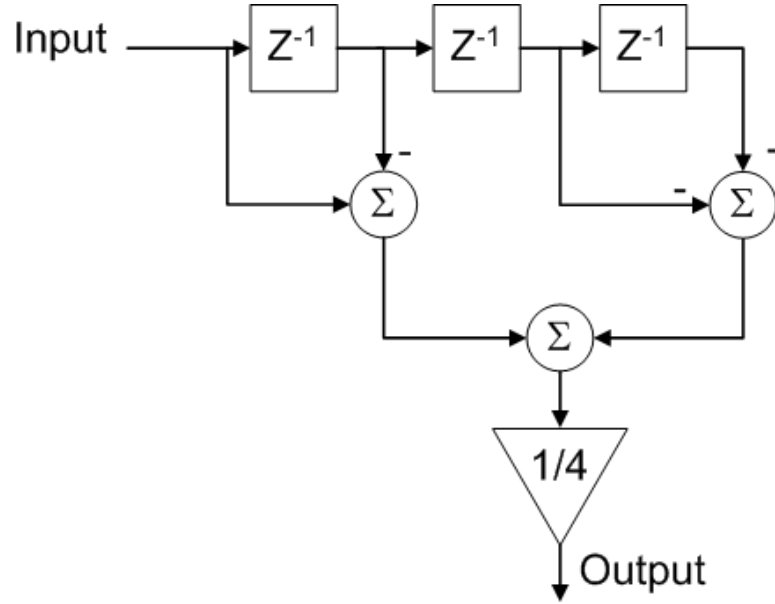
Figure B.1 Matched filter implementation of MVU estimator for perfect 4-symbol sequence.

ISI equivalent filter initially contain -1, the excitation matrix $\mathbf{X}$ becomes:

$$\mathbf{X_{IL}} = \begin{bmatrix} x_n & x_{n-1} & x_{n-2} & x_{n-3} & x_{n-4} \\ x_{n+1} & x_n & x_{n-1} & x_{n-2} & x_{n-3} \\ x_{n+2} & x_{n+1} & x_n & x_{n-1} & x_{n-2} \\ x_{n+3} & x_{n+2} & x_{n+1} & x_n & x_{n-1} \\ x_{n+4} & x_{n+3} & x_{n+2} & x_{n+1} & x_n \end{bmatrix} = \begin{bmatrix} 1 & -1 & -1 & -1 & -1 \\ -1 & 1 & -1 & -1 & -1 \\ -1 & -1 & 1 & -1 & -1 \\ -1 & -1 & -1 & 1 & -1 \\ -1 & -1 & -1 & -1 & 1 \end{bmatrix} \quad \text{(B.3)}$$

The variance of the MVU estimator for this excitation matrix is:

$$\mathbf{V_B} = \mathrm{Var}(\hat{\mathbf{B}}) = \frac{1}{SNR}(\mathbf{X_{IL}}^*\mathbf{X_{IL}})^{-1}$$

$$= \frac{1}{SNR} \left(\begin{bmatrix} 1 & -1 & -1 & -1 & -1 \\ -1 & 1 & -1 & -1 & -1 \\ -1 & -1 & 1 & -1 & -1 \\ -1 & -1 & -1 & 1 & -1 \\ -1 & -1 & -1 & -1 & 1 \end{bmatrix} \cdot \begin{bmatrix} 1 & -1 & -1 & -1 & -1 \\ -1 & 1 & -1 & -1 & -1 \\ -1 & -1 & 1 & -1 & -1 \\ -1 & -1 & -1 & 1 & -1 \\ -1 & -1 & -1 & -1 & 1 \end{bmatrix} \right)^{-1}$$

$$= \frac{1}{SNR} \begin{bmatrix} 0.2222 & -0.0278 & -0.0278 & -0.0278 & -0.0278 \\ -0.0278 & 0.2222 & -0.0278 & -0.0278 & -0.0278 \\ -0.0278 & -0.0278 & 0.2222 & -0.0278 & -0.0278 \\ -0.0278 & -0.0278 & -0.0278 & 0.2222 & -0.0278 \\ -0.0278 & -0.0278 & -0.0278 & -0.0278 & 0.2222 \end{bmatrix} \quad \text{(B.4)}$$

As before, the term 'average variance' will be used to refer to the average of the variances of the estimators for the individual ISI equivalent coefficients. For the IL sequence, the average variance of the MVU estimator is $\frac{0.2222}{SNR}$.

The estimator which acheives this average variance is given by:

$$\hat{\mathbf{B}} = (\mathbf{X_{IL}}^*\mathbf{X_{IL}})^{-1}\mathbf{X_{IL}}^*\mathbf{Y}$$

$$\begin{bmatrix} \widehat{b_{-1}} \\ \widehat{b_0} \\ \widehat{b_1} \\ \widehat{b_2} \\ \widehat{b_3} \end{bmatrix} = \frac{1}{6} \begin{bmatrix} 2 & -1 & -1 & -1 & -1 \\ -1 & 2 & -1 & -1 & -1 \\ -1 & -1 & 2 & -1 & -1 \\ -1 & -1 & -1 & 2 & -1 \\ -1 & -1 & -1 & -1 & 2 \end{bmatrix} \begin{bmatrix} y_{-1} \\ y_0 \\ y_1 \\ y_2 \\ y_3 \end{bmatrix} \quad \text{(B.5)}$$

Due to the symmetry of the square matrix in equation (B.5), the estimators of the individual ISI equivalent filter coefficients may be expressed in a very compact form, as originally presented in Section 5.2.1:

$$\hat{b}_n = \frac{y_n}{2} - \frac{\sum_{k=-1}^{3} y_k}{6} \quad -1 \leq n \leq 3 \quad \text{(B.6)}$$

The MVU set of estimators for the ISI equivalent filter coefficients when the IL sequence is transmitted which is represented by equations (B.5) and (B.6) may be
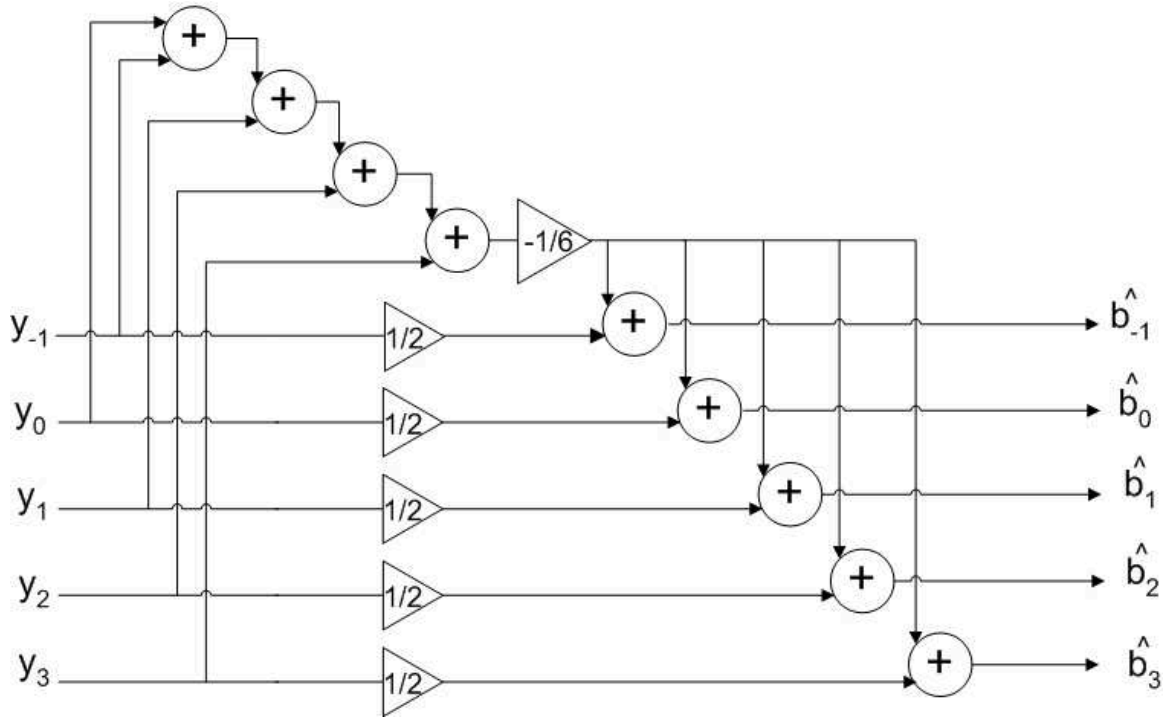
Figure B.2 MVU estimators for ISI equivalent coefficients using Impulse-Like sequence.

implemented using the structure shown in Figure B.2. The implementation shown in Figure B.2 is very economical, since it is able to take advantage of the fact that all of the estimators make use of the term $\sum_{k=-1}^{3} y_k$. When this sum is computed only once and all of the multiplications by $1/2$ are performed as shifts, the computational cost associated with the IL scheme is 9 complex additions and 1 complex scaling. In terms of operations on real numbers, this works out to 18 real additions and 2 real multiplications.

B.3   5-Symbol Barker-Based Sequence

As discussed in Section 5.2.4, Barker sequences have desirable autocorrelation properties which make them ideal for the purposes of timing recovery and equalization. If an 11-symbol Barker sequence is transmitted as part of the synchronization preamble, it is possible to capture a sequence of 5 outputs from the ISI equivalent

filter having the following excitation matrix $\mathbf{X_{BB5}}$:

$$\mathbf{X_{BB5}} = \begin{bmatrix} -1 & -1 & -1 & 1 & 1 \\ 1 & -1 & -1 & -1 & 1 \\ -1 & 1 & -1 & -1 & -1 \\ -1 & -1 & 1 & -1 & -1 \\ 1 & -1 & -1 & 1 & -1 \end{bmatrix} \tag{B.7}$$

For this excitation matrix, the variance of the MVU set of estimators is:

$$
\begin{aligned}
\mathbf{V_B} &= \mathrm{Var}(\hat{\mathbf{B}}) = \frac{1}{SNR}(\mathbf{X_{BB5}}^*\mathbf{X_{BB5}})^{-1} \\
&= \frac{1}{SNR} \left(\begin{bmatrix} -1 & -1 & -1 & 1 & 1 \\ 1 & -1 & -1 & -1 & 1 \\ -1 & 1 & -1 & -1 & -1 \\ -1 & -1 & 1 & -1 & -1 \\ 1 & -1 & -1 & 1 & -1 \end{bmatrix} \cdot \begin{bmatrix} -1 & 1 & -1 & -1 & 1 \\ -1 & -1 & 1 & -1 & -1 \\ -1 & -1 & -1 & 1 & -1 \\ 1 & -1 & -1 & -1 & 1 \\ 1 & 1 & -1 & -1 & -1 \end{bmatrix} \right)^{-1} \\
&= \frac{1}{SNR} \begin{bmatrix} 0.2222 & 0.0278 & 0.0278 & -0.0278 & -0.0278 \\ 0.0278 & 0.2222 & -0.0278 & 0.0278 & 0.0278 \\ 0.0278 & -0.0278 & 0.2222 & 0.0278 & 0.0278 \\ -0.0278 & 0.0278 & 0.0278 & 0.2222 & -0.0278 \\ -0.0278 & 0.0278 & 0.0278 & -0.0278 & 0.2222 \end{bmatrix} \tag{B.8}
\end{aligned}
$$

The average variance represented by equation (B.8) is equal to $\frac{0.2222}{SNR}$, which is equal to that of the IL sequence. This average variance is also the lowest possible value for any excitation sequence of length 5.

The set of MVU estimators which achieves the variance of (B.8) is obtained as

follows:

$$\hat{\mathbf{B}} = (\mathbf{X_{BB5}}^*\mathbf{X_{BB5}})^{-1}\mathbf{X_{BB5}}^*\mathbf{Y}$$

$$\begin{bmatrix} \widehat{b_{-1}} \\ \widehat{b_0} \\ \widehat{b_1} \\ \widehat{b_2} \\ \widehat{b_3} \end{bmatrix} = \frac{1}{6} \begin{bmatrix} -2 & 1 & -1 & -1 & 1 \\ -1 & -1 & 1 & -2 & -1 \\ -1 & -1 & -2 & 1 & -1 \\ 1 & -2 & -1 & -1 & 1 \\ 1 & 1 & -1 & -1 & -2 \end{bmatrix} \begin{bmatrix} y_{-1} \\ y_0 \\ y_1 \\ y_2 \\ y_3 \end{bmatrix} \tag{B.9}$$

Although not as obvious as in the case of the IL sequence, it is possible to optimize the computation of these estimates by factoring out some terms common to all of the estimators. To see this first define the sum S_{BB5} as follows:

$$S_{BB5} = -y_{-1} - y_0 + y_1 + y_2 - y_3 \tag{B.10}$$

Each of the inidividual ISI coefficient estimators may then be written in terms of S_{BB5}:

$$\widehat{b_{-1}} = -\frac{S_{BB5}}{6} - \frac{y_{-1}}{2} \tag{B.11}$$

$$\widehat{b_0} = \frac{S_{BB5}}{6} - \frac{y_2}{2} \tag{B.12}$$

$$\widehat{b_1} = \frac{S_{BB5}}{6} - \frac{y_1}{2} \tag{B.13}$$

$$\widehat{b_2} = -\frac{S_{BB5}}{6} - \frac{y_0}{2} \tag{B.14}$$

$$\widehat{b_3} = -\frac{S_{BB5}}{6} - \frac{y_3}{2} \tag{B.15}$$

A circuit which implements equations (B.11)-(B.15) is presented in Figure B.3. Comparing Figures B.2 and B.3, it is apparent that the implementation structure of the MVU estimators for the BB5 sequence is equivalent to that of the IL sequence. Therefore, the implementation costs are identical - 18 real additions and 2 real multiplications. The only difference is that some of the adders in Figure B.3 negate their inputs.
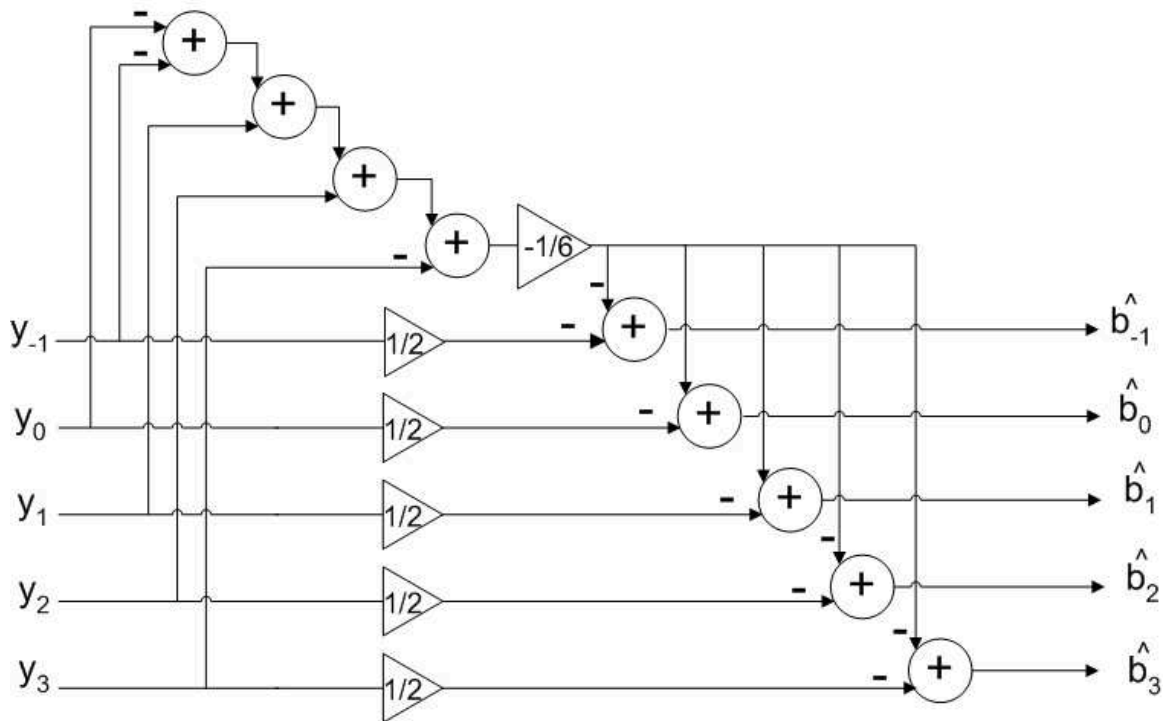
Figure B.3 MVU estimators for ISI equivalent coefficients using 5-symbol Barker-Based sequence.

B.4 11-Symbol Barker-Based Sequence

If an 11-symbol Barker sequence is transmitted, it is possible to make use of all 11 of the outputs from the ISI equivalent filter in order to estimate the channel ISI coefficients. When the complete 11-symbol Barker sequence is used for ISI estimation,

the excitation matrix $\mathbf{X_{BB11}}$ becomes:

$$\mathbf{X_{BB11}} = \begin{bmatrix} 1 & -1 & 1 & -1 & -1 \\ 1 & 1 & -1 & 1 & -1 \\ 1 & 1 & 1 & -1 & 1 \\ -1 & 1 & 1 & 1 & -1 \\ -1 & -1 & 1 & 1 & 1 \\ -1 & -1 & -1 & 1 & 1 \\ 1 & -1 & -1 & -1 & 1 \\ -1 & 1 & -1 & -1 & -1 \\ -1 & -1 & 1 & -1 & -1 \\ 1 & -1 & -1 & 1 & -1 \\ -1 & 1 & -1 & -1 & 1 \end{bmatrix} \tag{B.16}$$

Note that the above excitation matrix assumes that the ISI equivalent filter is initially filled with symbols from a previous repetition of the 11-symbol Barker sequence.

As before, the variance of the MVU estimator for this sequence may be computed using the excitation matrix:

$$\begin{aligned} \mathbf{V_B} &= \text{Var}(\hat{\mathbf{B}}) = \frac{1}{SNR}(\mathbf{X_{BB11}}^*\mathbf{X_{BB11}})^{-1} \\ &= \frac{1}{SNR} \begin{bmatrix} 0.0952 & 0.0119 & 0.0119 & 0.0119 & 0.0119 \\ 0.0119 & 0.0952 & 0.0119 & 0.0119 & 0.0119 \\ 0.0119 & 0.0119 & 0.0952 & 0.0119 & 0.0119 \\ 0.0119 & 0.0119 & 0.0119 & 0.0952 & 0.0119 \\ 0.0119 & 0.0119 & 0.0119 & 0.0119 & 0.0952 \end{bmatrix} \end{aligned} \tag{B.17}$$

Equation (B.17) indicates that the average variance of the MVU estimator for the ISI coefficients using the BB11 sequence is $\frac{0.0952}{SNR}$. As expected, this variance is lower than that of the IL and BB5 sequences. However, this improved performance comes at a cost in terms of computational complexity, as is apparent when the structure of

the MVU estimators is considered:

$$\hat{\mathbf{B}} = (\mathbf{X_{BB11}}^*\mathbf{X_{BB11}})^{-1}\mathbf{X_{BB11}}^*\mathbf{Y}$$

$$\begin{bmatrix} \widehat{b_{-1}} \\ \widehat{b_0} \\ \widehat{b_1} \\ \widehat{b_2} \\ \widehat{b_3} \end{bmatrix} = \frac{1}{42} \begin{bmatrix} 3 & 4 & 5 & -3 & -3 & -4 & 3 & -5 & -5 & 3 & -4 \\ -4 & 4 & 5 & 4 & -3 & -4 & -4 & 2 & -5 & -4 & 3 \\ 3 & -3 & 5 & 4 & 4 & -4 & -4 & -5 & 2 & -4 & -4 \\ -4 & 4 & -2 & 4 & 4 & 3 & -4 & -5 & -5 & 3 & -4 \\ -4 & -3 & 5 & -3 & 4 & 3 & 3 & -5 & -5 & -4 & 3 \end{bmatrix} \begin{bmatrix} y_{-1} \\ y_0 \\ y_1 \\ y_2 \\ y_3 \\ y_4 \\ y_5 \\ y_6 \\ y_7 \\ y_8 \\ y_9 \end{bmatrix} \quad \text{(B.18)}$$

It is not immediately obvious how to most efficiently implement the set of estimators represented by (B.18). A direct implementation of the MVU estimators would require 11 complex multiplications and 10 complex estimations per ISI coefficient, for a total of 55 complex multiplications and 50 complex additions. Compared with the number of computations required for the IL and BB5 estimators, this seems a bit excessive.

Fortunately, it is possible to optimize the calculations in order to greatly reduce the number of operations required. Close observation of the estimation matrix $\mathbf{K}$ indicates that each column contains only two values. Furthermore, the difference between the two values in each column is seven in all cases. This suggests that once one of the $\widehat{b_n}$ values has been calculated, the others may be expressed efficiently in terms of the already-computed coefficient. Since it makes no difference which coefficient is computed directly, we will proceed assuming that $\widehat{b_{-1}}$ is chosen. Then, $\widehat{b_{-1}}$ will be calculated as:

$$\widehat{b_{-1}} = \frac{3(y_{-1} - y_2 - y_3 + y_5 + y_8) + 4(y_0 - y_4 - y_9) + 5(y_1 - y_6 - y_7)}{42} \quad \text{(B.19)}$$

A circuit which implements this equation is shown in Figure B.4. Note that the multiplications by 3 and 5 could by implemented as $2^2 - 1$ and $2^2 + 1$ respectively. In this
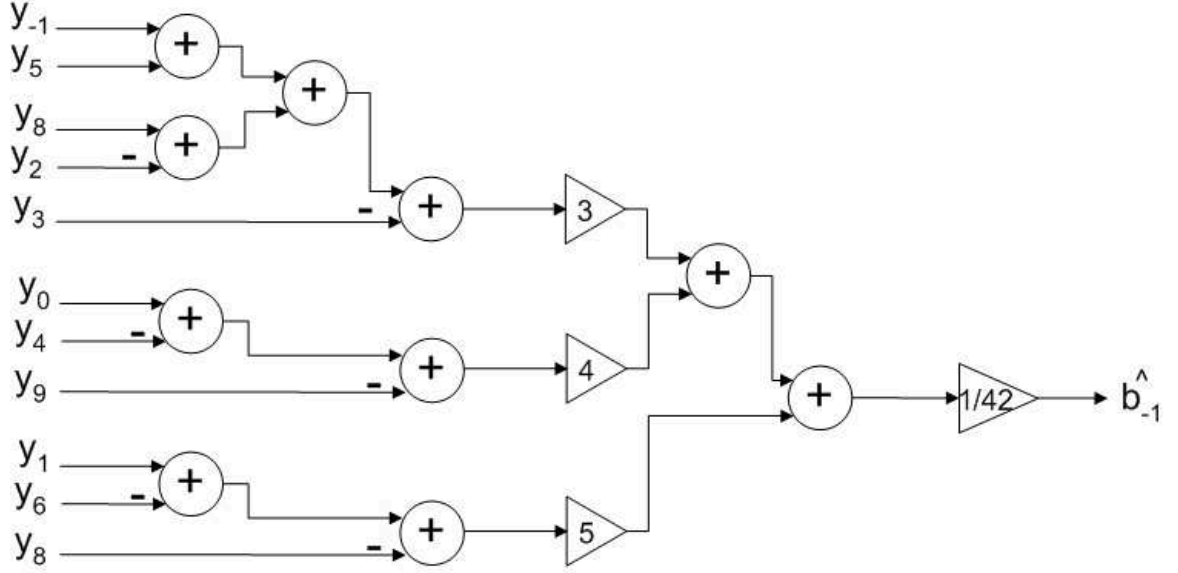
153

Figure B.4 MVU estimator for ISI coefficient $\widehat{b_{-1}}$ using 11-symbol Barker-Based sequence.

way, each multiplication may be implemented instead as an addition. Consequently, the computation of $\widehat{b_{-1}}$ requires 12 complex additions and 1 complex scaling, or 24 real additions and 2 real multiplications.

It is now possible to write the estimators for each of the other ISI coefficients in terms of $\widehat{b_{-1}}$:

$$\widehat{b_0} = \widehat{b_{-1}} + \frac{(y_2 + y_6 + y_9 - y_{-1} - y_5 - y_8)}{6} \tag{B.20}$$

$$\widehat{b_1} = \widehat{b_{-1}} + \frac{(y_2 + y_3 + y_7 - y_0 - y_5 - y_8)}{6} \tag{B.21}$$

$$\widehat{b_2} = \widehat{b_{-1}} + \frac{(y_2 + y_3 + y_4 - y_{-1} - y_1 - y_5)}{6} \tag{B.22}$$

$$\widehat{b_3} = \widehat{b_{-1}} + \frac{(y_3 + y_4 + y_9 - y_{-1} - y_0 - y_8)}{6} \tag{B.23}$$

Since the structures of the four estimators represented by equations (B.20)-(B.23) are identical, only the estimator for $\widehat{b_0}$ is depicted in Figure B.5. Each of these estimators will require 12 real additions and 2 real multiplications. In total, the set of ISI equivalent coefficient estimators for the BB11 sequence will require 72 real additions and 10 real multiplications.

154
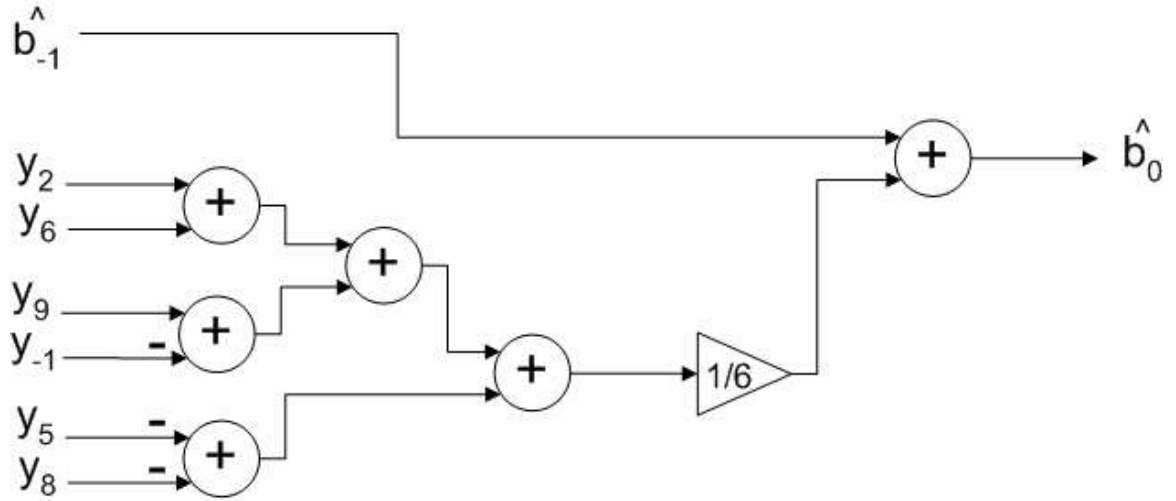
Figure B.5 MVU estimator for ISI coefficient $\widehat{b}_0$ using 11-symbol Barker-Based sequence.

B.5 Summary

The performance and complexity of the ISI coefficient estimators was summarized in Table 5.2 in the main body of the document. For the sake of convenience, the table is repeated here as Table B.1:

Table B.1 Performance and complexity of MVU estimators of ISI equivalent coefficients.

Sequence	Length	Implementation Complexity		Average Variance
	(symbols)	Multiplications	Additions	
P4	4	0	24	0.250 / SNR
IL	5	2	18	0.2222/SNR
BB5	5	2	18	0.2222/SNR
BB11	11	10	72	0.0952/SNR

C. Reciprocal of a Random Variable

Let ζ be a random variable (RV) with mean μ and variance σ^2. Define RV ϵ in terms of ζ by $\epsilon = \zeta - \mu$. Then $E[\epsilon] = 0$ and $E[\epsilon^2] = \sigma^2$. The random variable $1/\zeta$ can be written as

$$
\begin{aligned}
\frac{1}{\zeta} &= \frac{1}{\mu + \epsilon} \\
&= \frac{1}{\mu + \epsilon}\left(\frac{\mu - \epsilon}{\mu - \epsilon}\right) \\
&= \frac{\mu - \epsilon}{\mu^2 - \epsilon^2}
\end{aligned}
$$

Under the condition $\epsilon << \mu$, the RV $1/\zeta$ can be approximated by

$$
\frac{1}{\zeta} \approx \frac{\mu - \epsilon}{\mu^2}.
$$

This implies that under the condition $\epsilon << \mu$, the mean and variance of RV $1/\zeta$ are approximately $\frac{1}{\mu}$ and $\frac{\sigma^2}{\mu^4}$, respectively.

D. Raising a Random Variable to a Power

Let ζ be a RV with mean μ and variance σ^2. Define RV ϵ in terms of ζ by $\epsilon = \zeta - \mu$. Then

$$
\begin{aligned}
\zeta^m &= (\mu + \epsilon)^m \\
&= \mu^m \left(1 + \frac{\epsilon}{\mu}\right)^m .
\end{aligned}
\tag{D.1}
$$

Using the binomial theorem, RV ζ^m, for m a positive integer, is given by

$$
\zeta^m = \mu^m \sum_{k=0}^{m} g_k
\tag{D.2}
$$

where

$$
g_k = \frac{m!}{k!(m-k)!} \left(\frac{\epsilon}{\mu}\right)^k \quad ; \quad 0 \le k \le m
$$

The ratio g_{k+1}/g_k is

$$
\vartheta_k = \frac{g_{k+1}}{g_k} = \frac{(m-k)\epsilon}{(k+1)\mu}; \quad 0 \le k < m.
$$

Assume that $\epsilon/\mu << 2/(m-1)$. This assumption implies that

$$
1 >> \frac{(m-1)\epsilon}{2\mu} > \frac{(m-k)\epsilon}{(k+1)\mu} > \frac{(m-i)\epsilon}{(i+1)\mu}
\tag{D.3}
$$

for $i > k$. This has ϑ_k monotonic decreasing and implies

$$
g_1 >> g_2 >> g_3 >> \ldots >> g_m.
\tag{D.4}
$$

In this case equation (D.2) can be approximated by

$$
\begin{aligned}
\zeta^m &\approx \mu^m (1 + g_1); \quad (m-1)\epsilon << 2\mu \\
&\approx \mu^m + m\epsilon\mu^{m-1}; \quad (m-1)\epsilon << 2\mu.
\end{aligned}
\tag{D.5}
$$

Since $E[\epsilon] = 0$ and $E[\epsilon^2] = \sigma^2$, squaring equation (D.5) and taking the expected value has the variance of ζ^m approximately equal to $m^2 \mu^{2m-2} \sigma^2$.

E. Proof of Independence of Noise Samples at Output of ISI Equivalent Filter

As shown in Figure 5.1, the signal which enters the receiver is corrupted by John-son noise. In the receiver, the Additive White Gaussian Noise (AWGN) process is sampled to generate a discrete-time AWGN sequence which will be referred to as λ. The noise sequence is filtered by the receiver's shaping filter, which is a square root raised cosine filter in DOCSIS upstream systems:

$$g = \lambda \star h_{srrc} \qquad (E.1)$$

where g is the filtered noise output and h_{srrc} is the impulse response of the filter. In [55], it is shown that the autocorrelation of a filtered stochastic process is:

$$R_{yy}[n] = R_{xx}[n] \star h[n] \star h[-n] \qquad (E.2)$$

where $R_{yy}[n]$ is the autocorrelation of the output signal, $R_{xx}[n]$ is the autocorrelation of the input signal, and $h[n]$ is the impulse response of the filter. Since the autocorrelation of the AWGN input is $\sigma^2 \delta[n]$, applying equation (E.2) to the present case yields:

$$R_{gg}[n] = \sigma^2 h_{rc}[n] \qquad (E.3)$$

where $R_{gg}[n]$ is the autocorrelation of the filtered noise and $h_{rc}[n]$ is the impulse response of a raised cosine filter.

The filtered noise is then downsampled to the symbol rate, generating a sequence $\eta[n] = g\left[n\frac{T}{T_s}\right]$, where T is the symbol period and T_s is the sampling period. Conse-

quently, the autocorrelation of η is:

$$R_{\eta\eta}[n] = \sigma^2 R_{gg}\left[n\frac{T}{T_s}\right] \tag{E.4}$$

$$R_{\eta\eta}[n] = \sigma^2 h_{rc}\left[n\frac{T}{T_s}\right] \tag{E.5}$$

Since the raised cosine filter achieves the Nyquist criterion for zero ISI, the value of $h_{rc}\left[n\frac{T}{T_s}\right]$ is zero for all values of n except 0. If n is zero, $h_{rc}\left[n\frac{T}{T_s}\right]$ is equal to 1:

$$R_{\eta\eta}[n] \begin{cases} \sigma^2, & n = 0 \\ 0, & n \neq 0. \end{cases} \tag{E.6}$$

which, since the noise is Gaussian, implies that the samples of the downsampled process are independent random variables, and:

$$E[\eta_i \eta_j^*] = \begin{cases} \sigma^2, & i = j \\ 0, & i \neq j. \end{cases} \tag{E.7}$$

References

[1] E. Smith, "The emergence of CATV: A look at the evolution of a revolution," *Proceedings of the IEEE*, vol. 58, pp. 967 – 982, July 1970.

[2] CableLabs, *Data Over Cable Service Interface Specification DOCSIS 3.0-Physical Layer Specification.* CM-SP-PHYv3.0-I03-070223, 2007.

[3] CableLabs, *Data Over Cable Service Interface Specification DOCSIS 1.0 Radio Frequency Interface.* Society of Cable Telecommunications Engineers, 1997.

[4] S. Ovadia, *Broadband Cable TV Access Networks.* Prentice Hall, 2001.

[5] V. Betz, "FPGA challenges and opportunities at 40nm and beyond," in *Field Programmable Logic and Applications, 2009. FPL 2009. International Conference on*, p. 4, Sept. 2009.

[6] W. Patterson, "Field programmable gate arrays get enough speed and density for computer applications," in *Compcon Spring '90. Intellectual Leverage. Digest of Papers. Thirty-Fifth IEEE Computer Society International Conference.*, pp. 477 –480, Feb. 1990.

[7] I. Kuon and J. Rose, "Measuring the gap between FPGAs and ASICs," *Computer-Aided Design of Integrated Circuits and Systems, IEEE Transactions on*, vol. 26, pp. 203 –215, Feb. 2007.

[8] T. J. Kolze, "Upstream HFC channel modeling and physical layer design," *Proc. SPIE*, vol. 2917, pp. 240–251, 1996.

[9] H. Meyr, M. Moeneclaey, and S. A. Fechtel, *Digital Communication Receivers: Synchronization, Channel Estimation, and Signal Processing.* Wiley, 1998.

[10] U. Mengail and A. N. D'Andrea, *Synchronization Techniques for Digital Receivers.* Plenum Press, 1997.

[11] E. Pelet, J. Salt, and D. Fast, "Timing and carrier acquisition in upstream CATV channels," in *IEEE Industrial Electronics, IECON 2006 - 32nd Annual Conference on*, pp. 3267 –3272, Nov. 2006.

[12] Y. Kim, H. Ha, J. Lee, W. Oh, W. Kim, E. Lee, and Y.-J. Song, "Upstream channel synchronization for cable modem system," in *Advanced Communication Technology, The 9th International Conference on*, vol. 3, pp. 1864 –1867, Dec. 2007.

[13] f. harris and C. Dick, "Preamble structure for fast acquisition and equalization of QAM signals," *Proceedings of the Software Defined Radio Technical Conference*, Dec. 2009.

[14] J. Salt, E. Pelet, and B. Berscheid, "Demodulator for cable TV video-on-demand," *Consumer Electronics, IEEE Transactions on*, vol. 53, pp. 1642 –1646, Nov. 2007.

[15] S. Tretter, "Estimating the frequency of a noisy sinusoid by linear regression (corresp.)," *Information Theory, IEEE Transactions on*, vol. 31, pp. 832 – 835, Nov. 1985.

[16] S. Kay, "A fast and accurate single frequency estimator," *Acoustics, Speech and Signal Processing, IEEE Transactions on*, vol. 37, pp. 1987 –1990, Dec. 1989.

[17] M. Luise and R. Reggiannini, "Carrier frequency recovery in all-digital modems for burst-mode transmissions," *Communications, IEEE Transactions on*, vol. 43, pp. 1169 –1178, Feb/Mar/Apr 1995.

[18] U. Mengali and M. Morelli, "Data-aided frequency estimation for burst digital transmission," *Communications, IEEE Transactions on*, vol. 45, pp. 23 –25, Jan. 1997.

[19] S. Haykin, *Adaptive filter theory*. Prentice Hall, 1991.

[20] S. Qureshi, "Adaptive equalization," *Proceedings of the IEEE*, vol. 73, pp. 1349 – 1387, Sept. 1985.

[21] A. H. Sayed, *Fundamentals of Adaptive Filtering*. Wiley-IEEE Press, 2003.

[22] H. Nguyen and E. Shwedyk, *A First Course in Digital Communications*. Cambridge University Press, 2009.

[23] S. O. Kasap, *Principles of Electrical Materials and Devices*. McGraw-Hill, 2000.

[24] J. G. Proakis, *Digital Communications*. McGraw-Hill, 2001.

[25] B. Sklar, *Digital Communications: Fundamentals and Applications*. Prentice Hall, 2001.

[26] S. M. Kay, *Fundamentals of Statistical Signal Processing, Volume I: Estimation Theory*. Prentice Hall, 1993.

[27] D. Rife and R. Boorstyn, "Single tone parameter estimation from discrete-time observations," *Information Theory, IEEE Transactions on*, vol. 20, pp. 591 – 598, Sept. 1974.

[28] J. Wang and J. Speidel, "Packet acquisition in upstream transmission of the DOCSIS standard," *Broadcasting, IEEE Transactions on*, vol. 49, pp. 26 – 31, Mar. 2003.

[29] J. E. Volder, "The CORDIC trigonometric computing technique," *Electronic Computers, IEEE Transactions on*, vol. EC-8, pp. 330 –334, Sept. 1959.

[30] S. Golomb and R. Scholtz, "Generalized barker sequences," *Information Theory, IEEE Transactions on*, vol. 11, pp. 533 – 537, Oct. 1965.

[31] R. Merched and A. Sayed, "Extended fast fixed-order RLS adaptive filters," *Signal Processing, IEEE Transactions on*, vol. 49, pp. 3015 –3031, Dec. 2001.

[32] G. Carayannis, D. Manolakis, and N. Kalouptsidis, "A fast sequential algorithm for least-squares filtering and prediction," *Acoustics, Speech and Signal Processing, IEEE Transactions on*, vol. 31, pp. 1394 – 1402, Dec. 1983.

[33] J. Cioffi and T. Kailath, "Fast, recursive-least-squares transversal filters for adaptive filtering," *Acoustics, Speech and Signal Processing, IEEE Transactions on*, vol. 32, pp. 304 – 337, Apr. 1984.

[34] T. Wolf, C. Lemonds, and A. Gatherer, "Low complexity equalization for cable modems," *IEEE Proc. ISCAS*, vol. 5, pp. 522–524, May 1998.

[35] A. Gatherer, "The effect of microreflections on decision feedback equalization," *IEEE Trans. Signal Processing*, vol. 54, pp. 228–231, Jan. 1997.

[36] Y. Kim, Y. Kim, Y. Lee, W. Oh, and W. Kim, "Synchronization and channel equalization for upstream cable modem," *IEEE Proc. ISCE Symposium*, pp. 1–4, Apr. 2008.

[37] L. J. D'Luna (and 18 others), "A single-chip universal cable set-top box/modem transceiver," *IEEE Jour. Solid-State Circuits*, vol. 34, pp. 1647–1660, Nov. 1999.

[38] M.P.Sellars, J.Porter, S.D.Greaves, I.J.Wassell, A.Hopper, and W.J.Fitzgerald, "Performance of fast start-up equalizer for broadband indoor radio," *IEE Proceedings on Comm*, vol. 148, pp. 49–56, Feb. 2001.

[39] G. Ysebaert, K. Vanbleu, G. Cuypers, M. Moonen, and T. Pollet, "Combined RLS-LMS initialization for per tone equalizers in DMT-receivers," *IEEE Trans. Signal Processing.*, vol. 51, pp. 1916–1927, Jul. 2003.

[40] G. H. Lee, J. Choi, R. H. Park, l. Song, J. H. Park, and B. U. Lee, "Modification of the reference signal for fast convergence in LMA-based adaptive equalizers," *IEEE Trans. Consumer Electronics*, vol. 40, pp. 645–654, Aug. 1994.

[41] G. Wang and R. Kraemer, "Low-complexity initialization of adaptive equalizers using approximate channel inverse," *IEEE Symp. Signal Processing and Information Technology*, pp. 694–698, Dec. 2005.

[42] Z. Andalibi, B. Berscheid, E. Salt, and H. Nguyen, "A fast-converging equalizer for upstream DOCSIS channels," *Broadcasting, IEEE Transactions on*, vol. 56, pp. 311 –320, Sept. 2010.

[43] S. Crozier, D. Falconer, and S. Mahmoud, "Least sum of squared errors (LSSE) channel estimation," *Radar and Signal Processing, IEE Proceedings F*, vol. 138, pp. 371 –378, Aug. 1991.

[44] C. Tellambura, Y. Guo, and S. Barton, "Channel estimation using aperiodic binary sequences," *Communications Letters, IEEE*, vol. 2, pp. 140 –142, May 1998.

[45] E. De Carvalho and D. Slock, "Cramer-rao bounds for semi-blind, blind and training sequence based channel estimation," in *Signal Processing Advances in Wireless Communications, 1997 First IEEE Signal Processing Workshop on*, pp. 129 –132, Apr. 1997.

[46] M. Golay, "Complementary series," *Information Theory, IRE Transactions on*, vol. 7, pp. 82 –87, Apr. 1961.

[47] P. Donato, M. Funes, M. Hadad, and D. Carrica, "Optimised golay correlator," *Electronics Letters*, vol. 45, pp. 380 –381, Mar. 2009.

[48] K. S. Miller, "On the inverse of the sum of matrices," *Mathematics Magazine, Mathematical Association of America*, vol. 54, pp. 67–72, Mar. 1981.

[49] J. Mikulka and S. Hanus, "CCK and barker coding implementation in IEEE 802.11b standard," in *Radioelektronika, 2007. 17th International Conference*, pp. 1 –4, Apr. 2007.

[50] N. Mohamed, "Nonsinusoidal radar signal design for stealth targets," *Electromagnetic Compatibility, IEEE Transactions on*, vol. 37, pp. 268 –277, May 1995.

[51] J. Hassab and R. Boucher, "Optimum estimation of time delay by a generalized correlator," *Acoustics, Speech and Signal Processing, IEEE Transactions on*, vol. 27, pp. 373 – 380, Aug. 1979.

[52] J. G. Proakis and D. M. Manolakis, *Digital Signal Processing: Principles, Algorithms, and Applications.* Prentice Hall, 1996.

[53] D. Morgan, "Adaptive multipath cancellation for digital data communications," *Communications, IEEE Transactions on*, vol. 26, pp. 1380 – 1390, Sept. 1978.

[54] D. Cassioli and A. Mecozzi, "Minimum-phase impulse response channels," *Communications, IEEE Transactions on*, vol. 57, pp. 3529 –3532, Dec. 2009.

[55] A. Papoulis, *Probability, Random Variables, and Stochastic Processes.* McGraw-Hill, 2002.